Dissertation

Optofluidic components for biomedical applications

Vom Fachbereich für Physik und Elektrotechnik
der Universität Bremen

zur Erlangung des akademischen Grades
Doktor-Ingenieur (Dr.-Ing.)
genehmigte Dissertation

von

Dipl.Ing. Emanuel Weber

Rohrgasse 27
2500, Baden, Österreich

Bremen, 2014

Eingereicht am: 19.06.2014
Tag des Promotionskolloquiums: 7.10.2014

Referent: Prof. Dr.-Ing. Michael J. Vellekoop
University of Bremen
Bremen, Germany

Korreferent: Ao. Univ. Prof. Dipl.-Ing. Dr.techn. Franz Keplinger
Vienna University of Technology
Vienna, Austria

Meinen Eltern
Mechthilde und Gerhard

Contents

Summary **xi**

Kurzfassung **xiii**

Nomenclature **xv**
0.1 List of Abbreviations xv
0.2 List of Constants xvi
0.3 List of Variables xvi

1 Introduction **1**
1.1 The emergence of optofluidics 5
1.2 Objectives of this work 7
1.3 Outline 8

2 Theoretical considerations **11**
2.1 Fluidic aspects 11
2.1.1 Navier Stokes equation 12
2.1.2 Diffusion in fluidic systems 13
2.1.3 Flow profile 14
2.1.4 Droplet microfluidics 15
2.2 Optical aspects 19
2.2.1 Total internal reflection 19
2.2.2 Planar waveguide 22
2.3 Optofluidics 22

3 Micro-fabrication **27**
3.1 Bulk micromachining 27
3.1.1 Silicon 27
3.1.2 Borosilicate glass 31
3.2 Surface micromachining 33
3.2.1 SU-8 33
3.2.2 Dry resist 35
3.3 Soft lithography - PDMS 42

3.4 Peripheral connections 45
3.4.1 Fluidic system 45
3.4.2 Optical system 46
3.4.3 External instruments 47

4 On-chip light modulation 51
4.1 Introduction 51
4.2 Light modulation principles 52
4.2.1 Concept of L2-waveguide based light modulation . . 52
4.2.2 TIR concept for light modulation 54
4.3 Experimental results 54
4.3.1 L2-waveguide based modulation 55
4.3.2 TIR based light modulation 56
4.3.3 Comparison of the two light modulation units 60
4.4 Conclusions 61

5 Thermo-Optofluidics 63
5.1 Introduction 63
5.2 Thermo-optic coefficient 64
5.3 Chip design 65
5.4 Experimental results 67
5.4.1 Matching of refractive indices 68
5.4.2 Thermo-optofluidic light switching 68
5.5 Conclusions 71

6 Liquid concentration sensor 73
6.1 Introduction 73
6.2 Underlying principle 74
6.2.1 The divergence of the laser beam 76
6.2.2 The incident angle 78
6.2.3 Independence of flow-velocity and temperature . . . 80
6.3 Experimental setup 81
6.4 Determination of liquid concentrations 83
6.4.1 Device design 83
6.4.2 $CaCl_2$ study 83
6.4.3 Phosphate study 87
6.5 Detection of dissolved lactose 88
6.5.1 First characterization 88
6.5.2 Optimization for low lactose concentrations 89

6.5.3 Experiments on off-the-shelf lactose-free milk . . . 91
6.6 Determination of ethanol contents . . . 93
6.6.1 Device design . . . 93
6.6.2 Ethanol measurements . . . 94
6.7 Characterization of micro-droplets . . . 95
6.7.1 Motivation . . . 97
6.7.2 Device design . . . 98
6.7.3 Detection of micro-droplets . . . 99
6.7.4 Sizing of micro-droplets . . . 101
6.7.5 Identification of micro-droplets . . . 102
6.8 Conclusion . . . 104

7 Conclusions and future perspectives 107

Acknowledgments 111

List of Publications 113

Bibliography 117

About the Author 123

Summary

In the last years the term ”Optofluidics” has popped up in a large amount of scientific publications. The vastly increased interest underlines the potential of this new field of research. Nevertheless, the broad applicability of this technique for practical means is still to be demonstrated. The goal of this thesis is to prove Optofluidics as a powerful tool for distinct biological and medical applications. In particular, an optofluidic sensor design for the analysis of liquid samples shall be elaborated and hence demonstrate the applicability of this new field of research.

In the main part of this work, an optofluidic sensing unit for the determination of liquid concentration is presented. On a chip-area of less than two square centimeters, liquid samples are analyzed in a flow through manner and the concentration of dissolved molecules is derived. The principle is based on a change in the index of refraction depending on the concentration of molecules. A slightly diverging light beam experiences partial total internal reflection at the solid-liquid interface between chip material and liquid analyte in a micro-channel. The ratio between reflected and transmitted light is then used as a measure for the substitution of the sample solution. In an experimental evaluation, the sensor was tested with different dissolved molecules including phosphate and lactose. Depending on the analyte, a smallest detectable change in concentration of 10 to 40 mmol/L was determined. Keeping in mind the simplicity of the overall system this is remarkable.

Besides the sensing device, a new subfield of optofluidics was introduced for the very first time. Thermo-optofluidics deals with the integration of thermal elements in optofluidic systems. As a proof-of-concept a thermo-optofluidic light modulator was developed. Exploiting the opposing temperature dependency of the index of refraction of solids and liquids, waveguidance through a liquid core/solid cladding waveguide was reversibly turned on and off. Compared to solely solid based realizations more than twice the theoretical switching frequency can be achieved.

As a basic building block for microfluidic applications, an optofluidics based light modulation unit was developed. Exploiting the exchangeability of liquids this system provides an extremely stable light signal which is

completely flow independent. This system can be implemented on other microfluidic devices and enhance their functionality.

In conclusion, the applicability of optofluidics for different sensor as well as actuator systems was experimentally proven. All the devices were fabricated applying low-cost, rapid-prototyping fabrication techniques which allow the realization of cost-effective hand-held devices.

Kurzfassung

In den letzten Jahren ist das Schlagwort ”Optofluidics” immer öfter in wissenschaftlichen Publikationen aufgetaucht. Dieses Interesse streicht das Potential dieses neuen Forschungsgebietes hervor. Nichtsdestotrotz sind bislang wenige anwendungsbezogene Systeme mit dieser Technik hervorgegangen. Das Ziel dieser Dissertation ist es optofluidische Anwendungen im Bereich Biologie und Medizin zu entwickeln. Im Speziellen soll ein Sensorsystem erarbeitet werden mithilfe dessen Flüssigkeiten charakterisiert werden können.

Im Hauptteil dieser Arbeit wird ein optofluidischer Sensor für die Bestimmung von Konzentrationen in Flüssigkeiten vorgestellt. Auf einer Chipgröße von weniger als zwei Quadratzentimetern werden die Analyte in-line auf deren Konzentrationen untersucht. Das System nutzt die Tatsache aus, dass sich der Brechungsindex von Flüssigkeiten in Abhängigkeit von deren Molekülkonzentrationen verändert. Auf dem Chip wird ein leicht divergierender Lichtstrahl am Übergang vom Chipmaterial zu der zu untersuchenden Flüssigkeit in einem Mikrokanal teilweise total reflektiert. Das Verhältnis von reflektiertem zu transmittiertem Licht wird in weiterer Folge als Wert für die Konzentration von Molekülen in der Flüssigkeit herangezogen. Das System wurde mit unterschiedlichen Analyten, unteranderem mit Phosphat und Laktose, getestet und es wurde eine kleinste feststellbare Konzentrationsänderung von 10 bis 40 mmol/l bestimmt. Unter Berücksichtigung der Einfachheit des Systems ist diese Auflösung durchaus bemerkenswert.

Neben der Sensoreinheit wurde im Zuge dieser Arbeit das Gebiet der Thermo-Optofluidics zum aller ersten Mal vorgestellt. Dieses Untergebiet von Optofluidics integriert thermische Elemente in optofluidische Systeme. Als Proof-of-Concept wurde ein Lichtmodulator entwickelt. Das Konzept beruht auf der entgegengesetzten Änderung des Brechungsindex von Festkörpern und Flüssigkeiten in Abhängigkeit von der Temperatur. Mittels dieser Änderung wird die Wellenführung in einem flüssiger Kern/fester Mantel Wellenleiter ein- beziehungsweise aus-geschalten. Im Vergleich zu reinen Festkörpersystemen kann dadurch die theoretisch mögliche Schaltfrequenz mehr als verdoppelt werden.

Als Basisbaustein für mikrofluidische Anwendungen wurde ein optofluidischer Lichtmodulator entwickelt. Dieser Baustein nutzt die Austauschbarkeit von Flüssigkeiten um ein sehr stabiles Lichtsignal zu erzeugen das unabhängig von der Flussgeschwindigkeit ist. Dieses Element kann in andere mikrofluidische Systeme integriert werden um deren Funktionalität weiter zu erhöhen.

In dieser Arbeit wurde experimentell gezeigt, dass Optofluidics für unterschiedlichste Sensor- als auch Aktuator-Systeme einsetzbar ist. Die präsentierten Systeme wurde alle in kosteneffizienten, Rapid-Prototyping Verfahren hergestellt und erlauben somit die Entwicklung von leistbaren, kompakten Geräten.

Nomenclature

0.1 List of Abbreviations

Symbol	Description
$CaCl_2$	calcium chloride
CCD	charge-coupled-device
CMOS	complementary metal oxide semiconductor
DI	de-ionized
DNA	deoxyribonucleic
dpi	dots per inch
DRIE	deep reactive-ion etching
DRIN	gradient-index
HF	hydrogen fluoride
IR	infrared
KH_2PO_4	monopotassium phosphate
KOH	potassium hydroxide
L2	liquid core/liquid cladding
M	molar
MEMS	microelectromechanical systems
NA	numerical aperture
NaH_2PO_4	monosodium phosphate
PDMS	polydimethylsiloxane
PI	propidium iodide
PMMA	polymethyl methacrylate
PTFE	polytetrafluoroethylene

Symbol	Description
RIE	reactive-ion etching
rpm	revolutions per minute
SEM	scanning electron microscope
Ti	titanium
TIR	total internal reflection
UV	ultraviolet
vol. %	volume percent
ZZulV	Zusatzstoff-Zulassungsverordnung

0.2 List of Constants

Constant	Description	Unit
e	Euler's number	2.71828
k	Boltzmann constant	1.38064 x 10^{-23} J/K
π	Pi	3.14159

0.3 List of Variables

Symbol	Description	Unit
A	area	m^2
c	concentration	mol/liter
D	diffusion constant	m^2/s
D_H	hydraulic diameter	m
dn/dT	thermo-optic coefficient	1/K
E	electric field	V/m
ϵ	permittivity	F/m

Symbol	Description	Unit
ϵ_γ	surface energy	J
η	viscosity	kg/(m· s)
F	body force	N
J	diffusion flux	mol/(m^2· s)
k_0	amplitude of the wave vector in vacuum	
$k_{\|\|}$	projection of the wave vector	
l	length	m
λ	wavelength	nm
m	mass	kg
N	amount of molecules	
n	index of refraction	
p	pressure	Pa
P_{wet}	wetted perimeter	m
r	radius	m
R	average reflectivity	
$R_{\|\|}$	reflectivity of parallel polarized light	
$R_\perp$	reflectivity of perpendicularly polarized light	
Re	Reynolds number	
ρ	mass density	kg/m^3
ρ_f	local free charge	C
S	source or sink of concentration	mol/(m· s^2)
T	temperature	°C
t	time	s
θ	angle	°
v	velocity	m/s
x	place	
y_0	channel radius	m

Chapter 1

Introduction

Optofluidics, an idea that was born less than 10 years ago, starts to show its capabilities for a variety of applications. First seen as a by-product of microfluidics it is now fully accepted as a field of research on its own. The unique possibilities within optofluidics are the driving force of the increasing amount of activities on this topic. Optofluidics is ready to be taken to the next step. The applicability for different purposes has to be demonstrated which is the major goal of this thesis. In the course of this work, actuating as well as sensing elements are developed and realized for the first time proving the potential of optofluidics for practical means.

The last decades were characterized by a permanent pursuit for miniaturization and integration of system components into single devices. Especially in technical equipment this trend was strongly recognized and is still being continued. Today the modern society demands for user-friendly allround systems. Here the most prominent example might be voice telephony. Developed in the 19th century, as a way of connecting people all over the world, it has become indispensable and is taken as a matter of course for the majority of the modern society. Besides mobile telephony, today's modern cell phones provide their users with countless entertainment features on handheld devices. Gordon Moore [1] has already foreseen this way of miniaturization and integration in 1965 and there is still no end in sight.

This incredible amount of device features was enabled by continuous advances in micro-technology. With advanced techniques micro-devices can be equipped with structures in the nanometer range. Next to the development of smaller and smaller semi-conductor elements (e.g. transistors for processor board applications) another field of micro-devices, the microelectromechanical systems (MEMS) has arisen. MEMS devices incorporate, both electrical elements and mechanical structures in the micrometer range. Typical applications are integrated sensor and actuator systems. Widely applied examples are micro-accelerometers. They are integrated in airbag mechanisms as acceleration sensors and in modern mobile phones as sens-

ing unit for the automatic adaption of the screen orientation. Compared to macro-devices the mass and with that the inertia forces are drastically reduced resulting in much shorter reaction times.

The emergence of MEMS technologies has allowed a new field of research, microfluidics, to thrive. It deals with the controlled manipulation of liquids in micro-fabricated structures on-chip. Besides others, the investigation of biologically or medically relevant liquid samples is the driving force behind those efforts. The drastic reduction in sample volumes has enabled high throughput sensing devices to be developed. Another huge advantage of such systems is portability. Due to the small size microfluidic chips can be integrated in hand-held devices with fully autonomous operation. Two well known examples are pregnancy and blood glucose test devices. Without any need for bulky external instruments, those devices provide reliable results within a moment. Both devices employ functionalized substrates being highly sensitive for different molecules. In case of pregnancy tests those substrates are sensitive to human chorionic gonadotropin, a hormone produced only by pregnant women. A non-quantitative but highly qualitative information is obtained whether or not fertilization has taken place. Blood glucose tests are functionalized with an enzyme reacting directly with glucose molecules. In an electrochemical interaction a quantitative result is produced providing the operator with the blood sugar concentration within a few seconds.

The above mentioned microfluidic applications implement two basically different read-out mechanisms. Whereas the pregnancy test is based on a color change of the functionalized substrate, meaning an optical effect, the blood glucose test detects the produced electrical current during the chemical interaction, meaning an electrical mechanism. Anyway, both devices implement physical sensors for the characterization of liquids [2,3]. In general, for medical and biological purposes optical phenomena are often exploited. Compared to other principles, optical inspections are widely harmless to the analytes. Furthermore, light waves do not heavily interfere with other neighboring elements such as electric or magnetic circuits allowing them to be placed side-by-side on one device. Depending on the application, the operation wavelength of the analysis system reaches from the visible into the mid infrared region. The optical absorption of the device material is a major criterion for the choice of the employed wavelength. The surrounding material of the analyte has to be widely transparent at the chosen wavelength. If not, transmission of light to the analyte is inhibited, which mostly is a

requirement for the functionality of the system. In that sense the combination of sensing principle, optical properties of the device material, and the analytes of interest has to be chosen carefully.

In medicine and biology, the flow-cytometric analysis of biological samples such as particles and cells is a descriptive example of an optical system incorporating fluidic elements and is therefore shortly introduced. The operation principle is depicted in Fig. 1.1. The suspended analytes are introduced into the flow cytometer through the sample inlet. At the end of the sample inlet tube the suspension is heavily squeezed by the sheath flow. For the proper functioning of the instrument the suspended particles/cells have to line up one after each other before reaching the interrogation point. If particle/cell clusters are occurring, the sample suspension has to be diluted to reach a lower initial concentration of the analytes. Once a stream of single particles/cells is obtained, a meaningful analysis can be performed. At the interrogation point the analytes are exposed to a focused light beam. Each individual particle/cell passing through the interrogation point creates

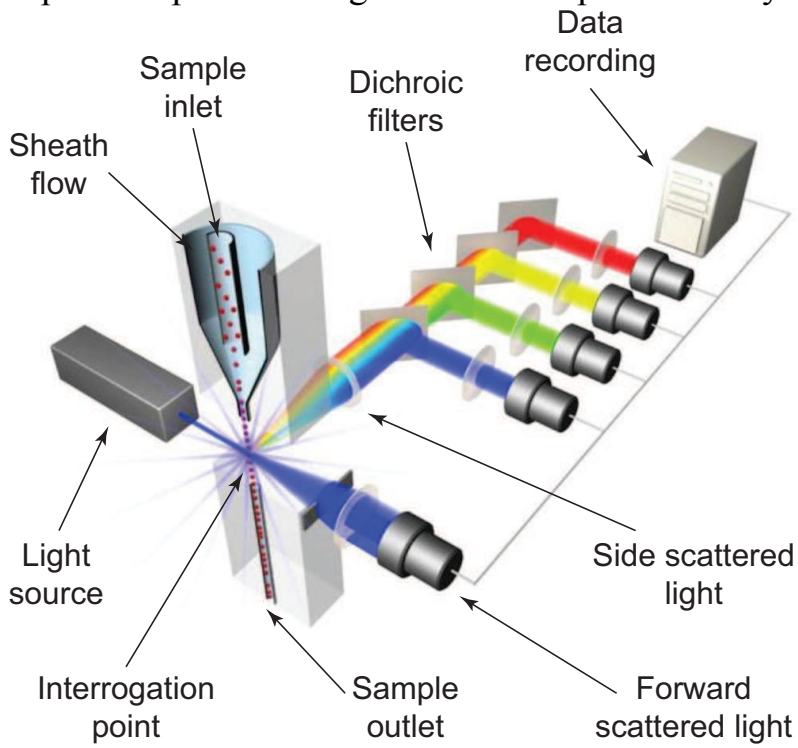

Figure 1.1: Schematic of the working principle of a bench-top flow cytometer. The suspended samples are squeezed to a stream of seriatim particles/cells. At the optical interrogation point light is scattered by the passing particles/cells depending on their optical properties. In general, photo multiplier tubes are used to record the forward as well as the side scattered light signals. The obtained data is logged and used for the characterization of the analyte. Figure adapted from *LifeTechnologies*©.

a distinct light scatter pattern. The forward as well as the side scattered light signals are detected. The forward scattered light provides information about the outer shape of the particle/cell. The side scattered light gives information about the internal granularity of the investigated sample. Furthermore, fluorescent signals, either due to auto-fluorescence or due to selective labeling, can be recorded by additional dichroic filters placed in the optical path. The gathered data provides information such as density, particle/cell size, and fluorescent activity of the suspension filled in the instrument.

Nowadays, flow cytometers are a well established tool in medical as well as bio-laboratories. Anyway, they are still far from being miniaturized, portable, point-of-care systems. Furthermore, well trained personnel is need for their operation. Different research groups have tackled these issues and have developed integrated versions of such instruments [4–10]. Fig. 1.2 shows a micro-flow cytometer chip applied for fluorescence based cell analyses presented by Weber *et al.* [11]. The dimensions of the device are 9x7 mm. As in its macro counterpart, the suspended cells are squeezed

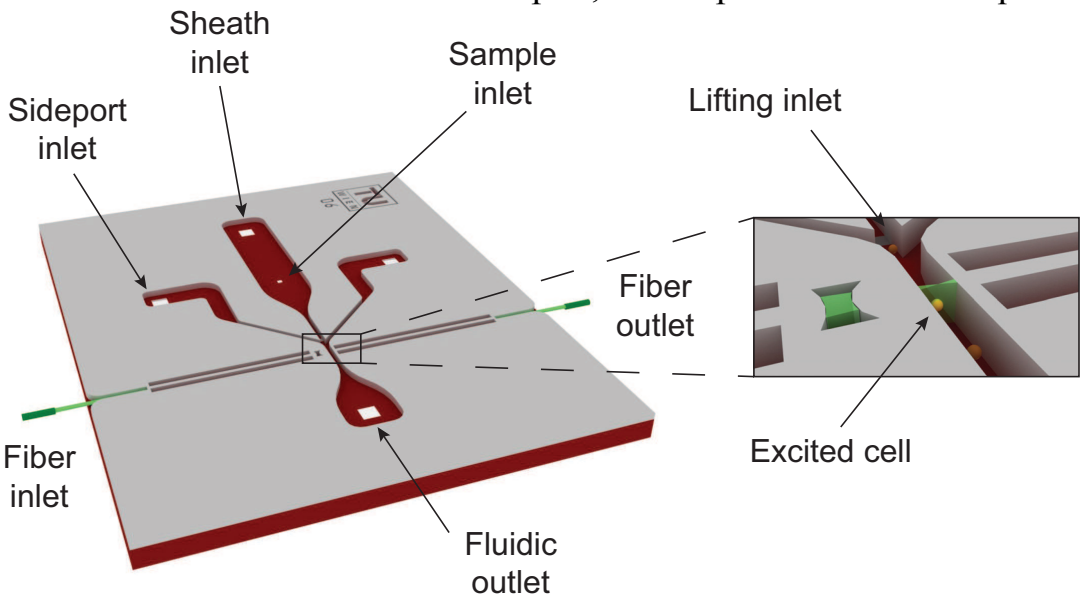

Figure 1.2: Schematic of the micro-flow cytometer chip with five liquid inlets (one sample, one sheath, one lifting, and two side ports). The principle of fluorescence excitation in a passing cell is illustrated in the magnification [11].

hydrodynamically to form a stream of seriatim cells. The first focusing of the analyte is realized by the sheath inlet. The sample enters the microfluidic system from the bottom at a constant flow rate. From the back it is overflown by the sheath liquid forming a narrow stream of cells pushed to the bottom. The lifting inlet is responsible to center the stream in the vertical direction right before the optical interrogation point. Two additional sideport inlets

further squeeze the sample stream to end up with individual cells flowing one after each other right through the center of the microfluidic channel. At the interrogation point the cells are exposed to focused monochromatic light. Two light signals are recorded. The first one is collected at the opposing side of the channel. The second one is bandpass filtered and collected from the top of the channel. A drop in the first signal indicates the presence of a cell in the interrogation point and is used as a counting unit. The second signal collects the fluorescent light emitted by the individual cells. Prior to the injection into the device the sample solution are treated with a fluorescent dye (propidium iodide) . Dead cells are labeled whereas alive ones are not. Calculating the ratio of cell count obtained from the first light signal and fluorescence signals gathered from the second one provides an absolute value of the cell culture viability.

This example is an impressive demonstration of the enormous capabilities of microfluidics. An inline and real-time measurement of cell culture viability can be performed on less than 1 cm^2 of space. Due to its small size a fraction of the sample volume is sufficient as compared to the analysis on a macro-flow cytometer. This fact goes hand in hand with a drastically reduced analysis time which is of huge importance for portable point-of-care devices. On the micro-scale new phenomena such as the laminar flow are of additional advantage e.g. for hydrodynamical manipulations of liquids. Now being aware of the potential of microfluidics and the already well known capabilities of optical sensing mechanisms gives rise to the question whether both together can fulfill tasks which neither is capable of on its own.

1.1 The emergence of optofluidics

Evolved from microfluidics, optofluidics has become much more than a by-product and is now seen as a new field of research starting to demonstrate its unique power to the scientific community [12–14]. The word *optofluidics* has popped up in scientific publications less than ten years ago. Fig. 1.3 depicts the number of publications per year with *optofluidic* in the title. The first appearance is dated in 2005. Starting from then the number is increasing rapidly reflecting the enormous interest in this new field of research. This trend indicates the potential of optofluidics seen by the researchers but what is it making optofluidics this powerful and obviously worth to be investigated?

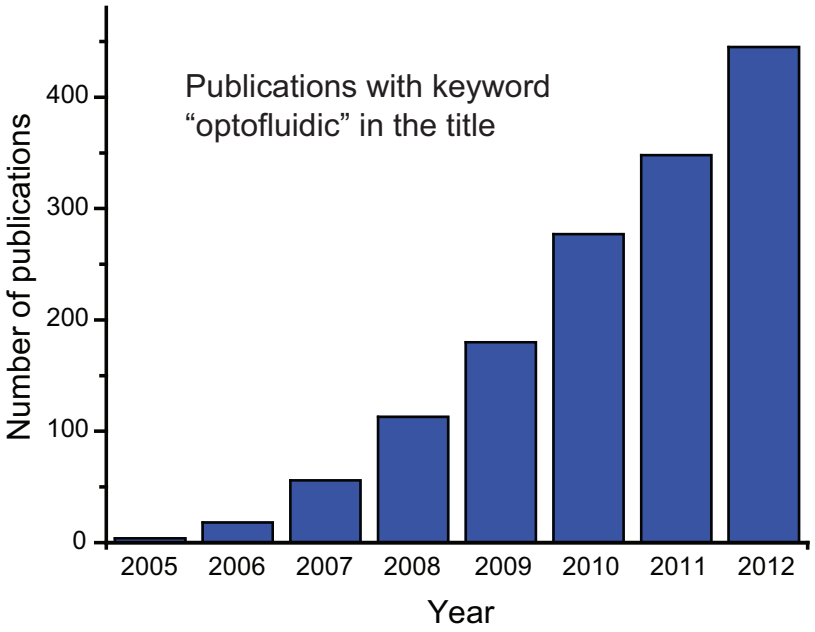

Figure 1.3: Absolute number of publications with the keyword ”optofluidic” in the title. Source *ISI Web of Science, July 2013*.

Optofluidics deals with fluids and optics on the micro-scale and is therefore often misinterpreted as microfluidics with integrated optical elements such as the micro-flow cytometer mentioned in the preceding section. In fact, optofluidics is defined as the integration of fluidic elements right in the functional optical path of the micro-system. The unique part is that liquids take over the role of optical elements and do not just coexist with them on the same device. This definition clearly separates optofluidics from microfluidics and optics. Certainly, it incorporates elements of both, but in combination it offers possibilities which can’t be obtained by simply adding the features of them. Novel phenomena occur which justifies optofluidics as an autonomous field of research on its own.

Liquid micro-lenses are one example of optofluidic elements [15, 16]. The idea is to form a lens shaped liquid object surrounded by another liquid with different refractive index. Compared to solid realizations liquids can easily be exchanged allowing a continuous reconfiguration of the focusing characteristics of the lens. Fig. 1.4 illustrates the basic concept for the creation of three dimensional liquid lenses on-chip. Two liquids with different refractive indices enter the microfluidic channels from the top. The main channel is then split and forms two arms, each one filled with both liquids equally. In a sharp turn of the microfluidic channel the inner liquid

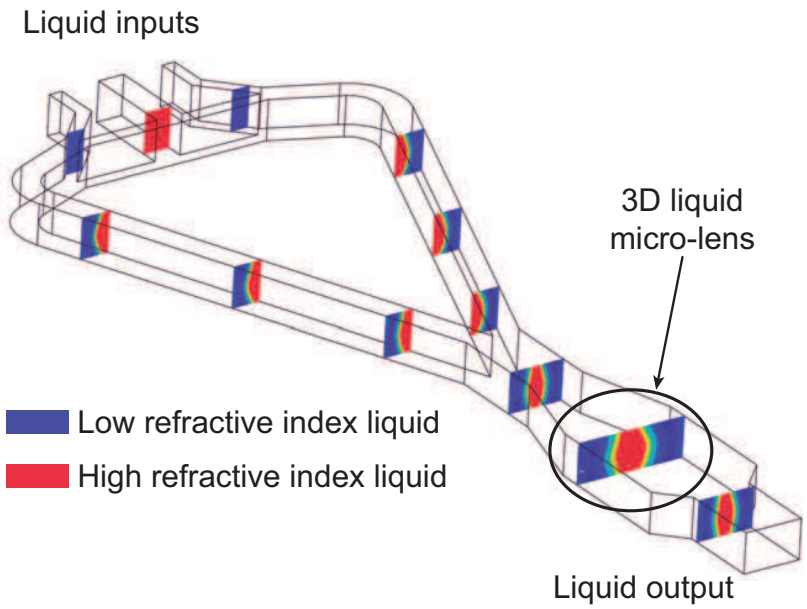

Figure 1.4: Concept for the creation of three dimensional liquid micro-lenses. Image adapted from Rosenauer *et al.* [16].

experiences higher forces towards the outside and displaces the outer liquid partially. Here the Dean effect [17, 18] is exploited. After the first turn the cross-section of each arm shows a half lens-like shape in two dimensions. After the two separated streams of liquids are joined again the channel expands. In this expansion the liquid lens is shaped in the third dimension and creates a 3D liquid micro-lens which can easily be reconfigured by applying different inlet velocities. Liquid micro-lenses are one demonstrative example of optofluidic applications and point out its advantages. Compared to solid realizations an enormous increase in flexibility is achieved. New phenomena occur, which can be exploited for the needs of the specific applications.

1.2 Objectives of this work

Optofluidics is a new field of research which shows high potential for the realization of various sensor systems. Especially, nowadays established optical analysis setups can benefit from its advantages. Here prominent examples can be found in medicine and biology. Nevertheless, optofluidics is still in development stage and devices based on practical applications are rare. More praxis oriented research is needed to demonstrate the full potential of

optofluidic sensor designs.

The goal of this thesis is to tackle this issue and design optofluidic sensor systems especially for use in medical and biological studies. The main research objectives are:

1. Novel optofluidic sensor designs for applications in medicine and biology shall be elaborated.

2. The applicability of different fabrication techniques for the device manufacturing shall be investigated.

3. The functionality of the fabricated prototypes shall be verified for relevant biological samples.

At the final state, the fabricated prototypes should operate with a minimum of peripheral equipment and should hold the potential to be further developed into a hand-held analysis device.

1.3 Outline

This thesis is divided into five main chapters. In Chapter 2 the theoretical aspects for the design of optofluidic devices are introduced. Both, the microfluidic as well as the relevant optical phenomena are described.

Chapter 3 is dedicated to the applied fabrication technologies. Two basically different approaches, bulk and surface micromachining, are followed. Each one provides unique advantages compared to the other one. The last section deals with soft lithography, a rapid prototyping technique which is widely applied in microfluidics and allows an extremely short design to device time. Finally, the peripheral connections to the micro-devices are explained.

In Chapter 4 an optofluidic waveguide modulator is presented and compared against an L2-waveguide shifter. The elaborated modulator is based on light reflection at a solid-liquid interface and operates without any mechanically moving elements. First, simulation results are shown followed by the experimental evaluation of the device functionality.

In Chapter 5 thermo-optofluidics, a novel field of application of optofluidics is introduced for the first time. It exploits the thermo-optic coefficient

of solid and liquid materials in a unique way. After giving the necessary theoretical considerations, a thermo-optofluidics based light modulation unit is presented pointing out the applicability of this new field of research.

Chapter 6 deals with an optofluidic sensor for the label-free determination of liquid concentrations. At first, the sensor design is explained theoretically followed by the experimental section. The device was successfully tested with different sample solutions including dissolved phosphate and lactose. As another field of application, droplet microfluidics is introduced and the capability of the sensor system for the investigation of microdroplets is pointed out.

In the final Chapter 7 the work presented in this thesis is summarized and the main conclusions drawn from the results are discussed. At the very end an outlook is giving providing ideas for the future continuation of the topics covered in this thesis.

Research project frame

The work presented in this thesis was conducted at three universities, the Delft University of Technology in the Netherlands, the Vienna University of Technology in Austria, and the University of Bremen in Germany within the framework of two European Marie-Curie Initial Training Networks, namely ”CellCheck - On-chip cell handling and analysis” with project number MCRTN-CT-2006-035854 and ”EngCaBra - Biomedical engineering for cancer and brain disease diagnosis and therapy development” with project number PITN-GA-2010-264417.

Chapter 2
Theoretical considerations

In this chapter the theory behind the optofluidic systems presented in the later chapters is introduced. First, the fluidic behavior of liquids in microchannels is analyzed followed by the optical fundamentals of wave guiding. At the end of this chapter, optofluidics, a novel field of research is examined in more detail.

2.1 Fluidic aspects

On the micro scale fluidic behavior can either be described by a molecular or by a continuum approach. For very small sample volumes molecular effects substantially influence physical parameters such as the fluid density. In such cases, the use of an average value would not well represent the investigated system. The decision whether to choose a molecular or a continuum approach is not very clear in fluid dynamics. In a continuum approach all quantities of interest (e.g. density, velocity, pressure) are assumed to be defined anywhere in the investigated geometry and vary continuously from point to point. The density (ρ) of a fluid in a certain volume is defined as

$$\rho = \frac{N \cdot m}{L^3}$$

where N is the amount of molecules in a cube with a side length of L and m stands for the mass of a single molecule. For a statistical variation of less than 1 % 10^4 molecules are needed. Taken water as the analyte the transitional length can be calculated to

$$L_{H_2O} = \sqrt[3]{\frac{N \cdot m}{\rho}} = \sqrt[3]{\frac{10^4 \cdot 3 \cdot 10^{-23}\, g}{10^6\, \frac{g}{m^3}}} = 6.7 \cdot 10^{-9}\, m.$$

A similar derivation is necessary for any other quantities of interest. Doing so, a characteristic length scale of 10 nm can be approximated. As long as

the characteristic length scale is much smaller than the dimensions of the fluidic channels the continuum approach is valid. Assuming typical dimensions in microfluidic systems of well above 1 µm [19] justifies the use of a continuum approach.

2.1.1 Navier Stokes equation

Taken the continuum assumption as valid, microfluidic systems can be described with Newton's second law for fluid particles, the Navier Stokes equations. Newton's second law for an ordinary particle is given by

$$m \cdot d_t \vec{v} = \sum_j \vec{F_j}$$

where m stands for the mass and v for the velocity of the particle. $\sum_j F_j$ represents any external forces acting on the particle. Dividing this equation by the volume and replacing d_t by the material time-derivative gives the first version of the Navier Stokes equation

$$\rho \cdot D_t \vec{v} = \sum_j \vec{f_j}$$

where the material time-derivative is defined as

$$D_t = \partial_t + (\vec{v} \cdot \nabla).$$

Substituting the forces acting in an isothermal incompressible Newtonian fluid (constant temperature, density, and viscosity) the Navier Stokes equation is given by

$$\rho D_t \vec{v} = -\nabla p + \eta \nabla^2 \vec{v} + \rho \cdot \vec{g}$$

where the left side represents the inertia forces (i.e. acceleration) and the right side the forces generated by the pressure gradient, the viscosity, and the gravity, respectively. To effectively solve this equation further simplifications are needed. In most microfluidic systems the inertia forces are dominated by the viscous forces. Therefore, the non-linear part $D_t \vec{v}$ can be neglected which leads to the simplified Stokes equation

$$\nabla p = \eta \nabla^2 \vec{v} + \vec{f}$$

where $\vec{f}$ represents external forces of particular interest (e.g. gravity and electrical forces). To verify the validity of the simplification the Reynolds

number (Re) has been introduced which basically is the ratio of inertial and the viscous forces,

$$Re = \frac{\rho D_H v}{\eta}$$

where v stands for the flow velocity and D_H for the hydraulic diameter. The hydraulic diameter is a characteristic length scale of the investigated system. In a channel with a circular cross section D_H equals the diameter d. For arbitrary perimeter D_H is defined as

$$D_H = \frac{4A}{P_{wet}}$$

where A stands for the area of the cross section and P_{wet} for the wetted perimeter. For cases in which $Re < 1$, the Stokes equation can be used to describe the system. In typical microfluidic systems this condition is fulfilled. As the Reynolds number scales linearly with the flow velocity, high flow rates require closer inspection of the theoretical situation. For Reynolds numbers, $Re \lesssim 2000$ laminar flow can be expected in the channels. In laminar systems the streamlines of the flow are widely parallel which inhibits any formation of turbulences. This circumstance allows mixing of fluids by diffusion only, which is exploited in many microfluidic devices but of disadvantage for micromixing applications.

2.1.2 Diffusion in fluidic systems

Microfluidic systems are commonly operated in the laminar flow regime. That means mixing of fluids in the channels is limited to diffusion only. The total diffusion flux (J) through a surface (δA) can be described using Fick's law

$$J = -D\nabla c$$

where D is the diffusion coefficient and c the concentration of species in the liquid. Substituting Fick's law in the conservation of species yields the diffusion equation

$$\frac{\partial c}{dt} = D\nabla^2 c + S$$

where S represents any source or sink of concentration. In Fig. 2.1 the diffusion in an elementary volume is illustrated.

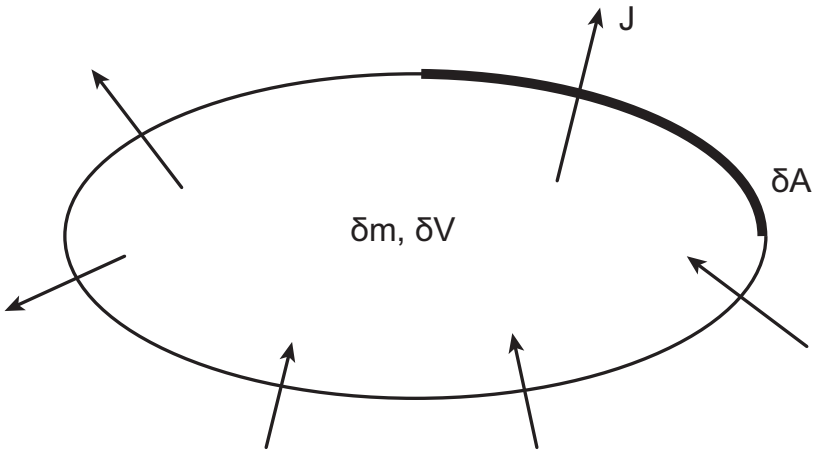

Figure 2.1: Schematic illustration of diffusion in an elementary volume.

In the laminar flow regime the diffusion constant can be derived using the Stokes-Einstein equation

$$D = \frac{k_b T}{6\pi\eta r}$$

where k_B is the Boltzmann constant ($1.38{\cdot}10^{-23}$ J/K), η the viscosity and r the radius of the species. The diffusion constant at room temperature for aqueous solutions including DI water is in the range of 10^{-9} m^2/s.

2.1.3 Flow profile

In microfluidic systems the velocity field in the channels requires closer consideration. Depending on the applied pumping system two basically different flow profiles are built up inside the channel. For external systems working with pressure differences as the pumping source (which is often applied in microfluidic setups), the *no-slip* condition at the channel walls is of high impact. Due to the width of the channels in the micrometer range, this zero flow velocity at the channel walls results in a parabolic flow profile (Fig. 2.2a). In the following chapters, only pressure driven systems are used.

It should be mentioned that there are pumping systems readily implemented capable of providing a constant flow profile in the channels as well. One such pumping principle is electro-osmosis. In an electro-osmotic driven flow, the flow velocity is constant over the entire width of the microfluidic channel (Fig. 2.2b).

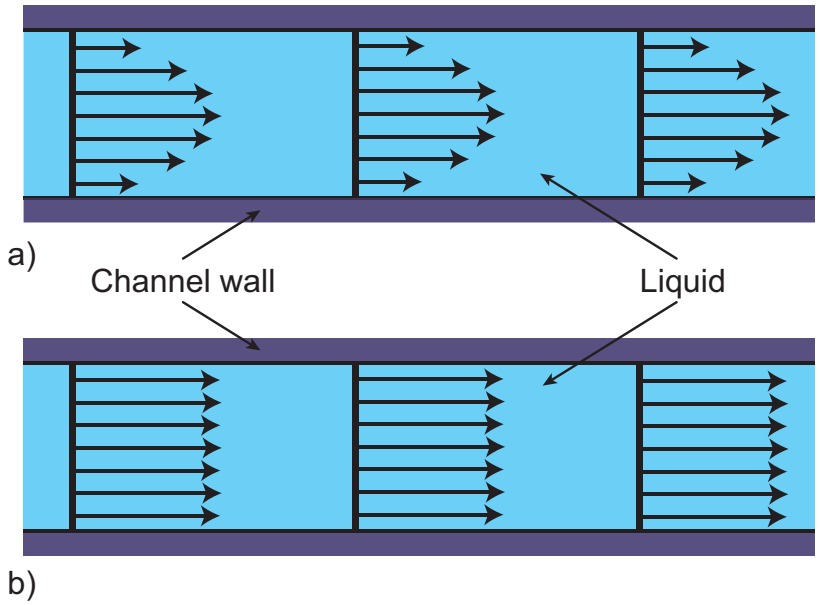

Figure 2.2: Flow profile in microfluidic channels. **(a)** In a pressure driven system a parabolic flow profile is obtained. The flow velocity at the channel walls is zero. **(b)** Driving the liquid in the channel with e.g. electro-osmosis results in a constant flow velocity.

2.1.4 Droplet microfluidics

Droplet microfluidics can be described as a controlled formation of emulsions in microfluidic channels. Two immiscible fluids, the droplet phase and the continuous phase, are brought into the same system to form micro environments for different applications. The two most popular ways of droplet formation are water-in-oil and oil-in-water droplets depending on the hydrophobic/hydrophilic characteristics of the applied device material. Hydrophobic materials result in water droplets surrounded by oil as the continuous phase whereas hydrophilic materials are used to form oil droplets surrounded by water. Surfactants can be added to the droplet as well as to the continuous phase for droplet stabilization [20]. The most simple way of passive droplet generation in microfluidic systems is based on a T-junction (Fig. 2.3). On the device two micro channels are merged. The continuous phase is pumped through the left inlet. The droplet phase approaches the continuous phase from the top. Depending on the device material, the chosen liquids, the channel geometry and the applied inlet velocities of the two phases different droplet shapes can be generated. For a T-junction arrangement and channels with a circular cross section, the droplet size can roughly

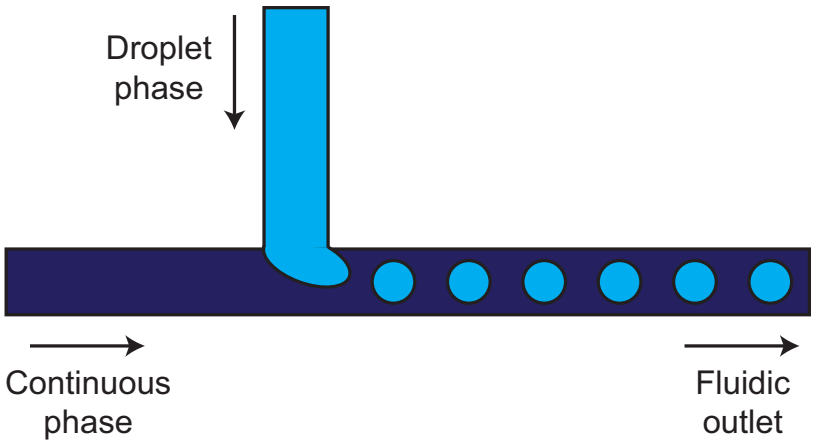

Figure 2.3: T-junction arrangement for micro droplet generation. The continuous phase is inserted from the left inlet. The droplet phase is inserted from the top, perpendicularly to the continuous phase.

be approximated by

$$r \approx \frac{y_0 \gamma}{2 v \eta}$$

where r is the radius of the droplet, y_0 is the channel radius, γ the interfacial tension between the two liquid phases, v the velocity of the continuous phase through the gap between channel wall and droplet, and η the viscosity of the continuous phase. Typical dimensions of the microfluidic channels implemented for droplet generation are in the range of 100 µm channel width. The produced micro droplets have a typical total volume in the picoliter range. These small volumes make micro droplets enormously attractive for applications with limited sample volumes such as, for example, in medical diagnostics.

Once micro droplets have been created, they can be manipulated in different ways. Two often required manipulations are controlled trapping and merging of droplets. Trapping at defined positions allow for a continuous observation of the micro droplets with implemented or peripheral sensing units. One typical peripheral measurement method is light microscopy. Size and shape of the droplet as well as inner changes can be recorded over time at the trapping position. Spectral analyses such as Raman spectroscopy [21, 22] are other examples for peripheral measurements. Next to external instruments, sensing elements can also be directly implemented at the trapping position on-chip. Proper placement of electrodes for example, allows the continuous monitoring of the electrical conductivity which can be correlated to changes of the droplet constitution. Furthermore, one could

also think of integration of optical sensing elements to record the change in optical properties such as light absorption and index of refraction. A simple method for trapping of single droplets is based on a spatially confined expansion of the channel [23, 24]. Fig. 2.4 shows the cross-section of a microfluidic channel with integrated micro droplet traps. This technique can

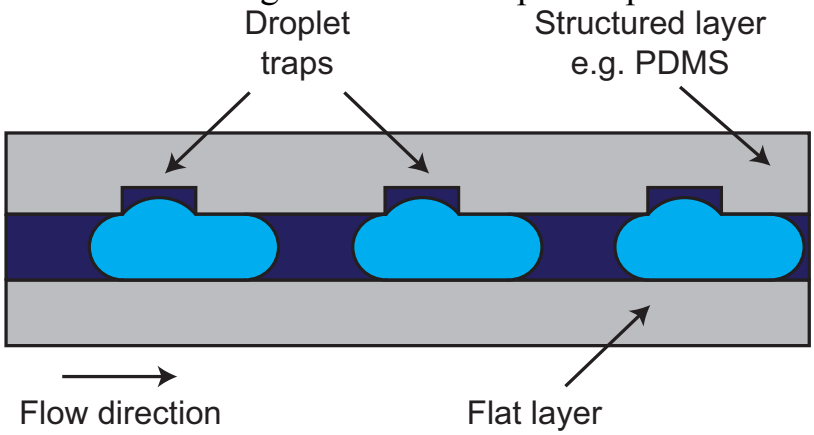

Figure 2.4: A micro channel with non-uniform height working as a trap for micro droplets. At the expansions of the channel the droplets can stay in a lower surface energy state and are fixed in their positions against the drag of the flow.

be applied for droplets which are squeezed inside the microchannel only. Spherical droplets not touching the channel wall are not trapped using this principle. In that sense this method can also be applied for droplet sorting based on their size. The principle behind is based on the circumstance that squeezed droplets are sensitive to depth modulation of the micro channel. Each interface between two liquids has a surface energy ϵ_γ which is defined as

$$\epsilon_\gamma = \gamma \cdot A$$

where γ is the interfacial tension and A the area of the interface. The lowest surface energy is obtained for fully spherical droplets. The more the geometry deviates from spherical the higher the surface energy. As anywhere in nature, the lowest energy state is the preferred one. Therefore, droplets tend to reach spherical shape. Squeezed droplets are forced to remain in a higher surface energy level. The integrated spatially confined expansions of the channel allow the droplets to stay in states of lower surface energy. As long as the strength of the trap due to the lower surface energy is higher than the drag force of the flow the droplets remain trapped. The critical value for the flow velocity is defined once the drag force reaches the strength of the trap. This principle allows passive trapping of droplets at positions defined by the geometry. Additionally, the droplets can easily be released again by

simply increasing the flow velocity above the critical value.

Another principle for droplet trapping integrates electrodes close to the microfluidic channel [25]. A schematic of the working principle is given in Fig. 2.5. Under the impact of an electric field, emulsions are subjected to a

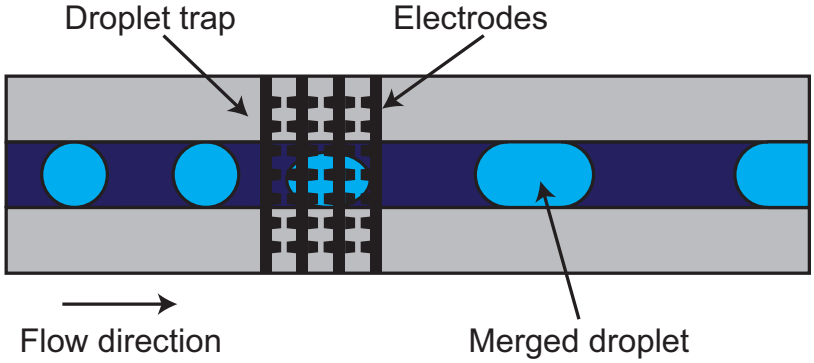

Figure 2.5: A micro channel with integrated electrodes working as a droplet trap. Droplets are decelerated and deformed in the presence of an electric field. As a consequence two succeeding droplets are merged.

body force which is given by

$$F_E = \rho_f E - \frac{1}{2} E^2 \nabla \epsilon + \frac{1}{2} \nabla \left[\rho_m \left(\frac{\partial \epsilon}{\partial \rho_m} \right)_T E^2 \right]$$

where ρ_f is the local free charge density, E the electric field strength, ϵ the permittivity, ρ_m the mass density, and T the temperature. The three terms are attributed to the coulomb, the dielectric, and the electrostriction force, respectively. In the case of incompressible fluids the last term can be neglected. If a droplet is passing through the electric field, it experiences a body force which causes the droplet to be trapped and deformed. As the deformed droplet does not occupy the entire channel anymore, the continuous phase can easily flow by until a second droplet approaches. The electric field induces coalescence and the two droplets get merged inside the electric field. Due to the doubled volume, the newly formed droplet experiences a higher drag force. Once the drag force exceeds the force of the electric field, the droplet is pushed out the trap and continues flowing through the channel. Depending on the channel geometry, the electrode placement, the strength of the electric field, and the flow velocity, droplets of any shape can be trapped and merged using this principle.

These and other techniques provide droplet microfluidics with an enormous flexibility. Droplets can be steered and manipulated through a complex microfluidic system allowing various tasks to be performed. More detailed information about single phase and two phase fluidic systems can be

found in [26–31].

2.2 Optical aspects

Optical systems are implemented for a variety of applications especially in sensing systems. Compared to other principles optics provide a contact-free analysis of the samples. Furthermore, it is widely harmless to the analytes and can easily be combined with other, for example, electrical principles without any kind of negative interaction. In the following section, the heart for such systems, the principle of light guiding, is introduced.

2.2.1 Total internal reflection

The phenomenon behind any kind of light guiding is total internal reflection. In brief, reflection of light at a given interface without any light transmission to the other side of the interface. If total internal reflection occurs inside a waveguide light losses are at the very minimum.

At the interface of two dielectric media a plane wave is given by

$$E_{i,r,t} = E_{0i,r,t} \cdot e^{-j(k_{||i,r,t} \cdot x - \omega t)}$$

where E stands for the electric field, $k_{||}$ for the projection of the wave vector on the interface, and x and t for place and time, respectively. The indices i, r, t stand for incident, reflected, and transmitted. At the interface the phase angle of all three waves has to be identical,

$$k_{||i} = k_{||r} = k_{||t}.$$

The magnitude of the phase vector is defined as

$$|k_{||i,r,t}| = n_{i,r,t} \cdot k_0$$

where n stands for the refractive index and k_0 for the amplitude of the wave vector in vacuum. Fig. 2.6 shows the phase angle diagram for total internal reflection. For total internal reflection, the refractive index of the material on the incident side (n_i) has to be bigger than the refractive index of the material on the transmission side (n_t). If now the incident angle θ_i exceeds the critical angle θ_{crit}, the projection of the incident wave vector is bigger than the magnitude of the transmitted one. In that case no free plane wave exists

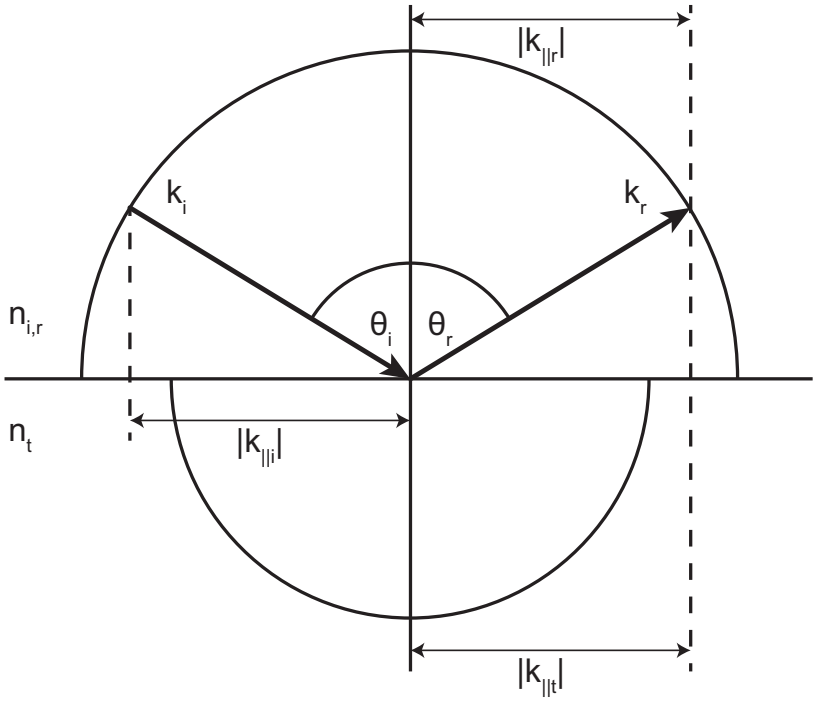

Figure 2.6: Phase angle diagram at total internal reflection.

in the medium on the transmission side and the incident wave experiences total internal reflection. The critical angle is defined as

$$\theta_{crit} = arcsin\frac{n_t}{n_i}.$$

In cases of $\theta_i > \theta_{crit}$ the only losses of light can be attributed to the evanescent field. Fig. 2.7 schematically depicts the propagation of the first mode of an electric field in a waveguide. The shape of the mode propagating along the illustrated waveguide follows a Gaussian distribution. At both contact regions (core-cladding) the mode rapidly decays inside the cladding material. The intensity escaping the core is the evanescent field. Although exploited for certain sensing devices, the evanescent field is of disadvantage for waveguiding applications. At the core-cladding boundary the magnitude of the electric field is E_0. Inside the cladding material the electric field decays rapidly depending on the refractive indices of the applied materials (Fig. 2.8). The penetration depth d_p of the evanescent field is defined at the point where the electric field reaches E_0/e. It can be calculated using

$$d_p = \frac{\lambda}{2\pi\sqrt{n_i^2 sin^2\theta_i - n_t^2}}$$

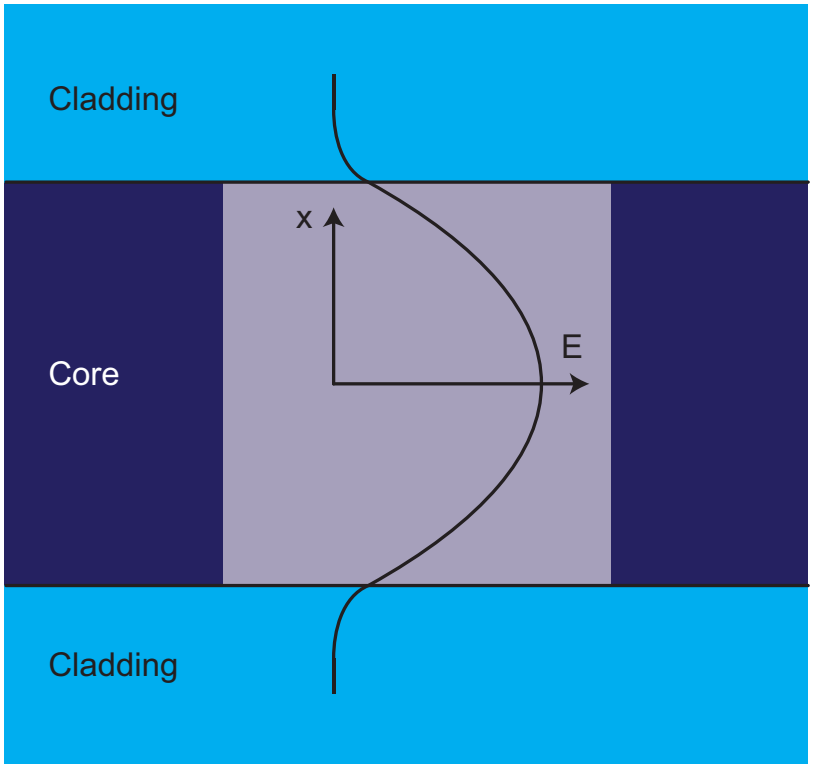

Figure 2.7: Propagation of the first mode of an electric field in a waveguide.

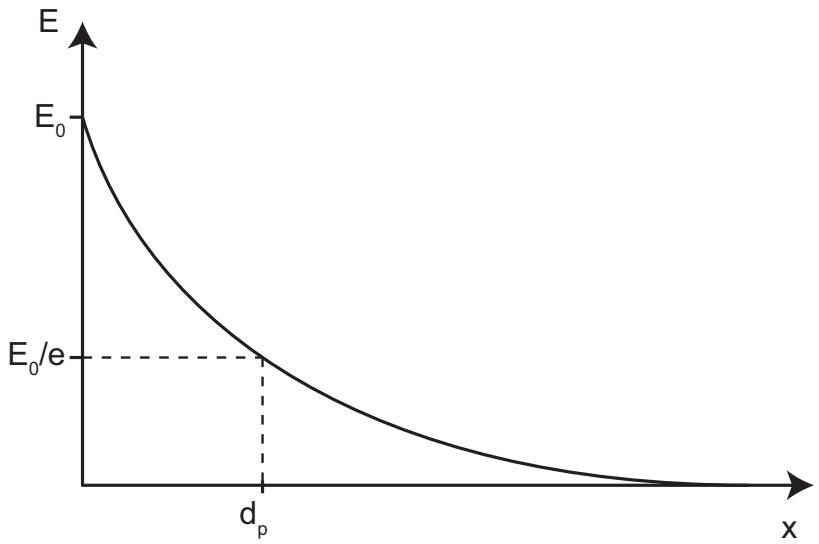

Figure 2.8: Decay of the evanescent field in the cladding material. The penetration depth depends on the refractive indices of core and cladding.

where λ is the operation wavelength. Close to the critical angle the evanescent field shows its maximum penetration depth and hence high optical losses. It decays rapidly at higher incident angles.

2.2.2 Planar waveguide

A planar waveguide exploits total internal reflection inside a core layer to confine light in two dimensions. The core layer with a higher refractive index is sandwiched between two cladding layers of lower refractive index. Fig. 2.9 illustrates the working principle. Light is coupled into the core of

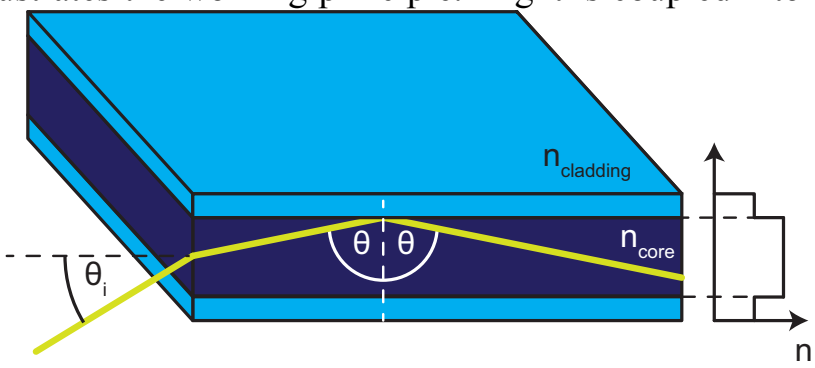

Figure 2.9: Schematic of a planar waveguide. The core layer is sandwiched between two cladding layers. Light is confined within the core layer by total internal reflection.

the planar waveguide. If light rays hit the core-cladding interface in an angle above the critical angle, they are totally reflected and confined within the core layer. The planar waveguide can couple in a range of incident angles which are defined by the numerical aperture (NA)

$$NA = \frac{1}{n_0} \cdot n_{core} \cdot \sqrt{1 - sin^2\theta_{crit}} = \frac{1}{n_0}\sqrt{n_{core}^2 - n_{cladding}^2}$$

where n_0 is the refractive index of the surrounding material (in this case air with n of 1). As long as $\theta_i < NA$ the condition for total internal reflection is fulfilled and light can be guided inside the waveguide. More detailed information about those optical effects can be found in [32, 33].

2.3 Optofluidics

Optofluidics is a new field of research which has emerged within the last decade. Having its roots in microfluidics and optics it has become much more than just a combination of those fields. In optofluidic systems liquids take over the functional role of optical elements. On the macro scale one could think of an optical bench with different elements such as light sources, mirrors, optical filters, or beam splitters with one or more of those elements replaced by liquids. Let's have a look at a simple example. Fig. 2.10 shows

the light absorption spectrum of a widely applied liquid, DI water, from the UV to the IR region. As can be seen DI water shows low absorbance

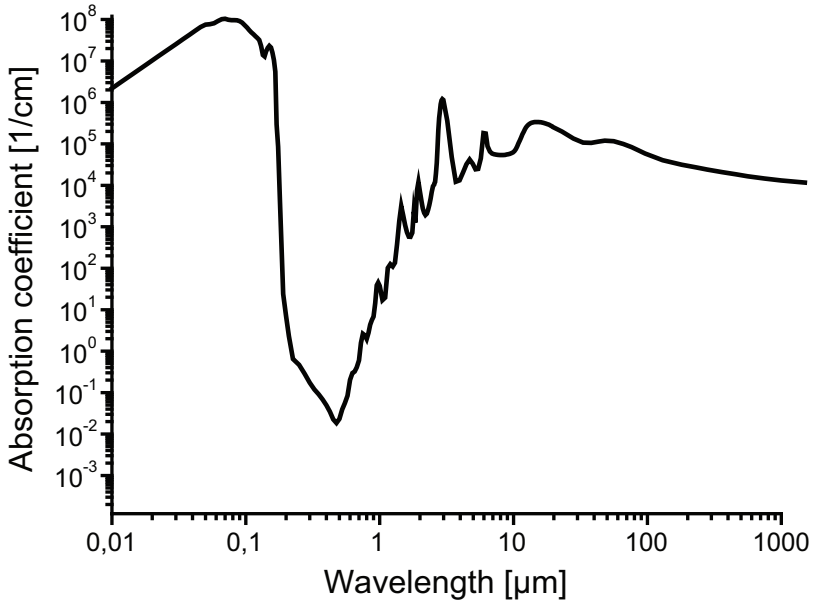

Figure 2.10: Absorption coefficient of DI water at room temperature from 10 nm to 1 mm wavelength [34].

around the visible wavelength region (0.39 to 0.7 µm). Shorter as well as longer wavelengths on the other side are highly absorbed. Placing a sufficiently thick layer of DI water in the optical path of a light beam works as a bandpass filter with a center wavelength right in the visible range. Different liquids show different absorption spectra. By placing multiple liquid filters in series, the spectra can be tuned such that only a certain range of wavelengths can be transmitted. Now taking this assembly and placing it on-chip results in an optofluidic bandpass filter. Of course bandpass filters can be realized with solid materials as well. This example is meant as an illustration of how a basic optofluidic system could look like. Anyway, one huge benefit in using a liquid filter could be the exchangeability of liquids. Replacing one liquid by another liquid with different absorption spectrum allows to adjust the overall filter characteristic in-line. For solid realizations this is not possible. The filter spectrum is defined by the materials. A change in this spectrum requires a complete redesign of the system.

Exploiting the light absorption characteristics of liquids is one of the basic building blocks for optofluidic setups. Often high transmission of light at the operating wavelength is a pre-requirement. In advanced optofluidic systems usually more than one physical property of the employed liquids need to be considered. The implementation of liquids with low light ab-

sorbance at the operating wavelength and carefully chosen refractive indices is a typical application. Here, one descriptive example are L2-waveguides (Fig. 2.11). The working principle of L2-waveguides and planar waveguides is basically the same. In both, light is confined in a region of high refractive index sandwiched between regions of lower one. In the case of L2-waveguides, those regions are formed by streams of liquids in a microchannel. The core liquid is chosen with a higher refractive index as the cladding. Two commonly chosen fluids are DI water (n of 1.33) and a 5 M $CaCl_2$ solution (n of 1.44). The numerical aperture of L2-waveguides built up with those two liquids is

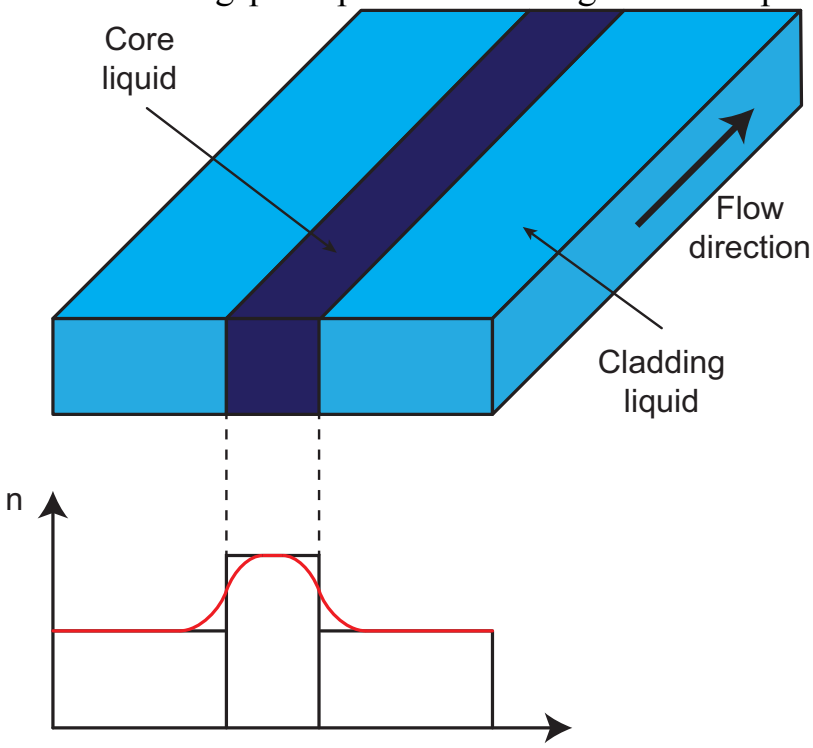

Figure 2.11: Schematic of an L2-waveguide. The core stream with an increased refractive index is sandwiched between to streams of cladding liquid with lower index. Neglecting diffusion, the profile of the refractive index looks like a step. Due to diffusion effects, which strongly depend on the applied flow velocities, the profile gets smoothened.

$$NA = \frac{1}{n_0} \cdot \sqrt{n_{core}^2 - n_{cladding}^2} = 0.552 \tag{2.1}$$

where n_0, n_{core}, and $n_{cladding}$ are the refractive indices of the surrounding material (usually the chip material, here assumed as air), the core, and the cladding liquid, respectively. One effect which substantially influences the functionality of L2-waveguides is diffusion. In regular planar waveguides

the profile of the refractive index looks like a step, high in the core and low in the cladding region. Diffusion prohibits such a clear separation of core and cladding region. Depending on the flow velocity, the liquids diffuse into each other at the contact region resulting in a smoothened profile of the refractive index. This profile resembles the profile of graded index (GRIN) waveguides [35] which provides superior waveguiding performance. For L2-waveguides a permanent flow of liquids is necessary. At a steady state the liquids would fully diffuse into each other and preclude any waveguiding. This automatically introduces a permanent consumption of liquids.

L2-waveguides are just one application of optofluidics. Liquid lenses, liquid based laser systems as well as various analysis devices are a few other possible applications.

Chapter 3
Micro-fabrication

This chapter deals with the micro-fabrication technologies which are applied for the manufacturing of the investigated devices presented in the following chapters. Two basically different fabrication techniques are presented. Bulk micromachining, which is based on selective etching of the substrate material and surface micromachining where multiple layers of various materials are deposited on the substrate material.

Parts of the work presented in this chapter have been published in [36–42].

3.1 Bulk micromachining

Bulk micromachining is a widely applied technique especially for the realization of MEMS (microelectromechanical systems). The standard base material for such kind of devices, the bulk material, is a silicon wafer. Anyway bulk micromachining itself is not limited to silicon substrates. Borosilicate glass wafers, for example, can be processed using similar techniques as well. The chosen substrate materials are then structured using different etching processes. Therefore, the structures are first patterned using etching masks. Those masks can be e.g. silicon dioxide or silicon nitride layers. After the etching process of the bulk material has been finished, the etching masks are removed again.

3.1.1 Silicon

Silicon is the most widely used material in micro-fabrication technologies. Especially for the design of integrated circuits silicon is the material of choice. Therefore, also the technologies necessary for the machining of silicon are well studied and fully mature. In Fig. 3.1 a standard one-sided polished silicon wafer is shown. If pure silicon is exposed to oxygen, oxida-

tion starts immediately. Therefore, the top as well as the bottom side of the wafer are covered with a silicon dioxide (250 nm), silicon nitride (80 nm) stack. This stack is then often used as an etching mask. The crystal orientation of the wafer is <100> and the diameter is 100 mm. Although possible

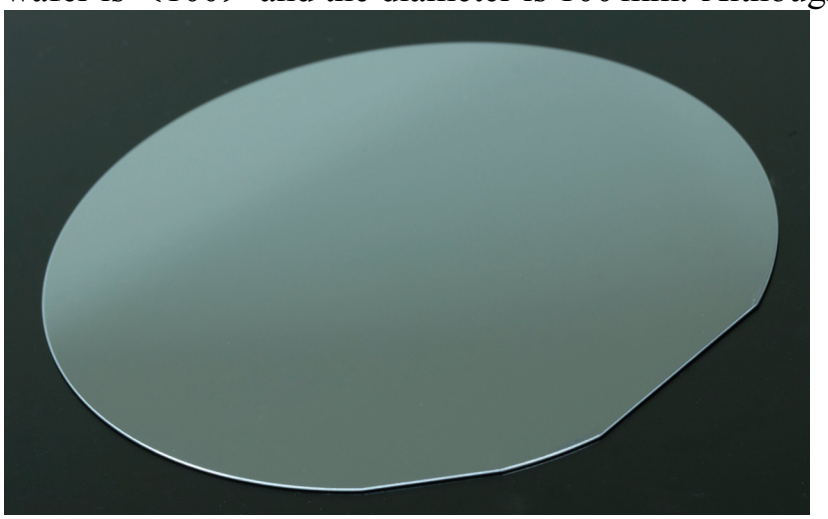

Figure 3.1: Standard one-sided-polished <100>-silicon wafer. The Diameter of the wafer is 100 mm.

from the technology point of view, for the devices presented in the following chapters silicon is used as a carrier material only. The microfluidic and optical elements are not directly written in silicon but structured in layers deposited on the silicon substrate. The reasons are the relatively long fabrication time and the optical behavior of silicon in the visible range. Etching deep trenches with either sloped or vertical channel walls in bulk silicon is an extremely time consuming process. Depending on the applied method, etching rates of approx. 1.4 µm/min and 0.5 µm/min can be achieved for wet chemical etching and plasma activated dry etching, respectively [43]. The typical height of microfluidic channels is in the range of 100 µm resulting in processing times of more than one hour just for the etching step alone. Together with all the essential pre- and post processing steps, it is hardly possible to manually fabricate devices within a single working day. This is of huge disadvantage during the development state of a device. Here, a short design to device time is required.

Another limitation of silicon as the device material for optofluidic applications is its low optical transmittance in the visible wavelength region. Fig. 3.2 shows the absorption spectrum of intrinsic silicon. Silicon is nearly opaque for wavelengths below 1 µm. Already a layer of 1 mm inhibits visible light transmission without using a high power light source. However, the absorption characteristic changes with increasing wavelength. Silicon is

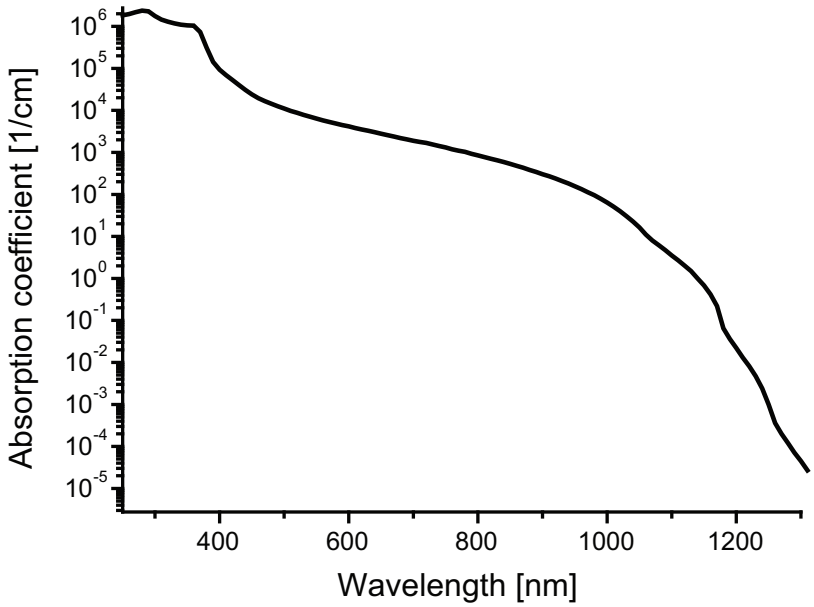

Figure 3.2: Absorption spectrum of intrinsic silicon at room temperature [44].

getting transparent for long wavelengths starting in the near IR region. This enables optical transmission and hence optical analyses on devices fabricated in silicon only. Nevertheless, the use of IR light implies two major drawbacks. First of all, IR light is not visible for the human eye. Special detectors or an IR-microscope are necessary for the visualization. Furthermore, the optical absorption of water drastically increases with increasing wavelength. For analyses or applications dealing with aqueous solutions, which is the widely applied standard, IR light is therefore not suitable and precludes the use of silicon as the device material.

As already mentioned, silicon can be applied as the carrier material for optofluidic systems. On such devices, the fluidic connections into the microfluidic channels are placed on the bottom of the chip. Therefore, the silicon substrates have to be fully etched through. Two basically different approaches are possible for the etching process: Wet and dry etching. Both, are anisotropic etching processes. Deep reactive-ion etching (DRIE) is a commonly applied dry etching process. Ions are accelerated perpendicularly towards the silicon surface. Those ions remove exposed silicon atoms from the surface. In that way trenches with upright channel walls can be achieved. Compared to wet chemical etching DRIE is a laborious technique. Furthermore, for fluidic inlets vertical channel walls are not necessary. Therefore, wet chemical etching with potassium hydroxide (KOH) as the etchant is chosen for the perforation of the silicon wafer. This tech-

nique is an anisotropic process as well. The etching rate strongly depends on the crystal orientation. In the <100> direction the etching rate is much higher than in the <111> direction. This results in sloped channel walls (Fig. 3.3).

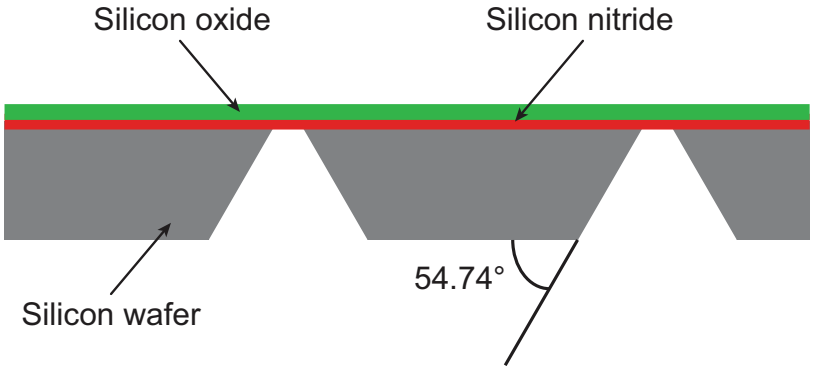

Figure 3.3: Wet chemical etching of a <100>-silicon wafer with a potassium hydroxide (KOH) dilution. The anisotropic etching process results in sloped channel walls with an angle of 54.74 ° with respect to the wafer surface.

An angle of 54.74 ° with respect to the wafer surface is obtained. Diluted KOH is the most widely applied liquid etchant for silicon. The etching process includes following main steps:

- Spin coating of standard photo resist (AZ6612) onto the bottom side of the whole wafer with a rotation speed of 3000 rotations per minute.
- Baking of the photo resist on a hot-plate with 107 ° for 5 min.
- Exposure of the resist through the desired mask for 20 s.
- Development of the resist by spraying of standard developer AZ826 for 20 s onto the wafer.
- Plasma etching of the silicon dioxide (250 nm), silicon nitride (80 nm) stack on the bottom side in the parallel plate RIE equipment (STS 320 PC).
- Stripping of the remaining photo resist.
- Etching of the holes with a 40% KOH solution (6 h 20 min).
- The silicon dioxide, silicon nitride stack on top of the wafer serves as an etch-stop.

- Removal of the remaining silicon dioxide, silicon nitride stack on the bottom side in the parallel plate RIE equipment (STS 320 PC).

After the etching process, the silicon dioxide, silicon nitride stack remains, covering the etched holes. These layers are essential for later steps such as spin coating of SU-8 on the perforated silicon wafer. Those films can be removed at a later stage by ultrasonic cleaning.

3.1.2 Borosilicate glass

The main constituents of borosilicate glass are silicon dioxide and boron oxide. It is widely applied in conventional optics for high performance elements such as macro-lenses. Depending on the exact composition, the index of refraction of this type of glass is around 1.52. Borosilicate glass provides full transparency in the visible range in contrast to silicon which is highly opaque. This is of huge advantage for optical applications. Fig. 3.4 shows the transmission spectrum of a common type of borosilicate glass with a thickness of 10 mm. The transmission rate is more than 90 % all over the

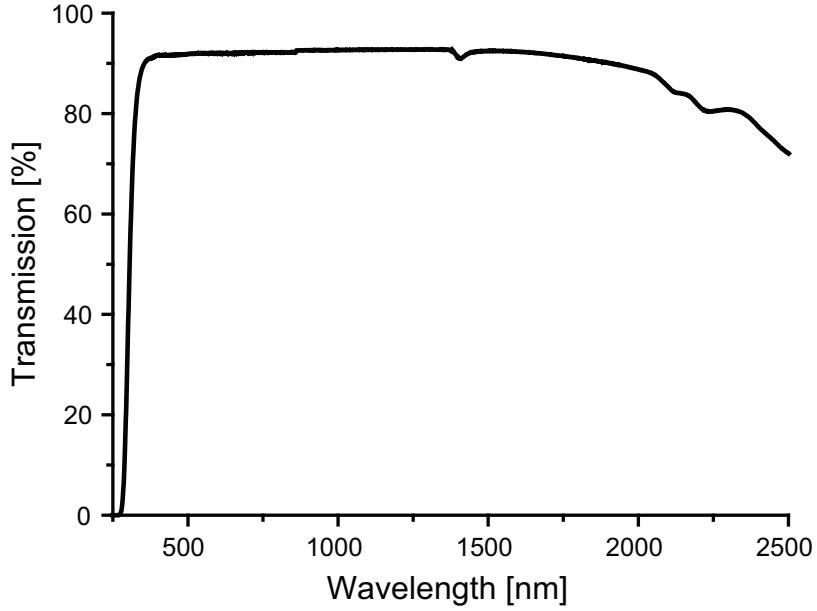

Figure 3.4: Transmission spectrum of uncoated N-BK7, a borosilicate glass, with a thickness of 10 mm [45].

visible wavelengths and in the beginning of the near IR region. At wavelengths exceeding 2 µm the transmittance starts to drop rapidly. For applications operation with longer wavelengths other materials have to be chosen (e.g. calcium fluoride glasses or silicon). Borosilicate fully satisfies the major requirement for optofluidic systems, meaning low optical absorbance

over a wide range of wavelengths. Unfortunately, the processing of borosilicate glass is far from being trivial. One possible way of structuring is micro milling. With this technology simple channel structures can be directly written in a glass substrate. For micro-optical applications the limitation in feature size and smoothness of the channel walls is here of disadvantage. Another way of glass processing is wet chemical etching using hydrofluoric acid (HF). Etching glass with HF is an isotropic process. The cross-section of obtained channel structures is not rectangular but semicircular. This significantly cuts the applicability of this technology. Furthermore, HF is a highly dangerous poison and has to be handled with great care. Considering those challenges, borosilicate glass is not applied as device material for the optical and microfluidic elements.

Anyway, borosilicate is used as substrate material for successive surface micromachining steps (e.g. deposition of SU-8). In Fig. 3.5 an application of an SU-8 device on a borosilicate glass substrate is shown. Here, a

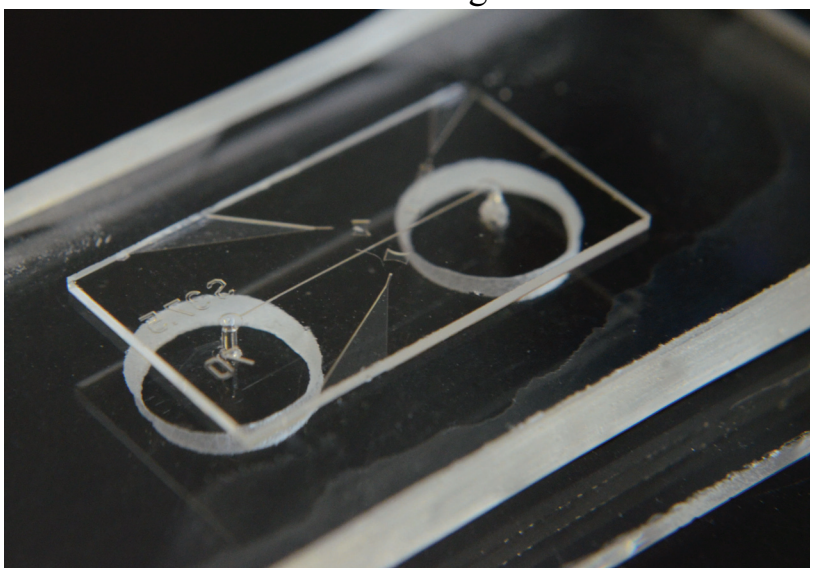

Figure 3.5: Application of borosilicate glass for device fabrication.

borosilicate glass wafer is used as substrate. After SU-8 deposition, exposure, and development the devices are diced in size and bonded on a PDMS slab. The other side of the PDMS slab is bonded to a borosilicate glass microscope slide. This microscope slide works as a carrier material and simplifies chip handling. The fluidic connections are placed on the bottom of the chip assembly. Therefore, the borosilicate glass slide is perforated using a sandblasting system.

3.2 Surface micromachining

In surface micromachining, elements are structured on a substrate by deposition and selective removal of additional layers of material. Compared to bulk micromachining the substrate material is not affected at all. Both the substrate and the deposited layers can be selected out of a variety of materials. A commonly used substrate material is silicon on a wafer level. Glass or polyester wafers are other examples for possible substrates. Different types of resists are typically chosen for the layer material. Here SU-8 is a prominent example.

3.2.1 SU-8

SU-8 (Microchem, USA) is a widely applied photoresist for bulk as well as for surface micromachining [46]. In bulk micromachining it is used as a mask for successive etching steps whereas in surface micromachining it is directly used as functional layer. In the course of this work, SU-8 is directly used as layer material. Fig. 3.6 shows a cross-section of a typical device constitution. A perforated silicon wafer is used as substrate. The SU-8

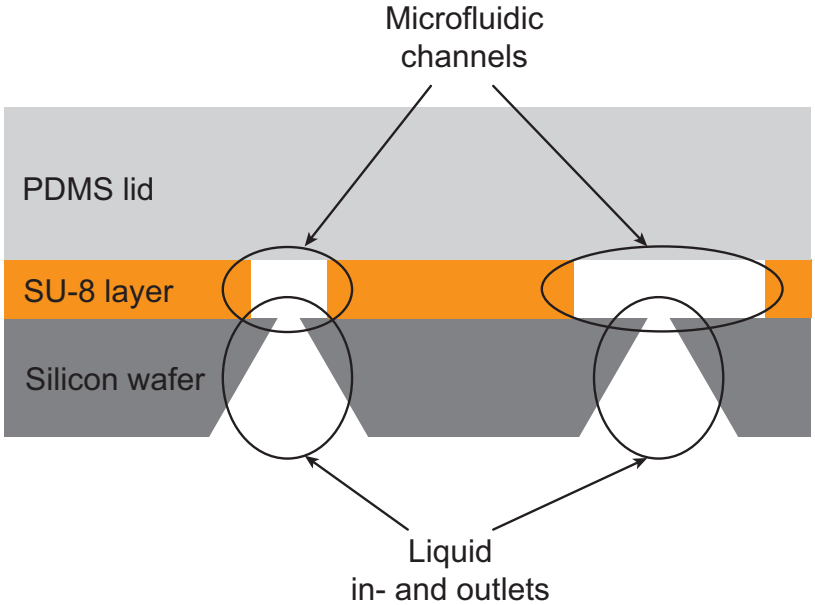

Figure 3.6: Cross-section of SU-8 structures applied on a silicon substrate. A PDMS layer is clamped on top of the SU-8 layer to seal the microfluidic channels.

layer (typical thickness of 100 µm) is deposited on top. To finally seal the microfluidic channels a PDMS layer is clamped on the SU-8 layer.

SU-8 is a negative photoresist. An unexposed negative photoresist is

fully soluble in the developer. It must be exposed to withstand the immersion. During the exposure to UV-light it becomes polymerized and with that resistant to the developer. On the contrary, an unexposed positive photoresist is not attacked during the development and must be exposed to increase its solubility in the developer. Both types of resist have their unique advantages. In general, positive photoresists allow smaller feature sizes to be fabricated. On the other hand, negative photoresists exhibit better adhesion to a variety of substrate materials including silicon and glass. Furthermore, they are more cost effective in both, purchasing as well as processing which makes them attractive for prototyping. The main process steps for the fabrication of SU-8 layers with a thickness of 100 µm are as following:

- Pre-bake of the silicon wafer on a hot plate at 120 °C for 2 min.
- Spin coating of an adhesion promoter (Ti-prime) and curing on a hot plate at 120 °C for 1 min.
- Spin-coating of SU-8 2100 at 3000 rpm for 30 seconds.
- Soft bake in an oven at 95 °C for 120 min.
- Exposure to UV-light for 130 s.
- Post exposure bake on a hot plate at 65 °C for 5 min and 95 °C for 10 min.
- Immersion in SU-8 developer for approx. 15 min.

Fabricated SU-8 structures are chemically inert and provide a high degree of biocompatibility. The material is hydrophobic and transparent at visible wavelengths. At 530 nm its index of refraction is approx. 1.59 [47]. For the optofluidic sensor applications presented in the following chapters the relatively low index of refraction compared to other materials (e.g. silicon, index of refraction at 530 nm of approx. 4.2 [48]) is of advantage. The closer the index of the device material to the index of the liquid analytes (aqueous solutions with an index of 1.3 to 1.5) the higher is the achievable sensitivity of the system.

Fig. 3.7 shows SEM images of a structured SU-8 layer with a thickness of 100 µm. On the left the achievable structure sizes are highlighted. The picture on the right shows a fiber groove used for clamping peripheral glass fibers onto the chip. With SU-8 aspect ratios (the ratio of element height to

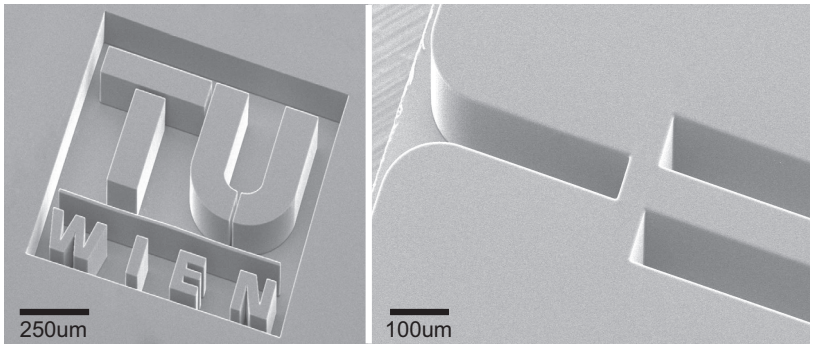

Figure 3.7: SEM images of device structures fabricated in SU-8.

element width) of up to 20 can be reached. This satisfies the requirements for most optofluidic as well as for a wide range of purely microfluidic applications. Compared to rapid prototyping techniques the achievable design to device time for SU-8 devices is still rather long. The obtained structure size and channel wall smoothness on the other hand are superior. The optimal trade-off between those two parameters has to be found for the given requirements.

3.2.2 Dry resist

One way of rapid prototyping is based on dry film lamination. The huge advantage of this technology is the extremely easy fabrication process. Layers of the desired resist are simply laminated on the given substrate. For structure sizes in the range of 100 µm, the lamination process can even be performed on conventional office laminators. To achieve smaller structure sizes, the lamination should be performed on high precision laminators in a clean room setting. Both, the applied substrate and the dry resist can be chosen individually and hence be optimized for the given specifications. In the following sections negative dry film resist, Ordyl SY330 and Ordyl SY317 having a thickness of 30 µm and 17 µm, respectively, are used. This dry resist is resistant to a wide range of chemicals. Furthermore, swelling is much reduced compared to other materials (e.g. PDMS). The dry resist structures can directly be used to form channels for microfluidic applications. The employed resist is fairly transparent in the visible light range. Fig. 3.8 shows the measured transmission of a 10 µm thick layer of Ordyl after the development. In the visible range a transmission of approx. 85 % is evident. Compared to silicon, which is fully opaque in the visible wavelength region, this resist can be employed for optofluidic applications operating with

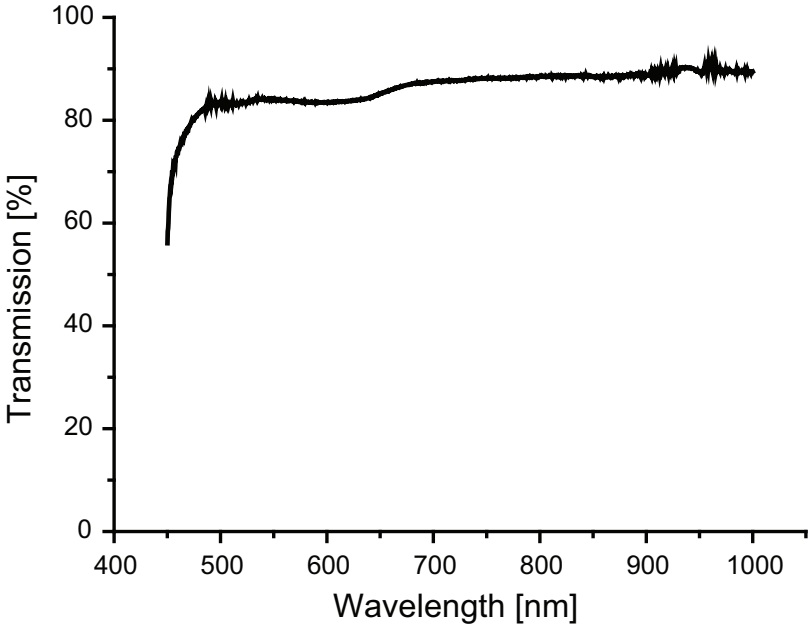

Figure 3.8: Transmission of a 10 µm thick layer of Ordyl after the development. Starting from 500 nm up to 1000 nm it shows a transmission rate of approx. 85 %.

visible light. Anyway, the loss of optical power in the dry resist should be accounted for. The input power must be set to a higher value accordingly. For proof of concept studies this is of minor relevance. In a final application, on the other hand, one should consider other materials with higher transmission rates at the wavelengths of interest. Another pre-requirement for microfluidic applications is impermeability to fluids. The chosen dry resist was tested for good sealing. Additionally, a gas test at a pressure of 2.5 bar was performed. During the entire test procedure the resist did not show any leakage or degeneration. The later-on presented optofluidic sensing devices are meant for biological or medical purposes. For this reason, the employed materials must show a high degree of biocompatibility. The materials must possess the quality of not having toxic or injurious effects on biological systems. In order to test the biocompatibility of the material living cells were cultured on an autoclaved piece of dry resist for a duration of five days. In comparison to a control culture, the cells behaved identical and no difference in the proliferation curves was detected [49].

As already mentioned, the substrate can be chosen out of a variety of materials. Examples are silicon, polyesters, and glasses. In the following the six main fabrication steps with a flexible polyester foil as substrate are described (Fig. 3.9). For other substrate materials the main steps stay the

same. The concrete parameters, such as temperature and durations, have to be fine tuned to reach optimal performance.

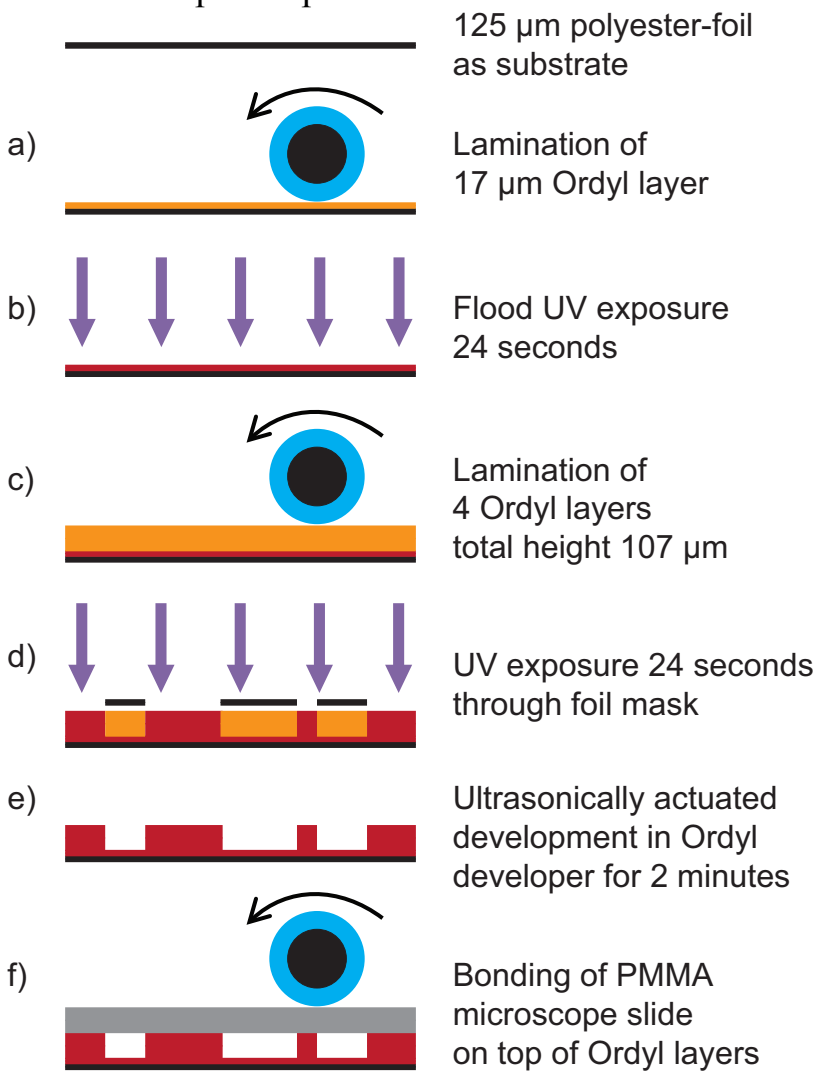

Figure 3.9: Process steps for the fabrication of dry resist micro-chips divided into 6 main steps; (**a**) A 17 µm thick resist layer is laminated onto a 125 µm polyester foil, (**b**) flood UV exposure of the 17 µm thick layer for 24 seconds to improve the adhesion of following resists, (**c**) consecutive lamination of four resist layers (one 17 µm and three 30 µm) to reach the final structure height of 107 µm, (**d**) UV exposure (24 s) through a high resolution printed foil mask (64000 dpi) to structure the elements, (**e**) after the post exposure bake (5 min, 70 °C), ultrasonically actuated development of the structures for 2 min, (**f**) bonding of a PMMA microscope slide on top of the structured resist (providing drilled in- and outlets) for sealing of the microfluidic channels by lamination.

A 125 µm thick polyester foil is used as a substrate for the devices. The surface of the substrate material must be clean and free of any contaminants for a good and permanent bonding to the dry resist. For this reason, the

polyester foil is cleaned with ethanol prior to processing. The dry resists are covered with a thin plastic foil on both sides. This foil ensures protection of the resist during handling and inhibits unintended bonding of the resist. Before lamination, one protective foil is removed. The dry resist film is then carefully aligned onto the previously cleaned substrate. Attention has to be paid to avoid air gaps between resist and substrate. At first, a 17 µm thick resist layer is laminated onto the polyester foil (Fig. 3.9a). The top of the dry resist must still be covered with the protective foil to prevent contamination of the laminator. After lamination, the first layer is flood exposed to UV light for 24 s (Fig. 3.9b). Especially if using contact alignment for the exposure, the protective foil on top is essential to preclude bonding of the resist onto the instrument. The 17 µm thick resist layer has two functionalities. At first, it improves the bonding of following layers allowing for the realization of higher aspect ratios. The adhesion between two layers of dry resist is superior to the adhesion of dry resist to substrate material. In that sense, the technology is widely independent from the underlying substrate material. Secondly, the microfluidic channels are covered with the same material on the channel wall as well as the channel bottom. Especially for biocompatibility reasons this is of huge desire since unwanted reactions can be suppressed to the biggest extent. If necessary, the channel top can be treated in a similar way. In that sense, the sample solutions in the microfluidic channels are in contact with dry resist only. In the next step the second protective foil is pulled-off as well and multiple resist layers are laminated (total thickness of 107 µm) on top of the 17 µm layer (Fig. 3.9c). The procedure is the same as for the first resist layer. After removal of one protective foil the dry resist is aligned onto the substrate and passed through the laminator. Then the second protective foil is pulled-off before the next layer of resist is aligned and laminated. All the lamination steps are performed at a temperature of approx. 90 °C. The optimum temperature must be defined depending on the properties of the employed instrument. One parameter which has a significant impact on the ideal temperature is the lamination speed. A lower speed asks for a lower temperature to prevent thermal damage such as excessive bending of the substrate as well as the dry resist foil. As the next step the microfluidic and optical elements are structured into the 107 µm thick resist layer using a high-resolution printed foil mask (64000 dpi; UV exposure for 24 s; Fig. 3.9d). After a post exposure bake for hardening of the dry resist (5 min at 70 °C), the development is performed under ultrasonic agitation for 2 min in resist developer (Fig. 3.9e). Depending on

the strength of the ultrasonic instrument, the necessary time for the development can be adapted. Subsequently, the individual devices can be cut in size using conventional scissors. To close the microfluidic structures a PMMA microscope slide (index of refraction approx. 1.49 [50]) is bonded on top of the structures by lamination (Fig. 3.9f). This PMMA slide is equipped with holes for the liquid in- and outlets. A conventional drilling machine is used for drilling the in- and outlet holes with typical diameters of 1 mm. As already indicated, the PMMA cover can be coated with a dry resist layer for biocompatibility reasons.

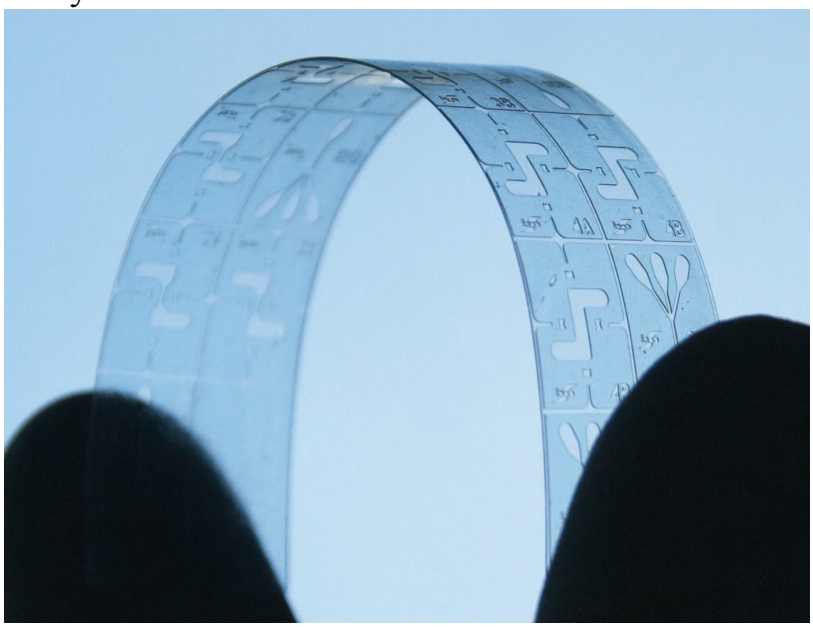

Figure 3.10: Photograph of fabricated devices before cutting and bonding. The microfluidic and optical elements are structured in dry resist. A polyester foil is used as substrate.

Fig. 3.10 shows an image of the finally obtained devices before cutting. The shape of the polyester foil in this case is rectangular. As can be seen the polyester foil provides the device with an enormous flexibility [51–53]. The substrate with the structured resist on top can be bended in any direction. This further increases the applicability of this technology. Care must be taken only to avoid cracking of the resist structures. In fact, after the development process the surface of the resist can be covered with micro-cracks anyway. The degree of surface roughness strongly depends on the specific development parameters. If a smooth surface is essential, an annealing step can be performed on the developed structures. For this reason, the fabricated structures are placed on a hot plate at approx. 90 °C for 5 to 10 min. During annealing, the micro-cracks can be removed to the biggest extend

and a smooth resist surface is obtained.

Besides flexibility, the huge advantage when using a polyester foil as substrate is the easy cutting process. No dicing machine is necessary. The individual chips can be cut in size with conventional scissors. This speeds up the fabrication process dramatically. Furthermore, any perimeters (even circular ones) can be defined. After cutting, the individual devices can be bonded on other substrates to close any microfluidic elements. Again, the substrate can be chosen out of several materials. Fig.3.11a shows a single device bonded on a PMMA microscope slide. For bonding, the chip is

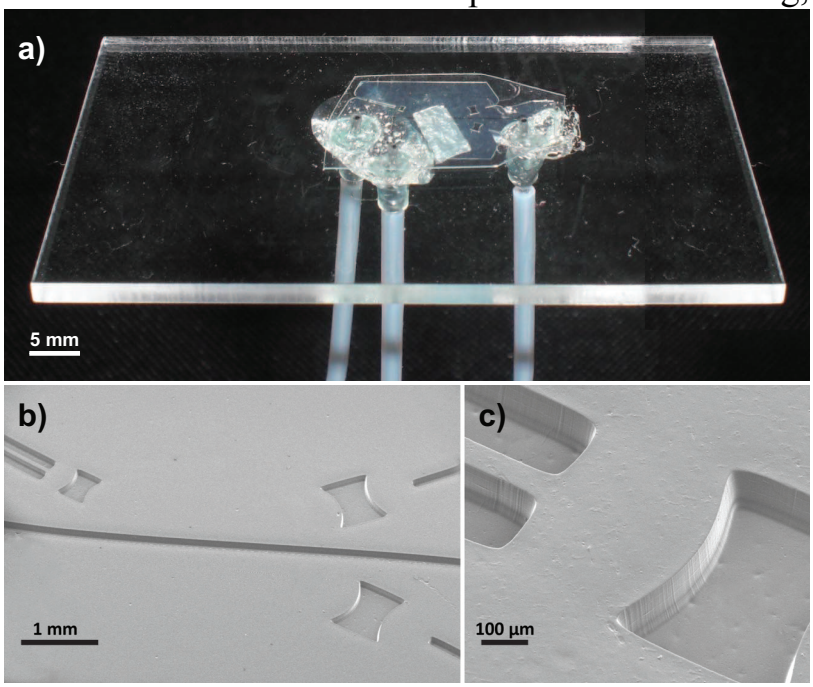

Figure 3.11: (a) Photograph of a dry resist device bonded on a microscope slide. The fluidic connections to the peripheral syringe pumps are managed by PTFE tubings. A highly reflective material (aluminum foil) is glued underneath the interrogation point to achieve a higher optical contrast in the microscope images. Scanning electron microscope images of **(b)** the optical interrogation point on-chip and **(c)** a magnification of an integrated air micro-lens.

simply laminated on a PMMA substrate. To improve bonding, this PMMA slide can be covered with a thin layer of dry resist as it is done for the bottom substrate as well. However, for optical applications this additional adhesion layers can be of disadvantage. These two layers on top and bottom can influence the waveguiding behavior of the system essentially. Integrated waveguides, for example, are meant to confine light inside a bar of dry resist in two dimensions. A continuous layer on two sides allows light rays to escape this bar and increase the optical loss. An optimum trade-off between

bonding strength and optical performance must be found. The PMMA slide on top can be provided with in- and outlet holes for fluidic connections. The slide can be as small as the single device itself. Anyway, for easier handling the use of a slide with dimensions of a few centimeters is preferable. In Fig.3.11b an SEM image of the interrogation region of an optofluidic sensing system is given. A straight microfluidic channel is placed in the middle. The integrated waveguide and the air micro-lenses are placed next to it. In Fig.3.11c a close up of the light input coupling region is shown. The air micro-lens is placed next to the ending of the integrated waveguide in a distance optimized for the numerical aperture of the waveguide.

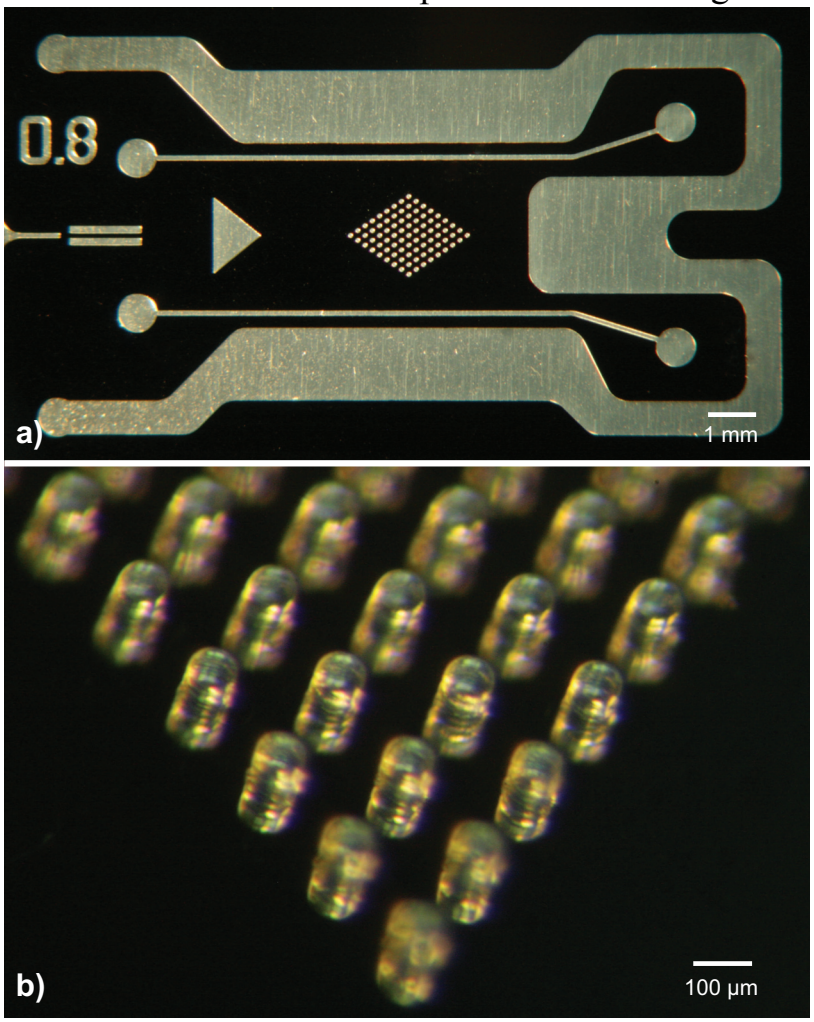

Figure 3.12: (a) Picture of one master device for PDMS replica fabricated in dry resist. **(b)** Close up view of achieved structure dimensions (aspect ratio approaching 2).

In Fig. 3.12 optical images of another device fabricated in dry resist is given. In a later step this device serves as a master for replica techniques.

Fig. 3.12a shows the entire chip comprising the light input coupling region on the left, a beam splitter and a deflection region in the middle, two microfluidic channels placed on both sides of the deflection region, and a broad microfluidic channel surrounding the entire design. Fig. 3.12b is a close up view of the deflection region and highlights the capability of this dry resist technology. Aspect ratios of up to 2 are feasible. Keeping in mind the design to device time of just a few hours this is truly remarkable.

3.3 Soft lithography - PDMS

The advantages of Polydimethylsiloxane (PDMS) are its low optical absorbance in the visible range (380 nm to 780 nm) and its refractive index [54–56]. Compared to most solid materials, the refractive index of PDMS (n of 1.41) is relatively low and close to the refractive index of DI water (n of 1.33). This adjacency is beneficial for optical analyses based on refractive index changes. Furthermore, PDMS is biocompatible which makes it attractive for applications in biological or medical studies. It is permeable to gases which can be exploited for the supply of e.g. oxygen to the analytes. Nevertheless, this permeability can be of disadvantage for certain applications as well. Although at very low rates, liquids can diffuse into PDMS which causes swelling of the device material. For long time analyses lasting more than a day this is a major drawback of PDMS. The investigated optofluidic sensing principles in this work are performed within just a few minutes. This circumstance justifies PDMS as an applicable device material.

PDMS devices are fabricated in a molding process. The liquid raw material is poured on a negative of the channel structures. After curing the PDMS device can simply be pulled-off the master device. This molding procedure can be repeated as many times as desired allowing low cost fabrication of devices at extremely high throughput. For the fabrication of the master devices, different substrate materials (such as, e.g. SU-8, silicon, dry resist) can be used. In the following paragraph the fabrication based on dry film resist is explained in detail. Two types of dry resist are used, Ordyl SY330 and Ordyl SY317 having a thickness of 30 µm and 17 µm, respectively (ElgaEurope, Italy). In addition to the dry resist fabrication process described in the preceding section, further process steps are essential (Fig. 3.13). After development of the dry resist (Fig. 3.13a), the finally obtained master devices are placed on a hot plate (approx. 60 °C) under

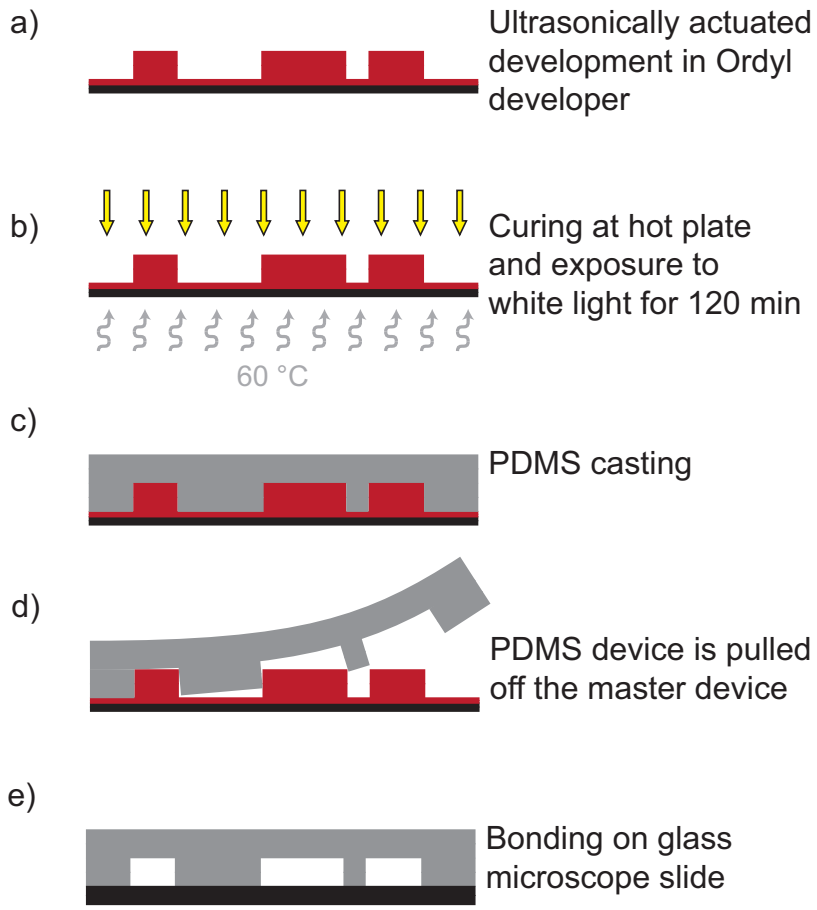

Figure 3.13: Additional fabrication steps for PDMS micro-chips starting from dry resist development. (**a**) Ultrasonically actuated development of the structures in dry resist developer, (**b**) curing of the master devices at 60 °C for 120 min under exposure to white light, (**c**) PDMS casting, and (**d**) final plasma activated bonding of the PDMS devices onto glass microscope slides.

exposure to white light (halogen lamp) for 120 min to allow curing of the resist (Fig. 3.13b). Those master devices are then used for PDMS casting (Fig. 3.13c). After curing of the PDMS the device can simply be pulled off the master device by hand (Fig. 3.13d). For sealing of the microfluidic channels the devices are plasma activated and irreversibly bonded on glass microscope slides (Fig. 3.13e). The use of dry resist as master device material and subsequent PDMS casting allows fabrication of devices within a few hours. This is of huge advantage especially for proof of concept studies. Fig. 3.14 shows an image of a PDMS master device. Here, a silicon wafer with a diameter of 100 mm serves as substrate for the dry resist structures. On the wafer 28 individual devices are visible. The shape of the master device is not limited to wafer size. In fact, any perimeter can be chosen.

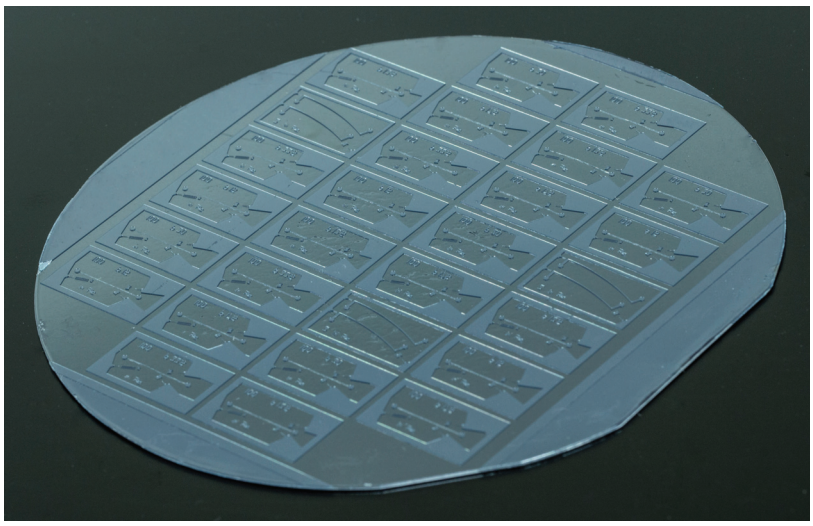

Figure 3.14: Photograph of a master device for PDMS replica. A layer of dry resist with a total thickness of 107 µm is structured on a 100 mm silicon wafer.

Depending on the arrangement of the individual devices, a space optimized substrate can be selected. A close-up few of a single PDMS device is shown in Fig. 3.15. A straight microfluidic channel is placed right in the middle

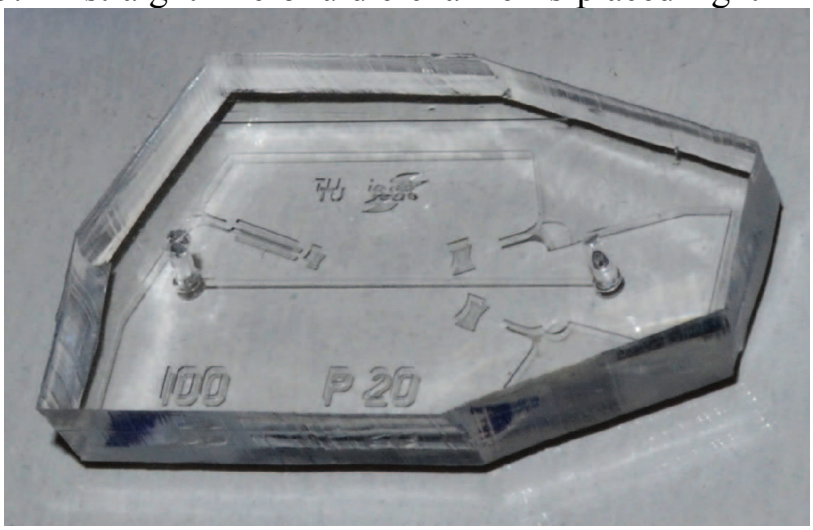

Figure 3.15: Photograph of a PDMS device fabricated using a dry resist master device.

of the device. On both sides of the channel a hole is punched through the PDMS for the liquid in- and outlet. Next to the channel three optical air micro-lenses and an integrated waveguide are visible. On the upper left corner of the chip as well as on both corners on the right, fiber grooves are integrated. Those fiber grooves allow external glass fibers to be clamped onto the device. For a final application the PDMS device is bonded to a

glass microscope slide to seal the microfluidic channels.

3.4 Peripheral connections

The sensor systems investigated in the following chapters are integrated directly on micro-devices. Nevertheless, a peripheral system is still needed for both, the fluidic as well as the optical part. In this section the connections employed for these reasons are introduced.

3.4.1 Fluidic system

For all the investigated microfluidic devices, external syringe pumps are employed as the fluidic pumping systems. Therefore, macro-tubings have to be connected to the chip, leading the fluids from the bulky syringe into the micro devices. A photograph of this fluidic connection is given in Fig. 3.16. An optofluidic chip is placed on a carrier substrate (a PMMA microscope slide in this case). The carrier substrate can be as small as the individual chip itself. Especially if thinking of a sensor element integrated in a hand-held device this could be advantageous. Nevertheless, during the development phase a carrier substrate with dimensions of a few centimeters might be the better choice. Fluidic connections into the micro-channels on-chip are

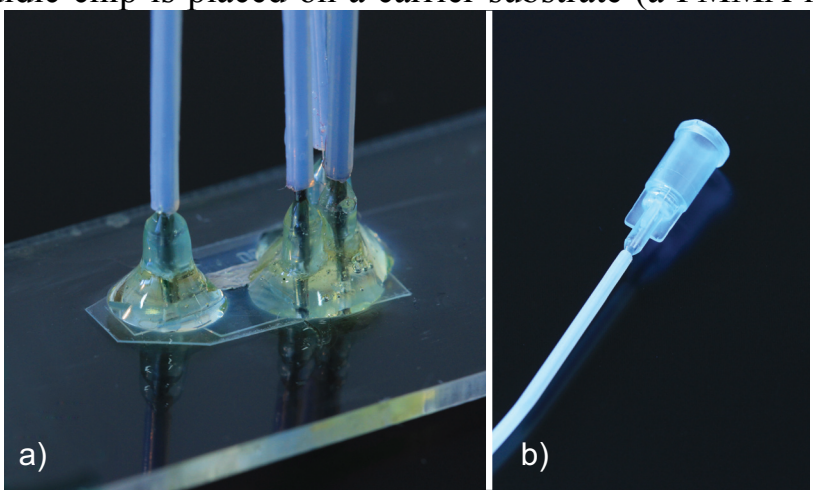

Figure 3.16: Fluidic connections to the optofluidic devices. **(a)** The substrate material (PMMA in this case) is provided with holes for liquid in- and outlets. PTFE tubings with inserted needles are plugged into those holes and glued to the substrate material. The optofluidic chip is placed on the other side of the substrate. **(b)** The other end of the PTFE tubings is equipped with a standard syringe connector for direct connections to the syringes containing the sample solutions.

provided through holes in the carrier substrate. These holes are drilled with a conventional drilling machine. On the other side of the substrate, PTFE tubings manage the peripheral fluidic connection to the syringe. The PTFE tubing on the chip side is equipped with a flat hollow needle inside. The needle stands out of the PTFE tubing, but less than the thickness of the substrate. The protruding part of the needle is plugged into the holes on the substrate and fixed using a two component glue (Fig. 3.16a). In addition, the applied glue ensures sealing of the in- and outlets to provide a fully airtight connection. Into the other side of the PTFE tubing a hollow needle with a standard syringe connector is inserted (Fig. 3.16b). This connector allows syringes filled with the specific liquids to be connected. The injection can either be done manually or by programmable syringe pumps. The sample volume inside the chip itself is in the pico liter range. Nevertheless, the attached PTFE tubings have volumes up to a few hundreds of micro-liters. For the experimental studies these volumes must be provided. In a final application, these connections can be removed and the necessary sample volumes are again in the pico liter range.

3.4.2 Optical system

The light source for the analyses presented in the following chapters is a solid-state laser system with an SMA-connector at the optical output. Using multi-mode glass fibers (core diameter of 50 µm, outer diameter of 90 µm) light is guided from the source into the optofluidic devices. In some of the developed optofluidic devices, the exiting light is again coupled into a glass fiber and guided towards an optical detector. This detector can be, for example, a simple photodiode or a photomultiplier tube. Although providing a lower sensitivity than photomultiplier tubes, a standard pre-amplified photodetector is used in the later on presented experiments to provide the possibility of a future integration on-chip. On the laser and the photodetector sides, the glass fibers are equipped with SMA connectors. The other sides of the fibers are free of any connector and provide bare endings only. These bare endings are inserted into fiber grooves on the micro-devices (Fig. 3.17). The wide opening of the fiber groove on the edge of the chip allows easy insertion of the glass fiber. The other side of the groove is narrowed down close to the outer diameter of the fiber. This prevents any movements of the fiber once it has been clamped inside the groove. In that way self-alignment of the glass fiber is ensured. Such fiber grooves can be implemented in

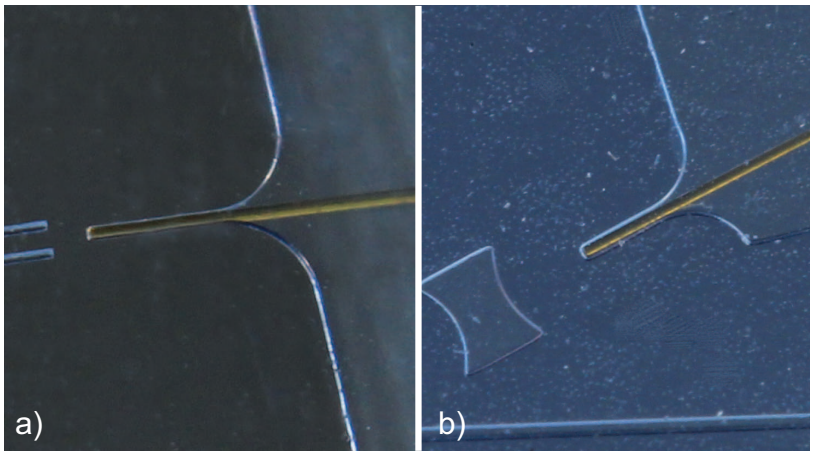

Figure 3.17: Optical connection to the micro-chip. The bare ending of a multi-mode glass fiber is inserted into fiber grooves. The wide opening of the grooves allows easy insertion whereas the other side is narrowed down to fully fix the fibers in their positions. The outer diameter of the employed glass fibers is 90 µm. **(a)** Fiber groove on a PDMS device placed close to an integrated waveguide. **(b)** Fiber groove on a dry resist device placed right next to an air micro-lens.

any device material as long as it provides sufficient transparency at the operating wavelength. Two examples are PDMS (Fig. 3.17a) and dry resist (Fig. 3.17b).

3.4.3 External instruments

All the investigated devices have their actual sensing and actuating units, respectively, directly integrated on chip. The optofluidic chip itself is then connected to external instruments using the previously described optical and fluidic systems. Elements such as the light source and photodetectors are not integrated on-chip but provided externally. A typical overall arrangement for an optofluidic experimental setup is illustrated in Fig. 3.18. The optofluidic chip is placed in the center of the setup. Glass fibers and PTFE tubings provide the physical connections into the device. As mentioned earlier, an external light source is used in all the experiments. The chip itself is placed on a mounting stage underneath an optical microscope. For the actual functionality of the system typically no visual inspection is necessary. Nevertheless, in the development phase a permanent verification of the ongoings inside the device is essential. Using a microscope the obtained results can be correlated to the actual behavior on-chip and are hence verified. For data recording, a digital camera can be assembled on top of the

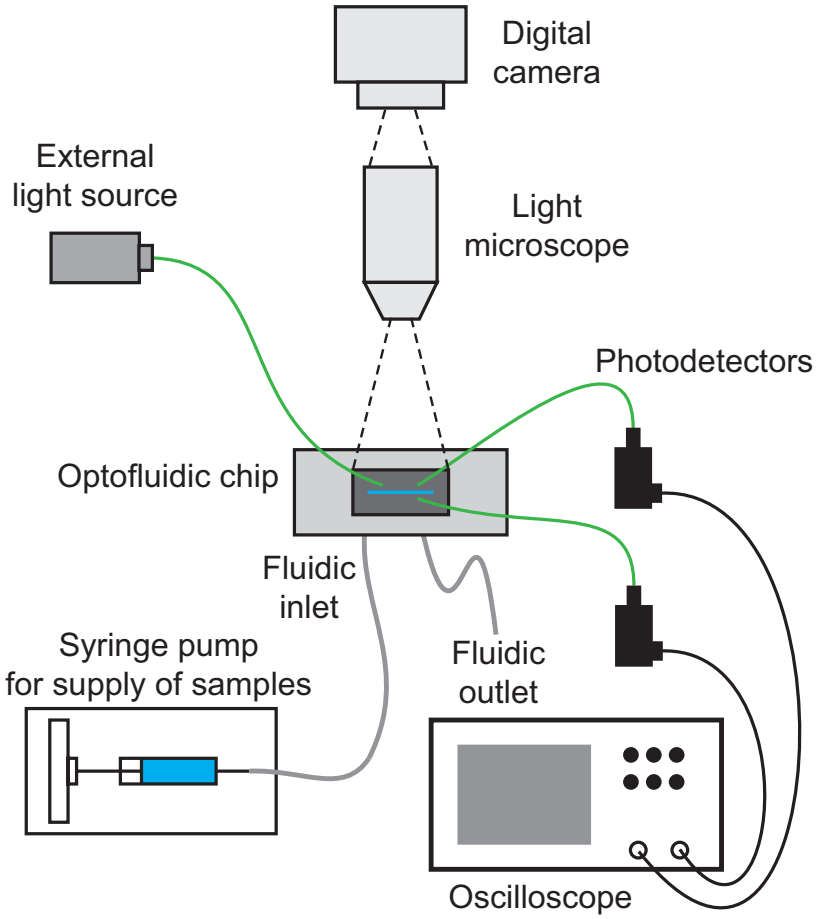

Figure 3.18: Schematic of a typical optofluidic experimental setup. The optofluidic chip is placed in the center underneath a light microscope having a digital camera attached. A syringe pump and PTFE tubings, an external light source and glass fibers, standard photodetectors, and an oscilloscope complete the setup.

microscope and can be connected to a PC. If a controlled flow of liquid is essential, a high-precision syringe pump can be integrated in the setup. For applications not demanding specific flow rates the injection can be done manually as well. The actual results can either be obtained through the microscope images or through light signals coupled into additional glass fibers. Those glass fibers are then connected to standard photodetectors. The use of photomultiplier tubes was intentionally avoided for two reasons. At first, standard photodetectors are much more cost effective than photomultiplier tubes. And secondly, photodiodes hold the potential for integration into the optofluidic chip whereas photomultiplier tubes don't. The electrical signals are then displayed on an oscilloscope.

In general, much attention is paid to the selection of the external com-

ponents. The peripheral system is tried to be kept as small and simple as possible. Furthermore, expensive instruments are avoided to allow a cost effective system to be built up. Finally, the main components are selected such that a future integration into the optofluidic chip is possible. Laser diodes and photo diodes are components which can already be integrated on-chip. For systems asking for a pumping system one could think of implementation of an electro-osmotic driven flow. Such pumping sources can be integrated and are much space optimized compared to the bulky external syringe pumps. In that sense, in future a cost effective, compact, hand-held system can be aimed for.

Chapter 4
On-chip light modulation

This chapter compares two basically different approaches for the realization of optofluidic light modulation units. After explaining the device designs both modulators are examined experimentally. Finally the advantages and disadvantages of each approach are discussed.

The work presented in this chapter has been published in [36,38,57,58].

4.1 Introduction

Optical principles are embedded in different ways for actuation as well as sensor elements [59] on microfluidic platforms. One example is fluorescent labeling, which is exploited for the visualization and examination of various biological and chemical reactions [60, 61]. For this kind of analysis, optics plays an important role in both excitation and detection. Optofluidics allows to integrate the two disciplines of fluidics and optics on a single chip where liquids not only coexist with light but take over the role of solid optical elements. They are directly integrated in the functional optical path. Once coupled into the device [62], light can interact with liquids for a vast variety of applications. Active elements, such as coherent light sources [63, 64], as well as passive ones, such as waveguides and lenses [16, 65–68], have already been successfully implemented. Compared to its solid counterparts, such optofluidic devices provide an enormously increased flexibility as well as tunability. Liquids can either be easily exchanged or streams of liquids in a microfluidic channel can be changed in size by alternating their inlet velocities resulting in continuously reconfigurable characteristics of the devices.

Especially for on-chip fluorescence excitation a sophisticated optical arrangement is crucial. The examined amount of sample in microfluidic devices is extremely low calling for a precise spatial control of possible stimuli (e.g., light for the excitation of fluorescence). Furthermore, a temporarily

confined time slot for the exposure of the analyte to light results in reduced photo bleaching issues. This has led to the investigation of various on-chip light modulation principles. Xu *et al.* [69] have developed a system comprising a sensing as well as switching unit based on fiber optics. Song *et al.* [70] published an integrated 2x2 optical switch based on pneumatically opened and closed air gaps. Campbell *et al.* [71] have developed a multi-layer 2x2 optical switch exploiting the different reflection/transmission properties of two liquids. Both groups apply mechanically moving parts for the light switching process. Although providing good switching characteristics, the use of mechanically moving parts automatically induces wearing and sticking issues. Seow *et al.* [72] proposed an optofluidic switch without any moving parts based on an L2-waveguide. In that work, flow rates are adjusted carefully to alter the width of the liquid core resulting in two possible light switching states. This principle based on an L2-waveguide does not employ any moving elements but depends on very stable flow conditions.

In the following sections, two on-chip optofluidic, contact-free light modulation units, both of them working without any moving elements are presented. The first modulator exploits the laminar flow conditions in a microfluidic channel to build up an L2-waveguide. Hydrodynamic pressure differences are then used to steer this waveguide. In a second realization the light modulation is performed without the need of a permanent flow through the device which allows more stable light configurations to be achieved.

4.2 Light modulation principles

For the realization of the on-chip light modulators two basically different optofluidic approaches are presented. The first concept based on an L2-waveguide was published in [57]. To provide a possibility of comparison between the two different designs a short summary is included in the following sections. The newly developed version utilizes total internal reflection phenomena at a steady-state.

4.2.1 Concept of L2-waveguide based light modulation

The concept of the hydrodynamic light modulator based on an L2-waveguide is explained in Fig. 4.1. Chung *et al.* have designed a similar device exploiting the same principle [73]. The microfluidic part consists of five liquid inlets, two for the pushing media, two for the cladding, and one

for the core solution. The difference in the refractive indices of cladding and core has to be sufficiently high to allow light guidance by total internal reflection inside the L2-waveguide. Applying DI water (*n* of 1.33) and a 5 mol/L $CaCl_2$ solution (*n* of 1.45) as cladding and core medium, respectively, satisfies this condition. The numerical aperture of this L2-waveguide configuration is

$$NA = 1/n_0 * \sqrt{{n_{\text{core}}}^2 - {n_{\text{cladding}}}^2} = 0.36,$$

where n_0, n_{core}, and n_{cladding} stand for the refractive indices of the device material (SU-8, *n* of approx. 1.60), the core, and the cladding liquid, respectively. Given this numerical aperture, light rays with incident angles up to 21° (with respect to the core stream) can be coupled into the L2-waveguide. The profile of the refractive index across the main channel is shown in Fig. 4.1 on the right side. In this case diffusion is neglected and constant inlet velocities are assumed at all inlets.

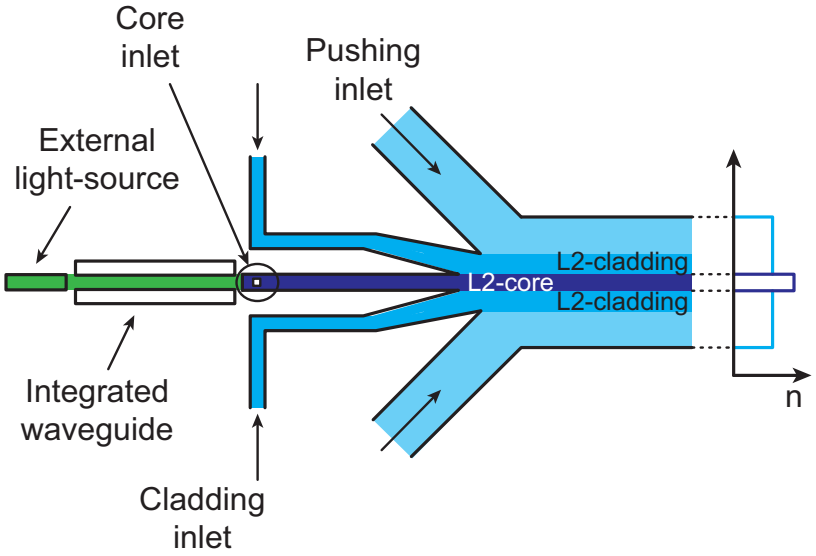

Figure 4.1: Working principle of on-chip light modulation based on an L2-waveguide. Two pushing inlets are used to steer the core and cladding media inside the channel. The output position of the light is defined by the position of the core stream. The profile of the refractive index across the main channel is indicated on the right side.

The two pushing inlets indicated on the top and bottom of the figure are used to steer the L2-waveguide consisting of the core and the two cladding streams. The hydrodynamic pressure applied at those two inlets defines the position of the waveguide in the channel. Using an external light source, light can be coupled inside the core of the L2-waveguide. The inlet flow-velocities define the position of the liquid core in the microfluidic channel

and with that the exiting position of the guided light at the outlet of the device. This concept requires a constant flow of liquid through the channel. In a stationary state, the solutions would fully diffuse into each other and prevent any light guidance. The principle can be used to define any light position within its working range. However, the constant need for fresh solutions holds the potential for improvement.

4.2.2 TIR concept for light modulation

This device takes advantage of the exchangeability of liquids in microfluidic devices. Lapsley *et al.* [74] have used a similar approach to build up an optical attenuator. The exploited principle is illustrated in Fig. 4.2. Light guided towards a microfluidic channel in a relatively flat angle is either reflected or transmitted depending on the refractive indices of the device material and the medium in the microfluidic channel. If the refractive index of the medium is sufficiently low (in relation to the index of the device material), incident light rays experience total internal reflection (TIR) at the solid-liquid interface (Fig. 4.2a). On the other hand, filling the channel with a solution matching the refractive index of the chip material allows light to be fully transmitted through the channel (Fig. 4.2b). The later on designed device is equipped with two microfluidic channels after each other (following the path of light). In that way, three distinct positions for the light on-chip can be configured. This concept does not depend on a constant flow of liquid through the device. In that way, an extremely stable output signal can be defined.

4.3 Experimental results

In all the experiments, DI water and a 5 M $CaCl_2$ solution are employed as the low and the high refractive index solution, respectively. A monochromatic light source (531 nm) is used as external light source. Reduced cladding glass fibers (core diameter of 50 µm, outer diameter of 90 µm) manage the peripheral light guidance. Glass fibers can be clamped onto the chip using the integrated fiber grooves on all the devices.

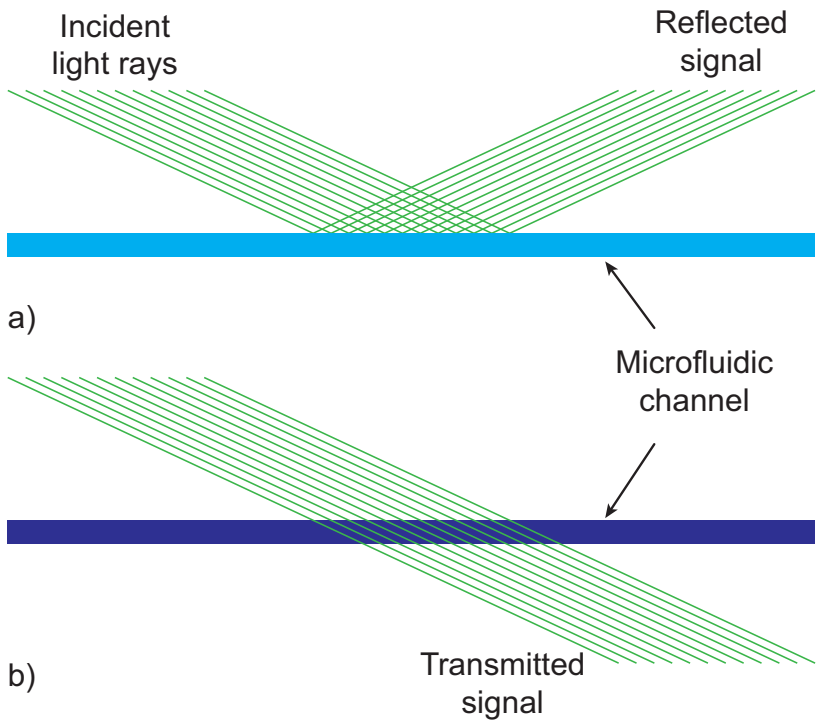

Figure 4.2: Operation principle of the total internal reflection (TIR) based modulator. The incident light rays hit a microfluidic channel. Depending on the refractive index of the liquid in the channel rays are either totally reflected or transmitted. **(a)** A low refractive index solution results in light reflection at the solid-liquid interface. **(b)** A high refractive index solution allows incident light to penetrate the channel.

4.3.1 L2-waveguide based modulation

For the L2-waveguide based device five syringe pumps are needed to adjust the fluid velocity for each inlet individually. To close the microfluidic channels a PDMS layer is clamped onto the chip using a standard cage mount system. In Fig.4.3 the fluidic design of the modulator is illustrated.

Right after the end of the microfluidic channel a ray tracing chamber is placed. This chamber is filled with a fluorophore (an aqueous Rhodamine B solution) to visualize exiting light rays. Fluorescence images of the output region are given in Fig. 4.4a. Three different light exiting positions are achieved in excellent accordance to the finite element simulations (COMSOL Multiphysics, Fig. 4.4b). In the first situation (Fig. 4.4a1, Fig. 4.4b1), the inflow of the upper pushing inlet is set smaller than the lower one resulting in a shift of the L2-waveguide to the upper outlet. If both pushing inlets are set to the same flow-velocity (Fig. 4.4a2, Fig. 4.4b2), light exits the de-

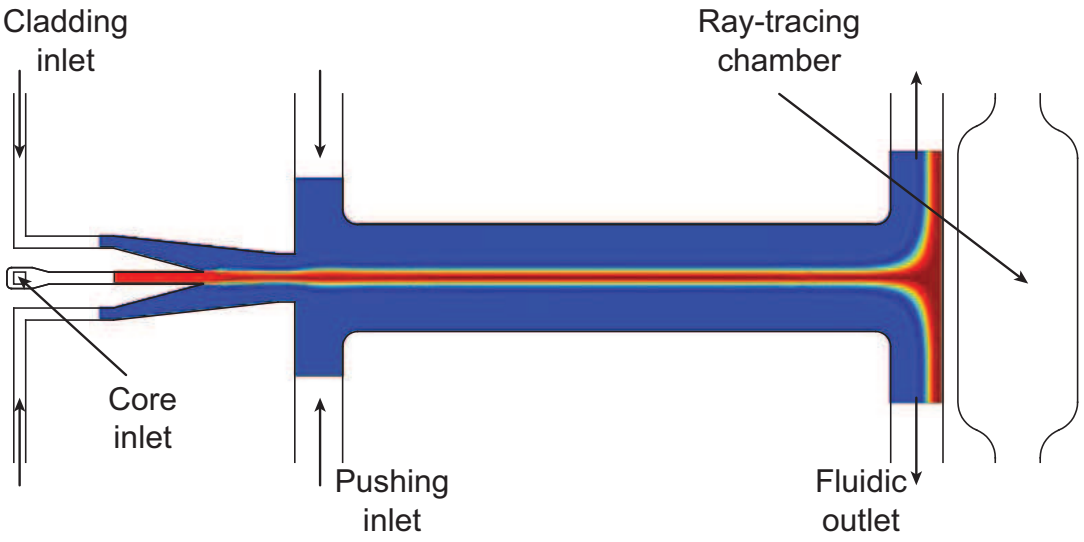

Figure 4.3: Final fluidic design of the L2-waveguide based modulator. A ray-tracing chamber is placed at the output region for light visualization.

vice from the middle. To steer the L2-waveguide downwards (Fig. 4.4a3, Fig. 4.4b3), the upper pushing flow-velocity is increased with respect to the lower one. In that sense a continuum of output positions for the guided light inside the core stream can be defined.

4.3.2 TIR based light modulation

Fig. 4.5 shows an image of the fabricated device. The PDMS chip is bonded on a glass microscope slide. In contrast to the hydrodynamic light modulator, the TIR based version does not need a controlled flow of liquids and hence no syringe pumps. The liquids can be inserted in the channel by means of manual injection. To allow visualization of light on the chip the PDMS device is soaked with a fluorophore. Fig. 4.6a depicts ray-tracing simulations of the three light switching possibilities. Corresponding fluorescence images are given in Fig. 4.6b. An integrated waveguide and micro-air lenses manage on-chip light confinement and focusing in-plane (two dimensions). In the current design there is no light confinement in the third dimension. As can be seen from the simulations, at a low refractive index medium light is totally reflected while at a high refractive index medium matching the index of PDMS light is entirely transmitted.

In Fig. 4.6b1 the first channel is filled with the low refractive index medium at which most light is reflected and output 1 is activated. In this case the second channel has no influence on the output. It can be filled with

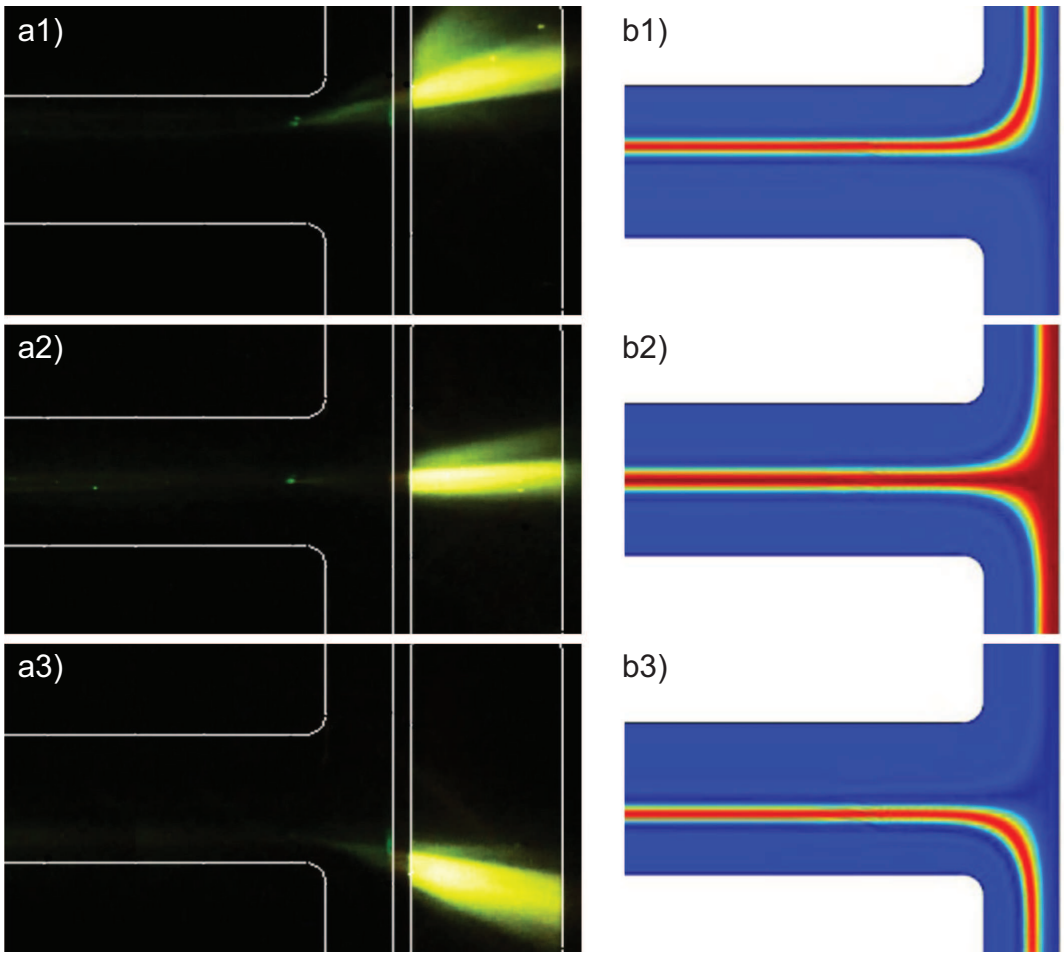

Figure 4.4: **(a)** Fluorescence images of the output region at three different flow conditions. Light exiting the L2-waveguide is visualized in a ray-tracing chamber filled with a fluorophore. **(b)** Finite element simulations (COMSOL Multiphysics) of the microfluidic flow conditions. The red stream represents the core whereas blue illustrates the cladding and pushing media.

either a low or a high refractive index solution. Due to the lacking confinement in the third dimension, there are also light rays visible crossing the channel. By changing the constitution of the device (sandwich structure), light confinement could be realized in this third dimension as well, which would further improve the performance of the device. Fig. 4.6b2 depicts the situation if the first channel is filled with a high refractive index solution and the second channel with a low one. There are no light rays reflected by the first channel anymore. At the second channel total internal reflection occurs and the output 2 is activated. The third switching state (Fig. 4.6b3) is obtained if both channels are filled with the high refractive index medium. In that case output 3 is activated. This principle can be extended by imple-

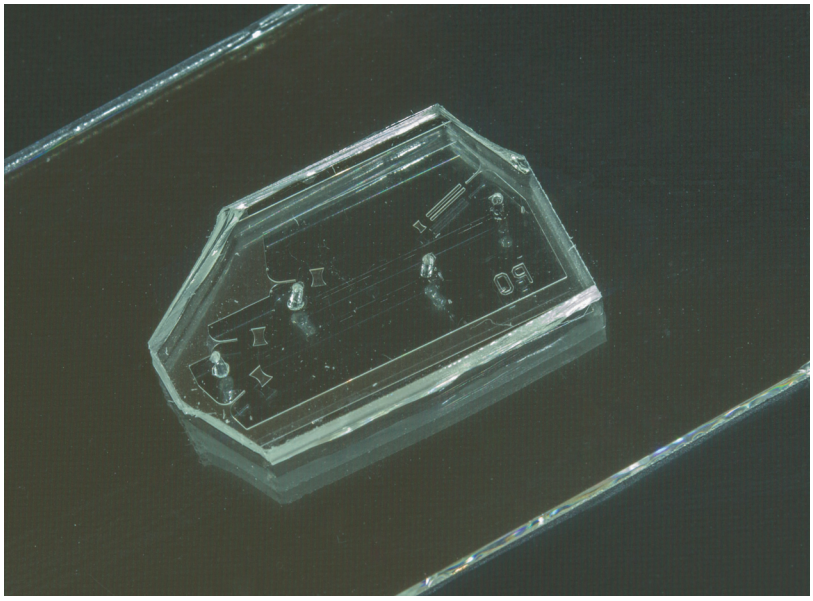

Figure 4.5: Photograph of the TIR based light modulation unit. The PDMS device is bonded on a glass microscope slide.

mentation of additional microfluidic channels.

In a final experiment, all output signals are recorded by externally attached photodetectors (each representing one optical output). Therefore, the bare endings of three glass fibers are inserted into integrated fiber grooves placed at each output. The other endings of the glass fibers (equipped with an SMA connector) are connected to standard pre-amplified silicon photodetectors. A digital storage oscilloscope is used to record the output signals of the detectors. The simplicity of this external read-out arrangement provides an extremely flexible optical connection to the chip and can be employed for diverse applications. The obtained results are shown in Fig. 4.7. Depending on the solutions in the two microfluidic channels (see table 4.1), one of the three outputs is at its maximum and activated while the other two are disabled. In the switching states I & V, both channels are filled with the low refractive index medium and output 1 is high. At state IV, the first channel is filled with the low refractive index solution and the second channel is filled with the high one. The difference compared to states I & V is the level of output 2 and output 3. In theory, those outputs are not influenced, but in practice, due to the missing confinement in the third dimension, there are small changes evident. In state II & VI, the high refractive index solution is filled in the first channel and the low one in the second which sets output 2 at its maximum. For state III, both channels are filled with the high refractive

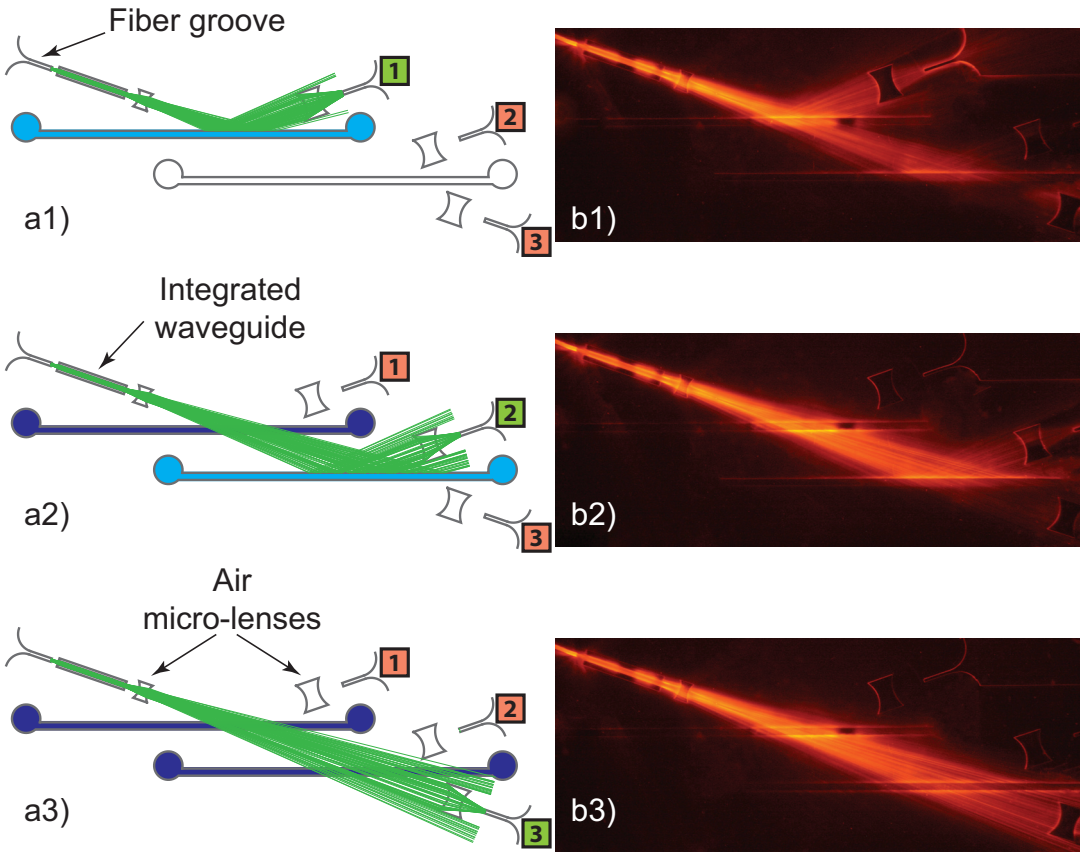

Figure 4.6: Illustration of the on-chip light switching process. **(a)** Simulation results and **(b)** corresponding fluorescence images of three distinct switching states. In a1) and b1) the first channel is filled with the low refractive index solution resulting in light reflection upwards and output 1 is activated. In a2) and b2) the first channel is filled with the high refractive index medium allowing light to penetrate through while the second channel filled with the low refractive index solution reflects the incident light and output 2 is activated. In a3) and b3) both channels are filled with the high refractive index solution allowing light to penetrate through both channels and output 3 is activated. The numbers in the squares indicate the three light detectors.

index medium and output 3 is activated. The overshoots at the beginning of each state are explained by the transition of one medium to the next one. At this interface light is reflected in all directions and short variations in the signals occur. For fluorescence applications this is of minor importance.

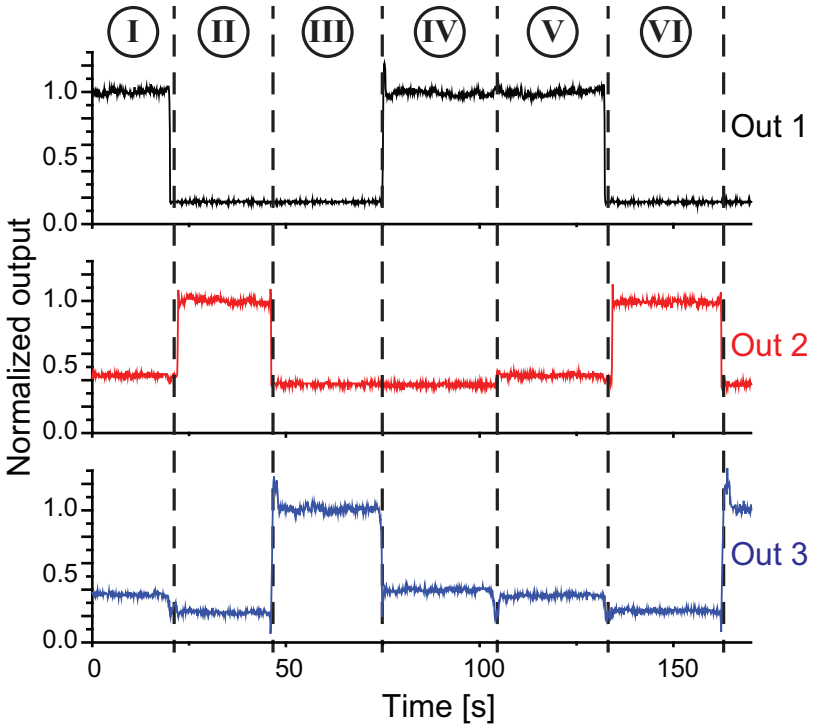

Figure 4.7: Output signals of the photodetectors. Depending on the solutions filled in the channels one of the three outputs is activated (high output signal). DI water is used as low refractive index and a $CaCl_2$ solution as high refractive index medium. See table 4.1 for the solutions in the channels at each labeled state.

	I	II	III	IV	V	VI
Channel 1	LOW	HIGH	HIGH	LOW	LOW	HIGH
Channel 2	LOW	LOW	HIGH	HIGH	LOW	LOW
Output	1	2	3	1	1	2

Table 4.1: Solutions in the two microfluidic channels for the six switching states labeled in Fig. 4.7. HIGH stands for a high refractive index solution (5 M $CaCl_2$) and LOW for a low one (DI water). In the last row the activated output for each state is indicated.

4.3.3 Comparison of the two light modulation units

The hydrodynamic modulator based on an L2-waveguide provides a continuum of possible light positions. The limits of the shifting ability solely depend on the geometry of the device. However, a continuous supply of solution is required. The core, the cladding, and the pushing streams have to be inserted at a certain minimum inlet velocity. This inlet velocity con-

trols the diffusion of core and cladding solutions. Very low inlet velocities prevent light guidance through the L2-waveguide as the necessary step in the refractive index between core and cladding material has vanished due to diffusion. Another issue when applying this principle is the stability of the exiting light beam. Whether the output position is stable or not depends on the stability of the inlet velocities of the solutions which are influenced by any vibrations and the precision of the syringe pumps. Furthermore, the need for multiple individual syringe pumps results in a rather complex and large experimental setup.

The TIR based device is not affected by the inlet velocities. Once the channels have been filled with the desired solutions the path of light on the chip is defined. Any changes in the flow conditions do not alter this path anymore as long as the liquids are not changed. In that sense, a robust and very stable light control is reached. Although not enabling a continuum of light positions, the amount of channels on the chip can be increased and with that the light modulation possibilities. This light modulator can be operated without any syringe pumps. The liquids can be inserted into the channels by manual injection.

4.4 Conclusions

Both presented optofluidic principles allow on-chip light modulation without incorporation of any mechanically moving elements. This avoids any wearing or sticking issues, enabling nearly infinite light modulation sequences to be performed. The TIR based device based on total internal reflection has shown superior working functionality. In contrast to the hydrodynamic design, the output position of the light is not affected by the flow conditions on-chip. Once the appropriate liquids are filled in the channels very stable light conditions are obtained. For the operation of the modulator no syringe pump is needed. Also the consumption of liquids is kept at a minimum since there is no need for a permanent flow through the device. Considering these advantages, the proposed TIR based concept can be, for example, implemented on a device for a spatially and temporally confined excitation of fluorescence. Especially the simplicity of the design allows the integration with other microfluidic elements on one and the same device to enable sophisticated lab-on-a-chip systems.

Chapter 5
Thermo-Optofluidics

This chapter introduces the novel field of thermo-optofluidics. In particular, the design and characterization of a light modulation unit based on temperature changes are described. At first, the chip design is presented followed by the experimental evaluation of the device performance.

The work presented in this chapter has been published in [42].

5.1 Introduction

The fusion of optics and microfluidics has allowed various new lab-on-a-chip devices to be realized [75]. Those optofluidic modules provide an enormously increased flexibility compared to its solid counterparts. Liquid micro-lenses, for example, can easily be reconfigured by employing different solutions and alternating their inlet velocities without the need of redesigning the basic layout [16]. With a single device, many different characteristics can be obtained which is not feasible if integrating solely solid elements. One parameter which is of importance for all those applications is the refractive index of the applied materials. As many parameters (e.g. wavelength, molecule concentration, buffer solution, temperature) have an influence on the refractive index, a change in this optical property can be utilized for analysis purposes as well as for actuator principles.

In the following sections, the influence of temperature changes on the refractive index of solid as well as liquid materials is exploited for the design of an on-chip light modulation unit. As published by Kamikawachi *et al.* [76] the index of various solids and liquids changes in opposite directions with increasing/decreasing temperature. If now a liquid core/solid cladding waveguide is exposed to temperature changes, the refractive indices of core and cladding material diverge at least twice as fast with respect to the applied temperature variations as they do for solely solid thermo-optic devices. In that sense on-off modulation of light guidance through the waveguide

can be obtained with doubled maximum frequency compared to solely solid thermo-optic devices.

5.2 Thermo-optic coefficient

Nearly any physical parameter is influenced by temperature changes. This is also true for the refractive index. Although experimental data is far from being comprehensive there are works published investigating the thermo-optic effect for various applications [77–81]. In the work of Espinola *et al.* [82] for example, one arm of an integrated Mach-Zehnder interferometer is exposed to temperature variations. Due to the temperature dependency of the refractive index, light propagating in this arm experiences a phase shift proportional to the temperature change. The thermo-optic coefficient dn/dT of silicon at the operating wavelength (1.5 µm) is $+1.84 \times 10^{-4}$. To achieve a π-phase shift and with that a full on-off light modulation a temperature difference of 8 °C is necessary. This temperature difference is directly proportional to the thermo-optic coefficient. Increasing the thermo-optic coefficient would reduce the necessary temperature difference and with that shorten the cooling/heating circles. Shortened cooling/heating circles, on the other hand, result in an increased switching frequency.

That is where liquids come into play. The thermo-optic coefficient of liquids is negative and hence opposite to the coefficient of various solid materials. For example, the thermo-optic coefficient dn/dT of DI water and ethanol at 1.5 µm are -0.8×10^{-4} and -4.0×10^{-4}, respectively. Exchanging a solely solid waveguide by a liquid core/solid cladding waveguide increases the effective thermo-optic coefficient of the assembly and allows superior modulation performances. Fig. 5.1 illustrates this circumstance. In solely solid-based systems, a temperature change of 10 °C is necessary for a difference in refractive index of 0.01. Doing this calculation for a liquid core/solid cladding waveguide shows a remarkable distinction. For reaching the same difference in refractive index, half the temperature change is sufficient. In these diagrams the thermo-optic coefficients of solid and liquid are arbitrarily chosen (1×10^{-4} and -1×10^{-4}, respectively). In reality the magnitude of the thermo-optic coefficients of most liquids is much higher than those of solids. In that sense the typical temperature change needed for the same difference in refractive index is even less than half.

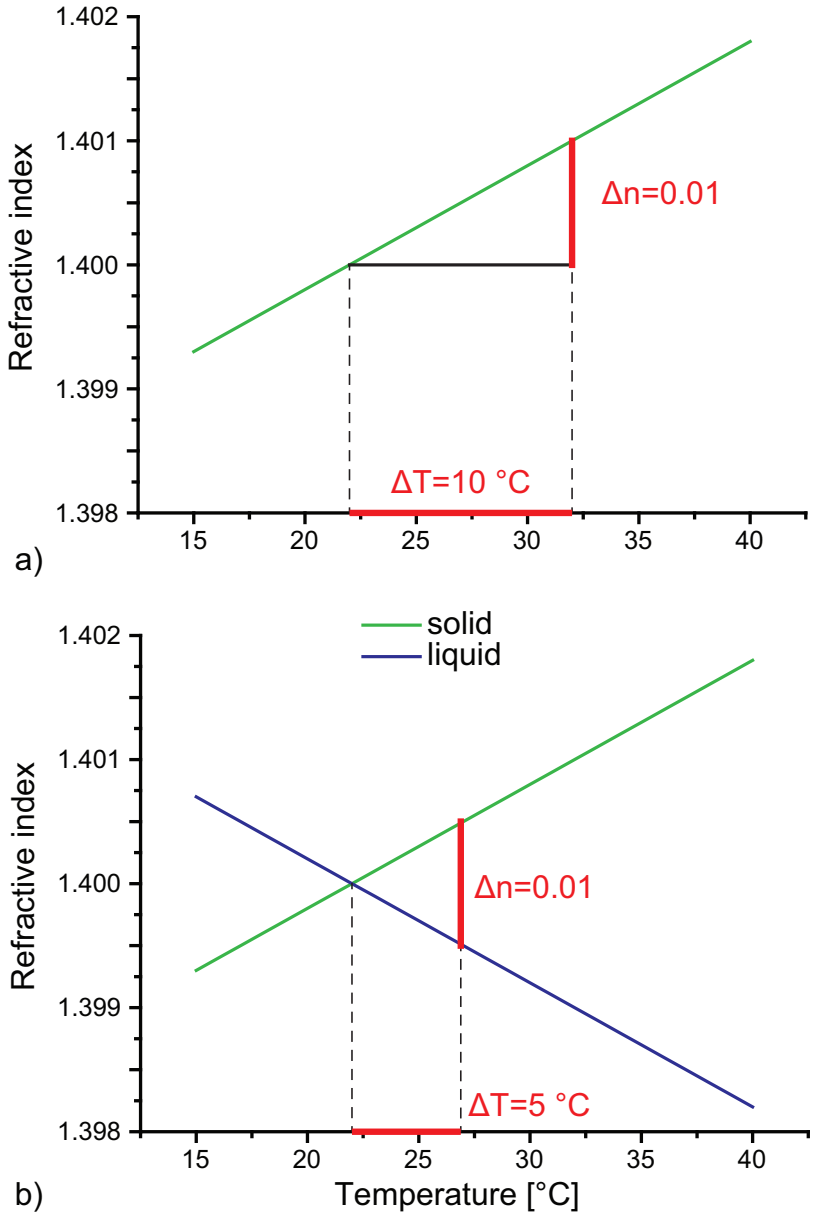

Figure 5.1: Thermo-optic coefficients of solids and liquids. **(a)** For solely solid based system a temperature change of 10 °C is necessary for a difference in the refractive index of 0.01. **(b)** A liquid core/solid cladding waveguide reaches the same difference in refractive index at half the temperature change. The thermo-optic coefficients of solid and liquid are arbitrarily chosen (1×10^{-4} and -1×10^{-4}, respectively).

5.3 Chip design

The main part of the device is an integrated liquid core/solid cladding waveguide as illustrated in Fig. 5.2. Light is coupled into the waveguide

from an external light source via peripheral glass fibers clamped into integrated fiber grooves. A straight microfluidic channel filled with solution works as core and the surrounding chip material as cladding of the waveguide. At the other end of the microfluidic channel, an integrated air microlens ensures focusing of the exiting light into the output glass fiber which is connected to a silicon photodetector.

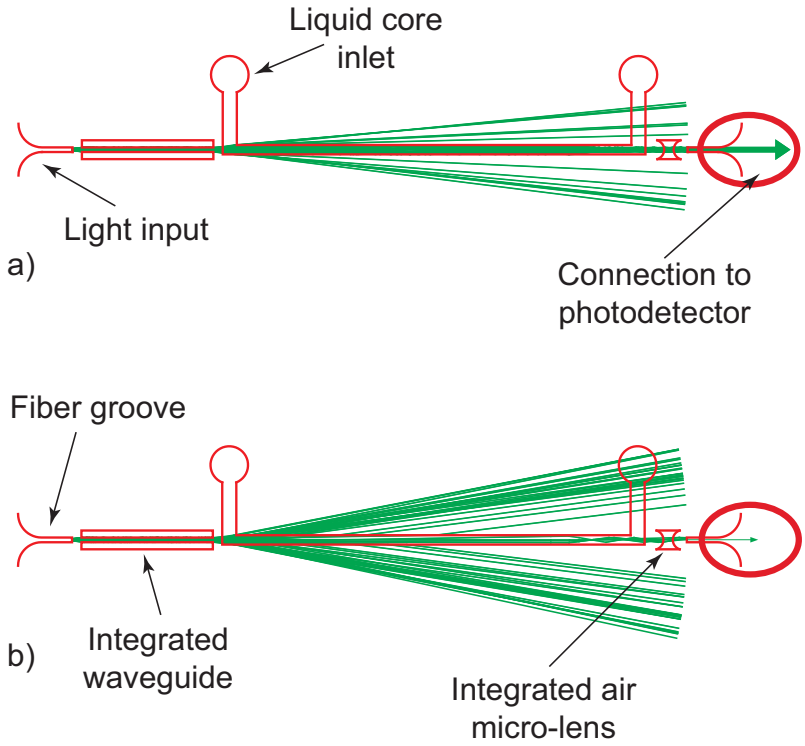

Figure 5.2: Schematic of the working principle. A liquid core/solid cladding waveguide is built up by PDMS as cladding and a $CaCl_2$ solution as core material. **(a)** The refractive index of the liquid core at room temperature slightly exceeds the index of PDMS and total internal reflection inside the waveguide is provided for a certain numerical aperture resulting in a high optical output (red circle). **(b)** At altered operation temperature the refractive indices of cladding and core change in opposite directions and total internal reflection is inhibited (low optical output).

Matching of the refractive indices of core and cladding material is essential for the functionality. For a *normally on* light modulation, the refractive index of the core solution has to be slightly higher than the index of the chip material. In that way, light is guided in the waveguide by total internal reflection if the whole assembly is kept at room temperature (22 °C). If the core medium as well as the chip material is exposed to altered temperature the situation is reversibly changed. The index of the chip material becomes higher than the index of the core and light guidance is switched off. As the

refractive indices of liquids and solids change in opposite directions with respect to temperature variations, highest switching rates can be obtained.

5.4 Experimental results

The experimental setup used for first experiments is depicted in Fig. 5.3. The thermo-optofluidic chip out of PDMS bonded on the glass microscope slide is placed on a Peltier element responsible for temperature management. An aluminum block underneath the Peltier element is employed as heat sink. To increase the heat transfer, thermal grease is deposited between glass slide and Peltier element and between Peltier element and heat sink. Light guidance from the external light source (diode pumped solid state laser, 531 nm, 20 mW) to the device and from the device to the pre-amplified silicon photodetector is managed by reduced cladding glass fibers.

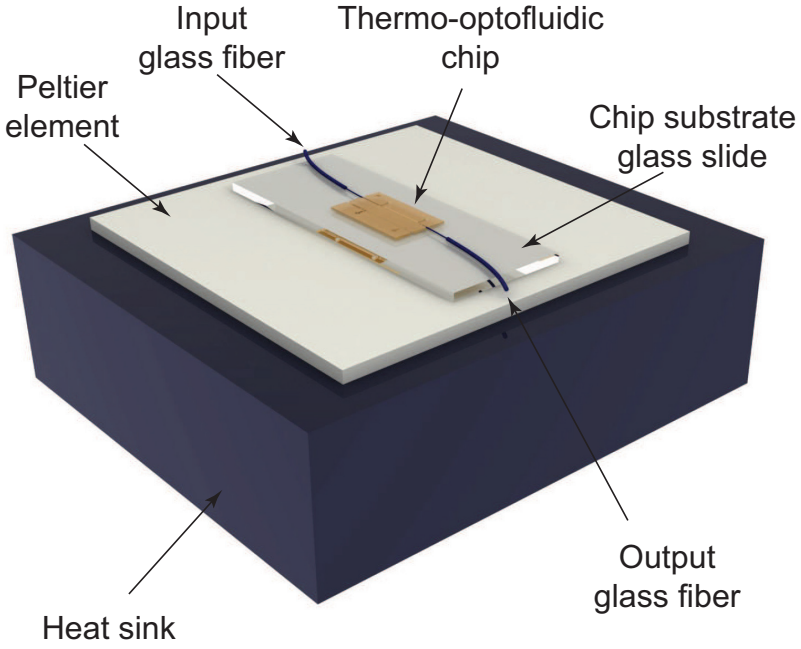

Figure 5.3: Illustration of the experimental setup. The thermo-optofluidic chip is bonded on a glass microscope slide. Temperature control is managed by a Peltier element on a heat sink (aluminum block). A thermal grease between the glass slide and the Peltier element as well as between the Peltier element and the heat sink ensures good heat transfer.

Fig. 5.4 shows an image of the final device. The PDMS chip is irreversibly bonded on a glass microscope slide.

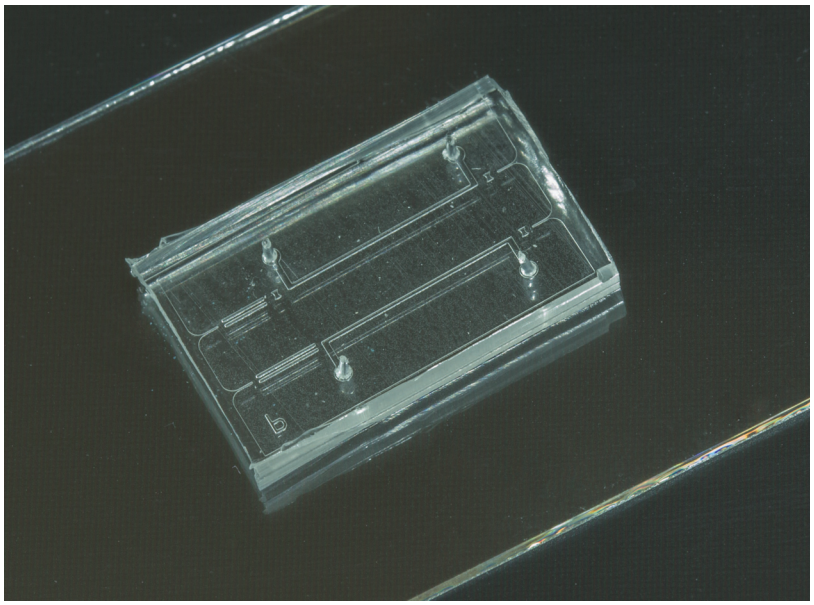

Figure 5.4: Photograph of the PDMS chip irreversibly bonded on a glass microscope slide.

5.4.1 Matching of refractive indices

As already mentioned in the thermo-optofluidic design section, matching of the refractive indices of core and cladding material is crucial for the overall functionality. The index of the core medium, an aqueous $CaCl_2$ solution, has to be slightly higher than the index of the chip material, PDMS. The refractive index of the solution increases proportionally with increasing $CaCl_2$ content [83]. Therefore, the relation between $CaCl_2$ concentration and the optical output power detected at the photodetector at constant temperature (22 °C) is recorded (Fig. 5.5).

At a certain concentration, the refractive index of the $CaCl_2$ solution exceeds the index of PDMS and a drastic increase in the optical output is evident. A concentration right after the drastic increase (3.15 mol/L) is used for the following experiments to keep the influence of temperature variations on the output at a maximum.

5.4.2 Thermo-optofluidic light switching

The microfluidic channel is filled with the 3.15 mol/L $CaCl_2$ solution without being exchanged during the entire experiment. For on-chip light path visualization the PDMS device is soaked with a fluorophore (Rhodamine B). Obtained fluorescence images are given in Fig. 5.6.

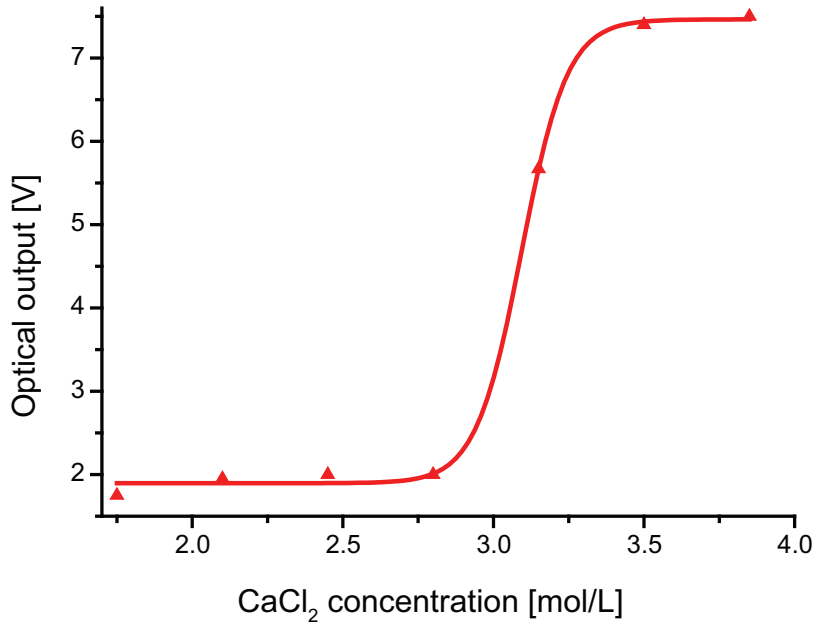

Figure 5.5: Output of the photodetector at constant temperature if differently concentrated $CaCl_2$ solutions (dissolved in DI water) are filled in the microfluidic channel. Once the refractive index of the solution exceeds the index of PDMS total internal reflection starts to occur inside the waveguide and a drastic increase in the optical output power is evident.

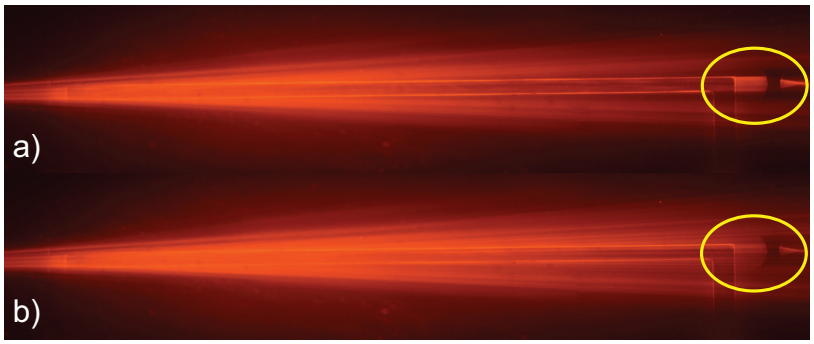

Figure 5.6: Fluorescence images of the PDMS devices soaked with a fluorophore for laser light visualization. **(a)** At room temperature light is confined within the core of the waveguide and results in a high optical output (yellow circle). **(b)** At altered temperature light confinement is reversibly turned off (low optical output).

At room temperature (Fig. 5.6a) light is well confined within the core of the waveguide and strong fluorescence is excited at the end of the channel. If the temperature of the arrangement is altered (a constant voltage is applied at the Peltier element) the refractive indices can be reversibly changed and total internal reflection inside the $CaCl_2$ solution is inhibited (Fig. 5.6b, at

the end of the channel almost no fluorescence signal is visible anymore).

To evaluate the reversibility of these changes in the refractive indices, the signal of the external photodetector is recorded and a sequence of temperature changes is applied (Fig 5.7).

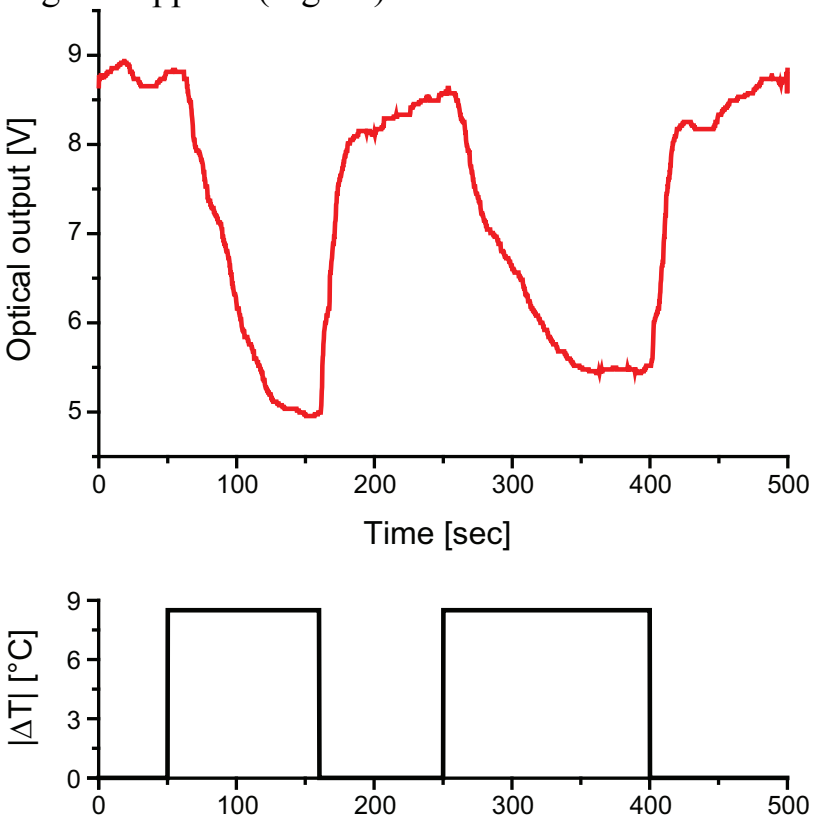

Figure 5.7: Reversible on-chip light modulation. Ideal temperature profile of the assembly is illustrated in the lower diagram. The output of the photodetector (upper diagram) clearly shows on-off switching of the guided laser light in the waveguide due to temperature changes. The slow response of the output signal to the temperature changes is explained by relatively long cooling/heating times of the whole device (glass slide, chip, and core medium). A spatial confinement of the temperature controlled area would drastically reduce the response time (integration of thermo-element on-chip).

In this experiment, the switching frequency is limited by the relatively long heating and cooling times. The entire thermo-optofluidic chip, the core solution, and the glass microscope slide have to be brought to the same temperature before a stable signal can be recorded at the output. A spatial restriction of the temperature controlled area by integration of a thermo-element on the chip would drastically increase the maximum modulation frequency. Nevertheless, reversible on-off switching of light guidance through the liquid core/solid cladding waveguide by applying temperature

changes is demonstrated for the presented setup.

5.5 Conclusions

A novel thermo-optofluidic principle for on-chip light modulation based on a liquid core/solid cladding waveguide has been elaborated. Taking advantage of the opposing change in the refractive index of core and chip material if exposed to temperature variations, the maximum light switching frequency can be increased by a factor of more than two compared to standard thermo-optic elements. This measurement design can be used for the realization of thermal actuators as well as for temperature sensing units and can easily be integrated with other microfluidic elements.

Chapter 6

Liquid concentration sensor

This chapter deals with the design and characterization of an optofluidic sensor device for the investigation of liquid concentrations. At first, the theoretical situation is analyzed and the experimental setup is described in detail. In the experimental part, the sensor is tested with different sample solutions. $CaCl_2$, phosphate, lactose, and ethanol are taken as analytes. As another application of this sensing principle the characterization and identification of micro-droplets is shown.

The work presented in this chapter has been published in [37,39,41,84].

6.1 Introduction

In the following sections, an optofluidic sensor principle for the determination of the concentration of dissolved molecules in liquids is presented. The investigated samples have an influence on the refractive index of the buffer solution which is exploited for sample characterization. In recent works, different approaches for the determination of the refractive index of liquids on-chip have been presented [85]. Lapsley *et al.* [86] have developed a planar, optofluidic Mach-Zehnder interferometer for the characterization of liquid samples. Chao *et al.* [87] have designed two different devices for the determination of refractive indices of liquids, one based on light refraction in a liquid filled prism and the second one using a refraction channel where light is coupled out of a liquid core waveguide in an angle corresponding to the refractive index of the core solution. Seow *et al.* [88] have exploited the principle of partial reflection to determine the refractive index of fluids. In this setup, the reflectivity as well as the angle of the exiting light are used as measure for the refractive index. Another device by Lapsley *et al.* [74] uses the reflection property of liquids with different refractive indices to build up a variable optical attenuator. Depending on the solution filled in the channel, the optical output power can be adjusted.

The later on presented devices are based on the principle of partial total internal reflection occurring at the solid-liquid interface when the center incident angle of a slightly diverging light beam is close to the critical angle. On the devices both signals, the reflected and the transmitted, are recorded. Compared to approaches performing the analysis using a single signal, a drastically increased stability is obtained. Furthermore, two signals provide a permanent verification of the measurement results allowing to discard changes in the signals generated by laser power instabilities. The improved stability allows for a more accurate analysis and has different practical applications. In food industry, for example, various phosphates play an important role as additives. The maximum amounts of additives for certain food products in Germany are regularized in the ”Zusatzstoff-Zulassungsverordnung” (ZZulV) [89]. For different phosphates a span between 0.5 g/kg and 50 g/kg, corresponding to a mono-phosphate concentration of approximately 3 mmol/L and 0.3 mol/L, respectively, is defined. Using one of the proposed designs, concentrations in the range of tens of millimol per liter can be identified making this principle a promising approach for control applications in this area.

Healthcare is another field of application. People suffering from lactose intolerance, for example, are advised not to consume high quantities of lactose containing products to avoid unwanted reactions in the body. Therefore, the amount of lactose in various products (solid as well as liquid) is of huge interest for medical purposes and obviously for food industry as well. A simple, fast, and robust way to determine the concentration would hence be desirable. The impact of dissolved lactose on the refractive index [83] can be exploited for the design and realization of a sensor system being capable of the above mentioned requirements. Products containing less than 0.1 g lactose per 100 g are considered lactose-free. For liquid products, this equals to a concentration of 3 mmol/L. For lactose intolerant people, the critical lactose concentration in products above which body reactions start to occur is approximately 30 mmol/L. With the elaborated sensor device, these lactose concentrations can be identified and provide valuable information for the patients.

6.2 Underlying principle

The operation principle of the sensor system is depicted in Fig. 6.1. On the chip a microfluidic channel filled with the analyte is hit by slightly diverging

laser light. The angle of the incident light (θ_i) is adjusted to result in partial total internal reflection at the solid-liquid interface. For a given chip material the critical angle, θ_c, is defined by

$$sin(\theta_c) = \frac{n_{analyte}}{n_{material}}$$

where $n_{analyte}$ and $n_{material}$ are the refractive indices of the analyte and the chip material, respectively. After focusing the laser light on-chip, the incident angles vary approximately $\pm 3°$ around the center angle. The center incident angle and the span of $\pm 3°$ define the working range of the system and can be optimized for the desired specifications.

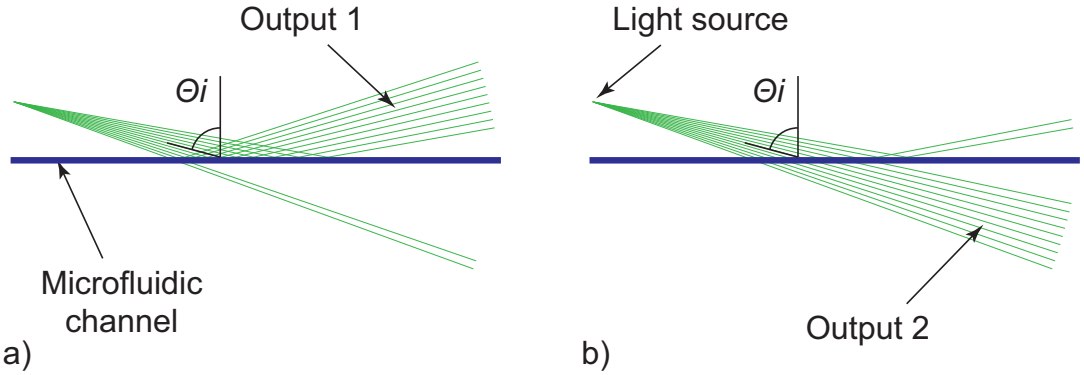

Figure 6.1: Schematic of the working principle for the determination of liquid concentrations. A straight microfluidic channel (blue line) is hit by slightly diverging laser light (green lines). (**a**) At samples having a low refractive index, most light rays are totally reflected, while (**b**) at samples with a high refractive index, most light rays are transmitted. The ratio of reflected to transmitted signal is used for sample characterization.

For the theoretical derivation dry resist is assumed as device material (*n* of 1.52). This value can simply be exchanged if other materials are used. For DI water (*n* of 1.33) as analyte the critical angle is calculated to 61.04°. If the center angle of the incident light is set in the vicinity of this value, a part of the light is totally reflected and subsequently results in a signal in output 1, whilst, at the same time, the other part is transmitted according to the Fresnel equations, which increases the signal in output 2 if DI water is filled in the analysis channel. A correlation of those two signals is then used to deduce the composition of the sample being analyzed.

The theoretical situation for a center incident angle of 65° is examined in detail. Light rays will approach the microfluidic channel in angles between 62° and 68°. Partial total internal reflection starts once the refractive index

of the sample exceeds

$$n_{analyte,min} = n_{material} \cdot sin(62°) = 1.34 \ .$$

Above a certain refractive index, no light ray will experience total internal reflection anymore. This value is calculated using the largest incident angle

$$n_{analyte,max} = n_{material} \cdot sin(68°) = 1.41 \ .$$

Those two values define the working range of the device with a center incident angle of 65°.

In order to characterize its performance, the device has been tested with $CaCl_2$ samples. Table 6.1 summarizes refractive indices of $CaCl_2$ solutions of different concentration at a measuring wavelength of 589 nm [83]. With the given working range, $CaCl_2$ concentrations between 0.5 mol/L and 3.5 mol/L can theoretically be differentiated. It should be mentioned at this point that the wavelength used for measurements in the following sections is 531 nm. This differs from 589 nm, which was used for the determination of the refractive indices of the $CaCl_2$ solutions in table 6.1. Although a significant difference is not expected, those absolute values should not be compared with the measurement results and are simply given to provide the reader with a feeling for the impact of $CaCl_2$ on the refractive index.

Table 6.1: Refractive indices of $CaCl_2$ solutions in different concentrations measured at a wavelength of 589 nm and a temperature of 20°C [83]

Concentration (mol/L)	Refractive index
0.045	1.3342
1.191	1.3625
2.122	1.3839
3.179	1.4066
4.062	1.4242
5.030	1.4420

6.2.1 The divergence of the laser beam

The Fresnel equations, which give the amount of reflected light at the solid-liquid interface for parallel and perpendicularly polarized light are

$$R_{\parallel} = \left| \frac{n_{material} \cdot cos(\theta_t) - n_{analyte} \cdot cos(\theta_i)}{n_{material} \cdot cos(\theta_t) + n_{analyte} \cdot cos(\theta_i)} \right|^2$$

and

$$R_{\perp} = \left| \frac{n_{material} \cdot cos(\theta_i) - n_{analyte} \cdot cos(\theta_t)}{n_{material} \cdot cos(\theta_i) + n_{analyte} \cdot cos(\theta_t)} \right|^2 ,$$

respectively. Where θ_i is the incident angle of the light. The exit angle of the transmitted light, θ_t, can be calculated using Snell's law

$$\frac{sin(\theta_i)}{sin(\theta_t)} = \frac{n_{analyte}}{n_{material}} .$$

The difference between $n_{analyte}$ and $n_{material}$ is intentionally kept as small as possible. In that case the reflectivity of parallel and perpendicularly polarized light does not significantly differ justifying the use of an average value which is defined as

$$R = \frac{R_{\parallel} + R_{\perp}}{2} .$$

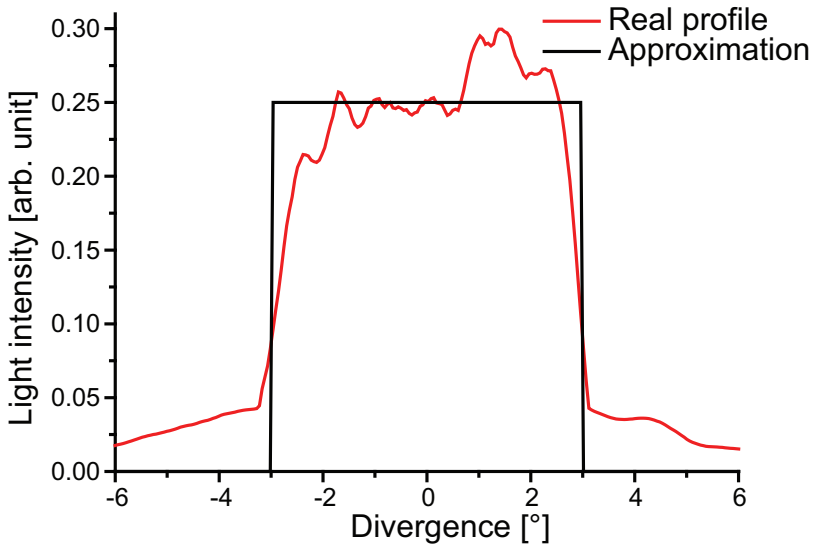

Figure 6.2: Incident beam optical power distribution right before the microfluidic channel. Between a divergence of -3° and +3° the profile is approximated as constant.

The incident beam optical power distribution at the microfluidic channel is approximated as constant over the divergence of $\pm 3°$ (Fig. 6.2). Comparing the calculated averaged reflectivities of a device with fully collimated incident beam (no partial total internal reflection occurs) and the proposed design with a beam divergence of $\pm 3°$ both at a center incident angle of 65° shows remarkable differences (Fig. 6.3). Realizations utilizing a fully collimated light beam solely depend on the reflectivity of the analyte according to the Fresnel equations. Such realizations show an inefficient characteristic to changes in the analyte composition. The proposed design with a

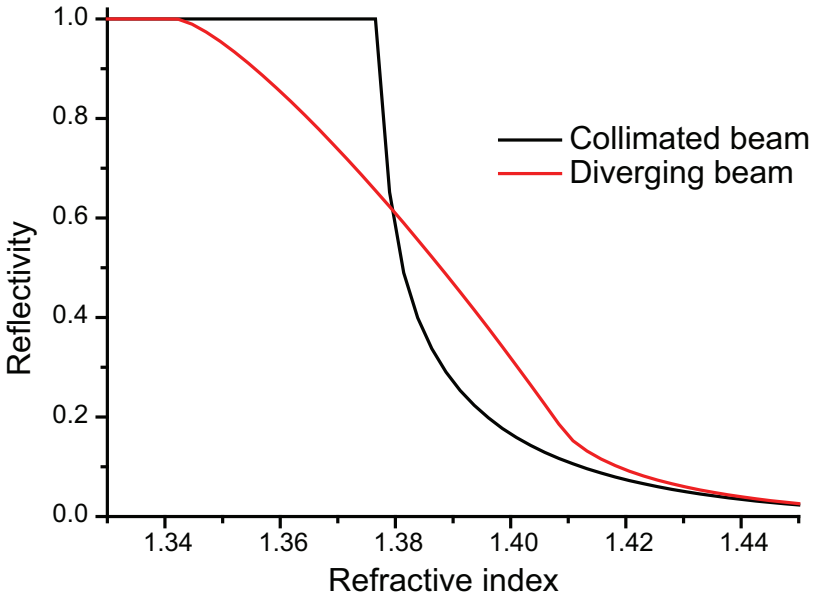

Figure 6.3: Calculated reflectivities at the solid-liquid interface for different refractive indices. The device with the diverging laser beam shows a linear relation over a large refractive index range, which is advantageous for sample characterization.

diverging laser beam provides a linear relation between obtained signal ratio and the refractive index of the solution over a huge range. This behavior facilitates a robust application of the principle for an accurate detection of dissolved molecules in the analyte. The theoretical upper end of the feasible working range is defined by the chip material. As long as the index of the chip material exceeds the index of the analyte, which is true for nearly all liquid samples, this method can be applied.

6.2.2 The incident angle

As mentioned before, the presented principle can be optimized for various ranges of interest. To cover a wide range of sample concentrations, four designs with different center incident angles are investigated. The center angles are set to 60°, 62.5°, 65°, and 67.5°. All those designs are optimized using ray-tracing simulations (ZEMAX, USA). The first angle is chosen to be sensitive for very low $CaCl_2$ concentrations and the last one for $CaCl_2$ concentrations close to 5 mol/L.

For a first characterization of the devices, $CaCl_2$ solutions with known concentration are filled in the channel and the signals of both outputs are recorded. Fig. 6.4 depicts the obtained results, where reflected light signals

of all four devices are illustrated by solid and corresponding transmitted light signals in identical color by dashed lines.

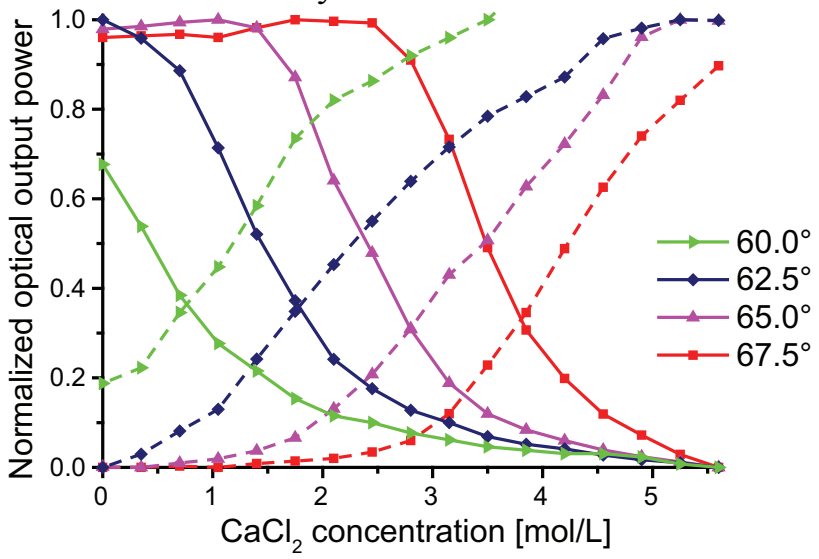

Figure 6.4: Offset corrected and normalized reflected (output 1) and transmitted (output 2) light signals for all four devices at different $CaCl_2$ concentrations. Solid lines represent reflected and dashed lines represent transmitted light signals recorded by external photodetectors. For different incident angles different working ranges are evident.

The output signals of the external photodetectors are offset corrected to eliminate the influence of dark currents and normalized by the maximum values before being printed in the diagram. As expected, the device with an incident angle of 60° shows sensitivity already for DI water. Neither the reflected nor the transmitted signal at 0 mol/L $CaCl_2$ is at its maximum or minimum, respectively. That means, at this point partial total internal reflections occurs. With increasing concentration, the reflected signal converges to zero while the transmitted signal reaches its maximum and defines the end of the working range of the device. The situation for the other devices is similar but shifted towards higher concentrations. The device with an incident angle of 67.5° shows sensitivity for concentrations up to 5 mol/L and above. Due to the finite solubility of $CaCl_2$ in DI water, the analysis is stopped at a concentration of 5 mol/L. Theoretically, these curves can be continued to any higher values as well.

The working ranges of the devices are summarized in table 6.2. Each one can be used over approximately 2 mol/L. By changing the divergence of the laser beam hitting the microfluidic channel, this span can be either enlarged or even further reduced. Depending on the application, a perfectly optimized design can be elaborated. The only limitations are the size of

the device (larger divergences call for longer analysis channels), the incident optical power which has to be increased at higher divergences, and the length of the optical path on-chip causing absorption losses and beam expansion. Considering those parameters for the given device, an increase in working range by a factor of two is feasible.

Table 6.2: Working ranges of the investigated designs

Incident angle	Lower limit	Upper limit
60.0°	0 mol/L	2 mol/L
62.5°	1 mol/L	3 mol/L
65.0°	2 mol/L	4 mol/L
67.5°	3 mol/L	5 mol/L

6.2.3 Independence of flow-velocity and temperature

To further evaluate the performance of the developed sensor system the influence of the flow-velocity is investigated. Samples are pumped through the device at different inlet speeds and the signals at both outputs are recorded. Fig 6.5 depicts the results. As anticipated by the theory the inflow velocity does not affect the results. Both signals stay stable over the entire flow

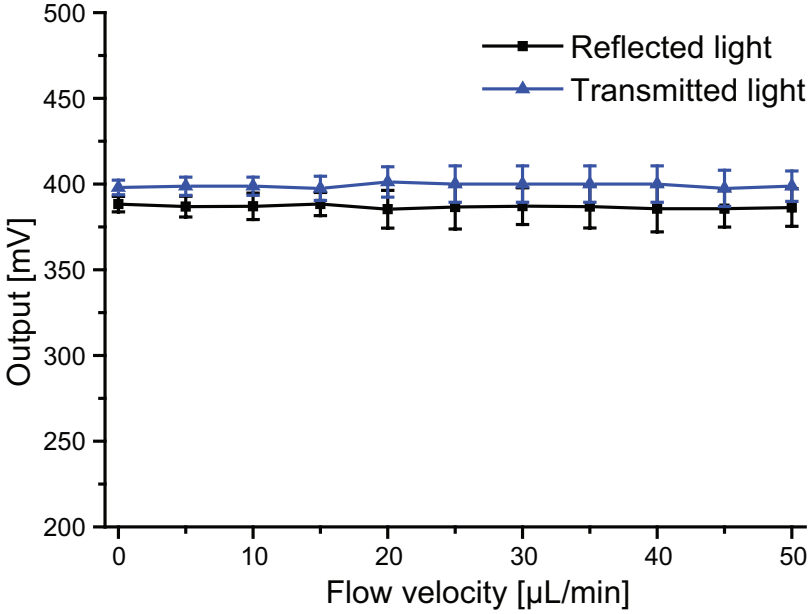

Figure 6.5: Reflected and transmitted light signals recorded at the two outputs for a single analyte. The results are not significantly influenced by the applied flow rate.

velocity range from 0 up to 50 µL/min.

Another important parameter for nearly any kind of analysis is the temperature dependency of the sensing element. To estimate the impact of temperature variations in the range of ± 1°C a worst case scenario is conducted. Fig. 6.6 illustrates the results of the simulation. The thermo-optic coeffi-

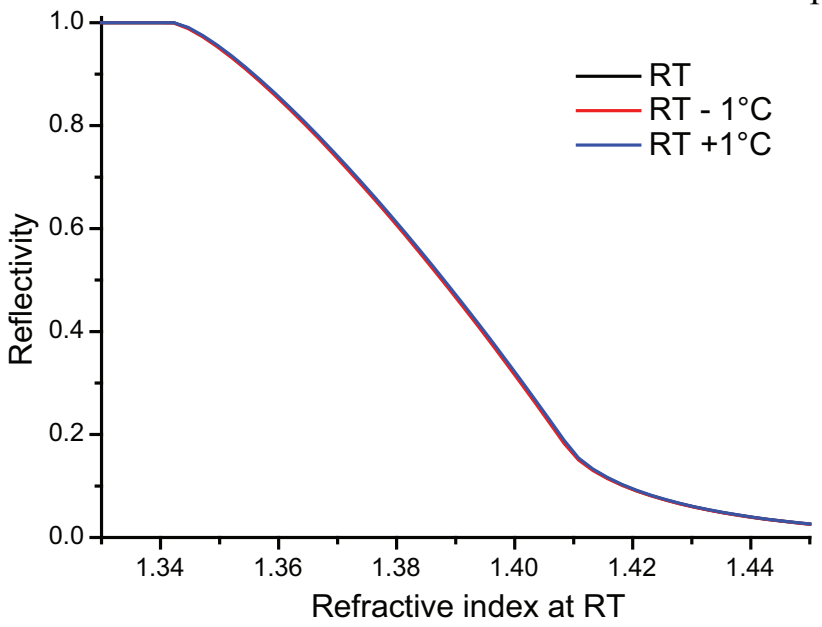

Figure 6.6: Influence of temperature variations of ± 1°C around room temperature (RT, 22°C). The maximum deviation is calculated to ± 1.7%.

cients of sample solution and chip material are intentionally set to a high value (|dn/dT|of $1*10^{-4}\,K^{-1}$). Over the entire range of investigated refractive indices, the maximum deviation from the index at room temperature is below ± 1.7%. This value equals approx. ± 8 mmol/L $CaCl_2$ concentration.

6.3 Experimental setup

A schematic of the overall setup, consisting of an external light source, three reduced cladding glass fibers, two pre-amplified silicon photodetectors, a digital storage oscilloscope, the sample solution, a fluidic waste box, and the optofluidic chip is given in Fig. 6.7. Except for the droplet study, a stop-and-go flow profile is applied in all the experiments to keep sample consumption at a minimum.

All experiments are conducted at room temperature (22°C) ± 1°C. Those temperature variations have only minor impact on the results. One end of all three glass fibers is equipped with an SMA connector for di-

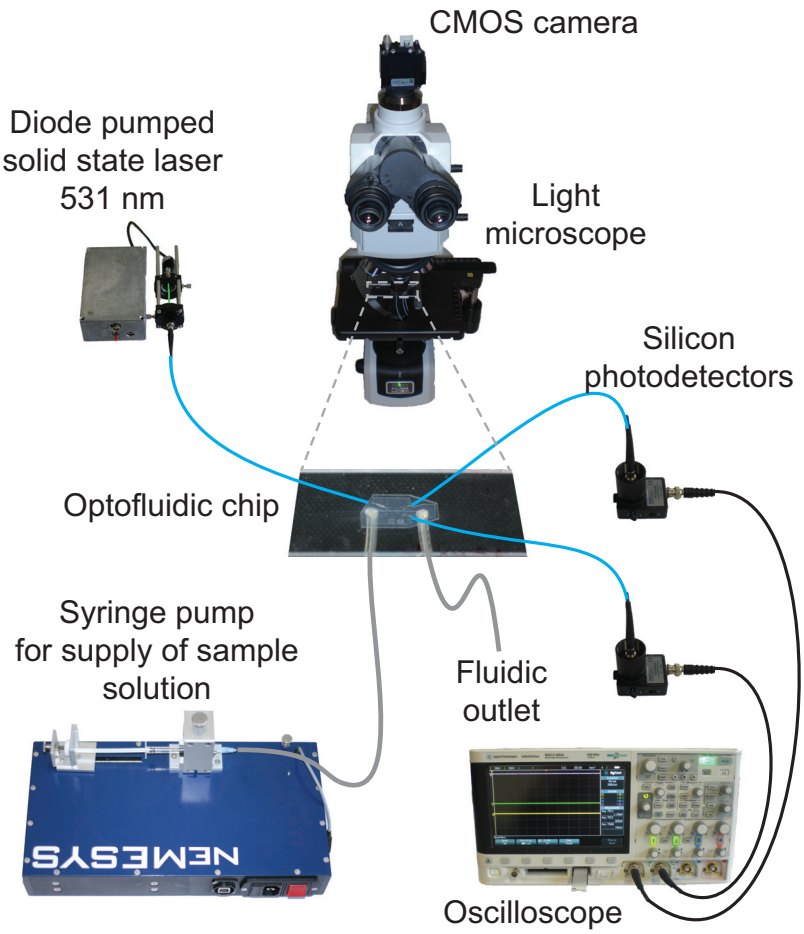

Figure 6.7: Overall experimental setup consisting of an external light source, three reduced cladding glass fibers (green lines), two pre-amplified silicon photodetectors, a digital storage oscilloscope, the sample solution, a fluidic outlet, and the optofluidic chip on the PMMA microscope slide. A light microscope having a CMOS camera attached is used for visual inspection.

rect connection to the light source as well as to the photodetectors. The bare other end is clamped onto the optofluidic chip using integrated fiber-grooves. The signals of the two photodetectors are recorded simultaneously using a digital storage oscilloscope. A syringe pump is used to manage the supply of sample solution through PTFE tubings into the microfluidic channel. For the droplet study, a second syringe pump is added to the peripheral setup. The outflow is collected in a waste box. To allow for visual inspection of the on-goings in the microchannel, the optofluidic chip is placed under a light microscope having a CMOS camera attached.

6.4 Determination of liquid concentrations

As a first characterization of the device, two studies with different sample molecules are conducted. One series of measurements is performed on $CaCl_2$ samples and a second one on phosphate dilutions. After the device design section, the obtained results are presented.

6.4.1 Device design

In Fig. 6.8 the device design for the analysis of liquid concentrations is shown. The microfluidic channel filled with the analyte is hit by slightly diverging laser light. An integrated waveguide ensures precise on-chip light positioning. The core of this waveguide has a width of 100 µm allowing most of the light exiting the peripheral glass fiber to be collected. An air micro-lens arranged after the integrated waveguide defines the divergence ($\pm 3°$) of the laser beam hitting the microfluidic channel. Two collecting lenses on the chip are responsible for focusing the reflected as well as the transmitted light, which are consecutively coupled into two separate peripheral glass fibers. Those lenses are bigger in size to counter beam broadening due to the divergence of $\pm 3°$. In that way, the major part of the reflected and transmitted light can be collected. To keep absorption losses at a minimum the lenses are placed next to the microfluidic channel as close as possible limited by the fabrication method only. The lens on the transmission side has a small lateral offset with respect to the incident light to compensate for light deflections by the microfluidic channel. The devices investigated in this section are fabricated in dry resist on a polyester foil bonded to a PMMA microscope slide (Fig. 6.9).

6.4.2 $CaCl_2$ study

Before starting with the determination of $CaCl_2$ concentrations, a calibration curve for each device is recorded. Similar to the angle study described in a preceding section, $CaCl_2$ solutions with known concentration are filled in the channel and the signals in output 1 and output 2 are measured. To increase the accuracy of the calibration curve, the signals for each concentration are recorded over five seconds and an average value is calculated. The ratio of corresponding reflected and transmitted value is then taken, normalized, and printed against the $CaCl_2$ concentration (Fig. 6.10).

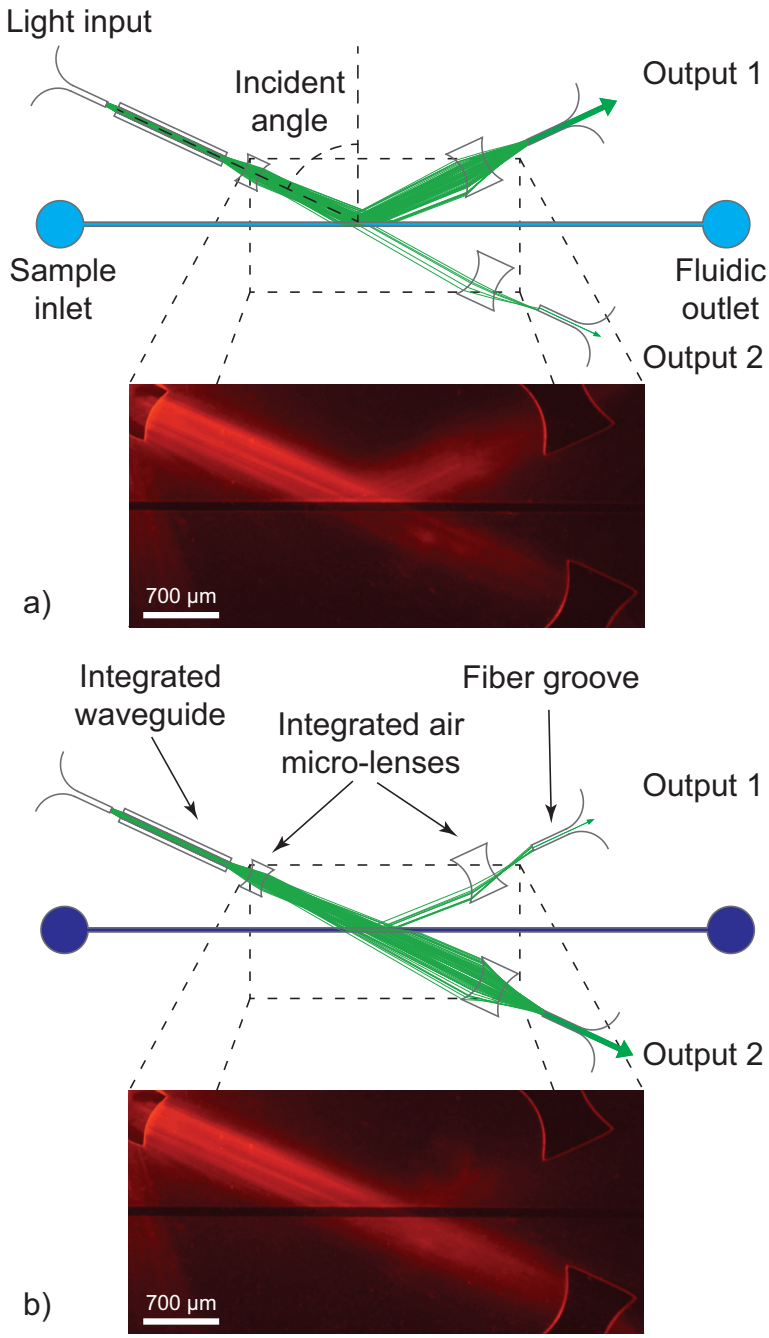

Figure 6.8: True-to-scale schematics of the operation principle and fluorescence ray-tracing photographs illustrating the real behavior of the device. The width of the microfluidic channel is 70 µm. At samples having (**a**) a relatively low refractive index a larger amount of light is reflected and results in a high signal in output 1 and a low signal in output 2; (**b**) a relatively high refractive index more light is transmitted and produces a high signal in output 2 and a low signal in output 1.

For each individual device, the collected data points are fitted on a curve

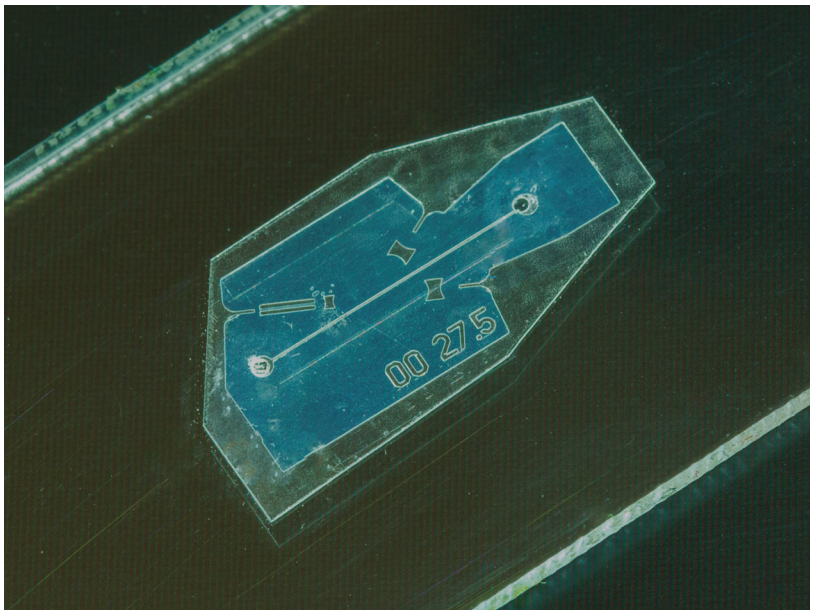

Figure 6.9: Photograph of the device for the analysis of liquid concentrations. A dry film resist is structured on a polyester foil and bonded to PMMA microscope slide.

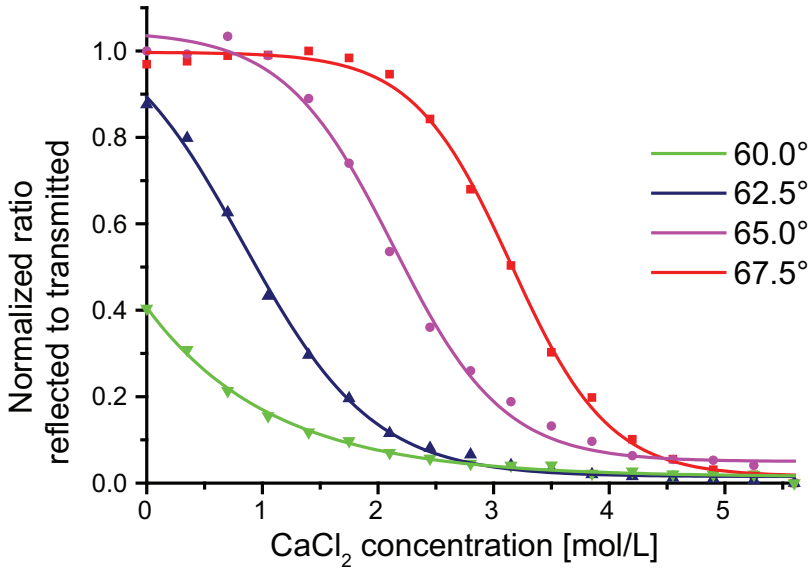

Figure 6.10: Normalized ratio of reflected and transmitted light signal printed against the $CaCl_2$ concentration. The obtained data points for each device are fitted on a Boltzmann sigmoid distribution.

using a best-fit algorithm (OriginPro, USA). The obtained best-fit function

is a Boltzmann sigmoid distribution defined by

$$y = \frac{A_1 - A_2}{1 + e^{\frac{x - x_0}{dx}}} + A_2$$

where A_1, A_2, x_0, and *dx* are constants obtained separately for each device (summarized in table 6.3 for all four devices), *x* gives the $CaCl_2$ concentration, and *y* stands for the absolute ratio of reflected and transmitted light signal. The obtained equations are then used to determine the $CaCl_2$ concentration out of the ratios of reflected and transmitted light signals. For practical applications, lower concentrations of dissolved molecules might be of more interest than higher quantities. Therefore, table 6.4 gives obtained values and the observational errors for the device with an incident angle of 60°, having the lowest working range (0 - 2 mol/L). The resolution amounts to approximately 40 mmol/L. The other devices give similar results within their working ranges. For $CaCl_2$ concentrations approaching 5 mol/L, fluctuations in the signal start to occur. These fluctuations can be attributed to scattering/diffusion effects within the sample solutions due to their increasing colloidal behavior.

Table 6.3: Constants for fitted Boltzmann sigmoid distributions

Device	A_1	A_2	x_0	dx
60.0°	380.74639	0.5431	-6.91827	1.07977
62.5°	2.62706	0.26287	0.83892	0.56033
65.0°	1.84164	0.67093	2.1333	0.47561
67.5°	1.89455	0.52888	3.15032	0.42376

Table 6.4: Measurement results of the $CaCl_2$ concentration determination experiments obtained with the 60° device

Reference value	Determined concentration	Observational error
1.05 mol/L	1.04 mol/L	0.01 mol/L
0.70 mol/L	0.68 mol/L	0.02 mol/L
0.35 mol/L	0.31 mol/L	0.04 mol/L
DI water	-0.04 mol/L	0.04 mol/L

6.4.3 Phosphate study

Two monophosphates, NaH_2PO_4 and KH_2PO_4, dissolved in DI water are used as the sample solutions. To evaluate the performance of the device (incident angle of 60°), aliquots of the samples at different phosphate concentrations (0 mol/L up to 1 mol/L) are taken and analyzed. As for the $CaCl_2$ experiment both signals, reflected and transmitted, are recorded and the ratio is calculated for each concentration. Fig. 6.11 depicts the obtained results. As can be seen, both phosphates show similar characteristics. With increasing concentration, the refractive index of the sample solution increases and results in a reduction of the reflected light signal and a concurrent increase in the transmitted one. The obtained data points are fitted on an asymptotic exponential curve. Deviations from the curve can be explained by imperfections in sample preparation resulting in small concentration errors. For lowest concentrations, the magnitude of the sensitivity is $0.41\,(\mathrm{mol/L})^{-1}$. Following the typical convention, the resolution is defined as three times the standard deviation of the noise in the system. Given that the mean standard deviation of the obtained ratios (reflected to transmitted light signal) for both phosphate experiments is $5.3 \cdot 10^{-3}$, a resolution of $16 \cdot 10^{-3}$ can be approximated. Using those two values the limit of detection can be cal-

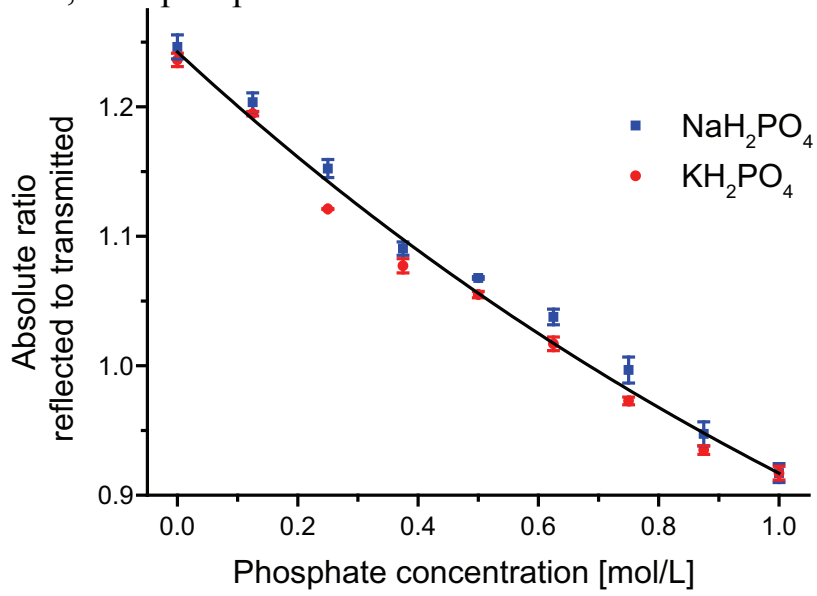

Figure 6.11: Absolute ratio of reflected and transmitted light signal printed against the phosphate concentration. Both phosphates, NaH_2PO_4 and KH_2PO_4, show a similar influence on the measurement results. Imperfections in sample preparation leading to concentration errors explain the small deviations from the fitted curve.

culated to

$$Limit\ of\ Detection = \frac{Resolution}{Sensitivity} = 39\,mmol/L\ .$$

6.5 Detection of dissolved lactose

The design of the device used for the lactose study is principally identical to the devices used for the $CaCl_2$ and phosphate studies. As the following experiments are performed on a PDMS device, the center incident angle is adjusted according to the refractive index of the device material. The first experiments on the device are performed using DI water as the buffer solution for the samples. In a final evaluation, commercially available lactose-free milk is taken for the analyses. Fig. 6.12 shows an image of a final PDMS device bonded on a glass microscope slide.

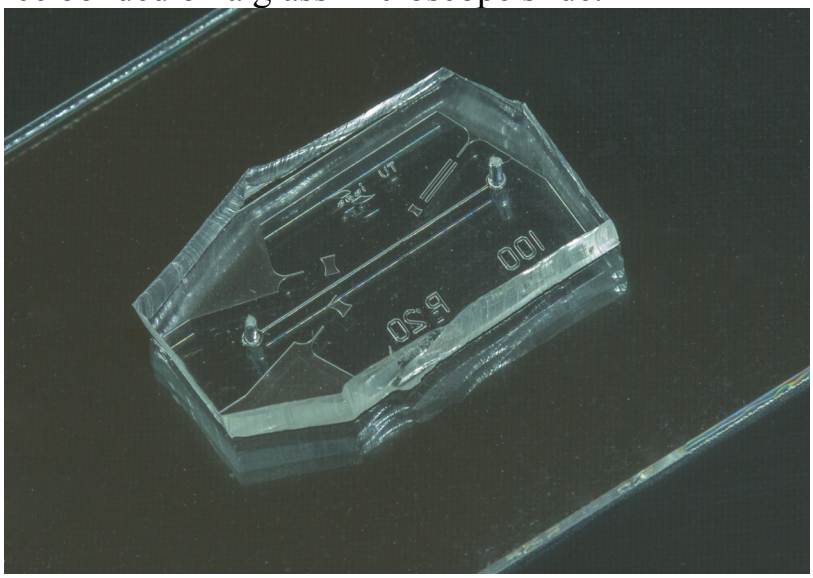

Figure 6.12: Photograph of the device for the analysis of dissolved lactose. The PDMS device is bonded to a glass microscope slide.

6.5.1 First characterization

The first investigated device is designed with a center incident angle of 72.5°. The divergence of the laser beam is set to ±3°. To characterize the performance of the device, lactose is dissolved in DI water at concentrations between 0 mol/L and 0.5 mol/L. Those solutions are then analyzed in the optofluidic chip one after another. Fig. 6.13 illustrates the obtained

ratios of reflected to transmitted light plotted over the concentration. A linear working range of the fitted sigmoid function over a defined region is evident. The gradient of the curve represents the sensitivity of the device at

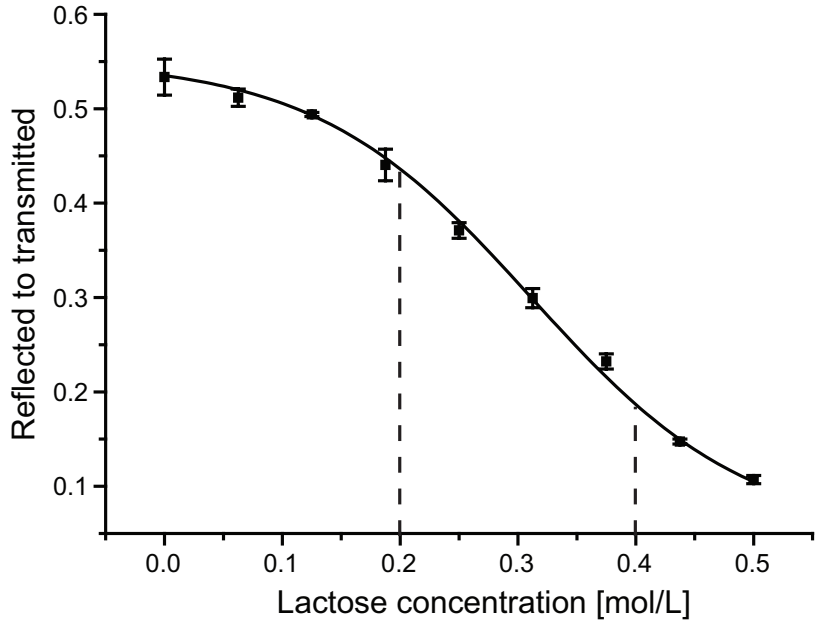

Figure 6.13: Ratio of reflected to transmitted light signal for the device with an incident angle of 72.5°. Highest sensitivity is obtained between 0.2 mol/L and 0.4 mol/L and defines the optimal working range.

the given lactose concentration. Highest sensitivity is obtained in the linear region between 0.2 mol/l and 0.4 mol/L. At lower concentrations the curve saturates. At those values, the amount of reflected and transmitted light does not change significantly anymore. Nearly all of the incident light rays are totally reflected. At higher concentrations, almost no light ray experiences total internal reflection. There still is a change in the reflected and transmitted signal according to the Fresnel equations. Anyway, the impact of changes in the refractive index on the output decreases, which degrades the performance of the device. To obtain higher sensitivity for other concentration regions, the center incident angle of the light beam has to be adjusted.

6.5.2 Optimization for low lactose concentrations

To optimize the performance of the sensor system for lowest lactose concentrations and to obtain the smallest value for the detection limit, a design with a reduced incident angle is developed. At reduced incident angle, the working range and with that the region of highest sensitivity will be shifted to smaller values. The optimized device is designed with an incident angle

of 70.0°. Fig. 6.14 depicts the ratio of reflected to transmitted light signal for this design.

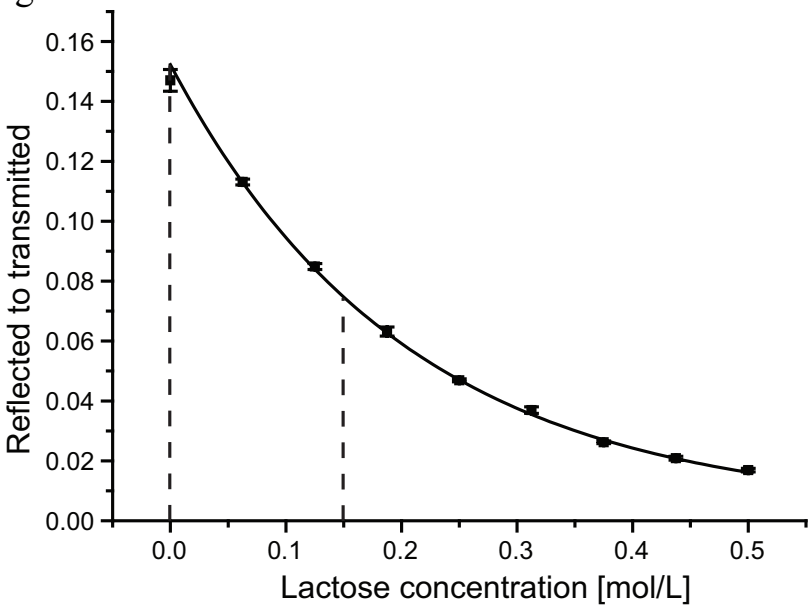

Figure 6.14: Ratio of reflected to transmitted light signal for the device with an incident angle of 70.0°. Compared to the device with an incident angle of 72.5 °, the working range is shifted to lower lactose concentrations. The optimal working range is defined between 0 mol/L and 0.150 mol/L.

Compared to the first device, a clear shift of the working range towards lower lactose concentrations is evident. The gradient of the curve is highest around 0 mol/L, meaning pure DI water. For concentrations exceeding 0.15 mol/L, the sensitivity decreases rapidly, which indicates the end of the optimal working range. In addition to changing the center incident angle to 70.0°, the light coupling region is also optimized. By fine tuning the external fiber coupling, an increased coupling coefficient and with that higher optical power on-chip is achieved while using the same light source. Considering the standard deviation obtained for the device with an incident angle of 70.0°, a smallest detectable change of below 10 mmol/L lactose is anticipated. To demonstrate this capability, lactose concentrations of 0 mol/L up to 100 mmol/L with a step size of 10 mmol/L are analyzed in the device. The obtained results are shown in Fig. 6.15.

For this analysis, four series of measurements are performed on different samples containing the same amounts of dissolved lactose. The variation in the sensor output for a given analyte is in the noise level of the optical setup and hence not detectable. With the optimized device, a discrimination of samples containing different lactose concentrations in a step size of 10 mmol/L is achieved over the entire working range. This step size is

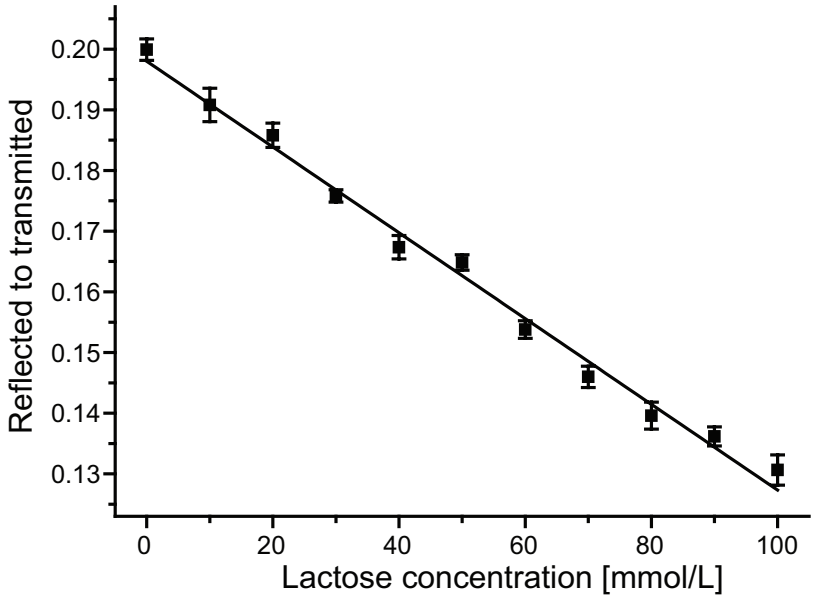

Figure 6.15: Response of the sensor device to dissolved lactose in DI water in the range from 0 to 100 mmol/L. Samples with different lactose concentrations in a step size of 10 mmol/L can clearly be discriminated. Concentration errors and laser power stability issues explain the small deviations from the fitted linear curve.

equivalent to a difference in refractive index of two consecutive samples of 5×10^{-4}. Imperfections in sample preparation (*i.e.*, concentration errors) and instable laser conditions are responsible for the small deviations from the fitted linear curve.

6.5.3 Experiments on off-the-shelf lactose-free milk

For a final evaluation of the performance of the system on a complex mixture, untreated lactose-free milk is taken as the buffer solution. Without any cleaning or washing steps, the lactose-free milk is spiked with known concentrations of lactose. Aliquots are then analyzed in two different devices. Fig. 6.16 depicts the obtained results. Again, four series of measurements are performed on both devices. In the diagrams, an overall increase of the standard deviations is evident. The main reason is the reduced transparency of milk compared to DI water at the employed wavelength (531 nm). The transmitted light signal experiences high absorbance and its impact on the ratio of the reflected-to-transmitted light signal decreases. Reducing the width of the analysis channel would minimize this effect. Furthermore, ingredients of the lactose-free milk (e.g., different types of sugar, salts)

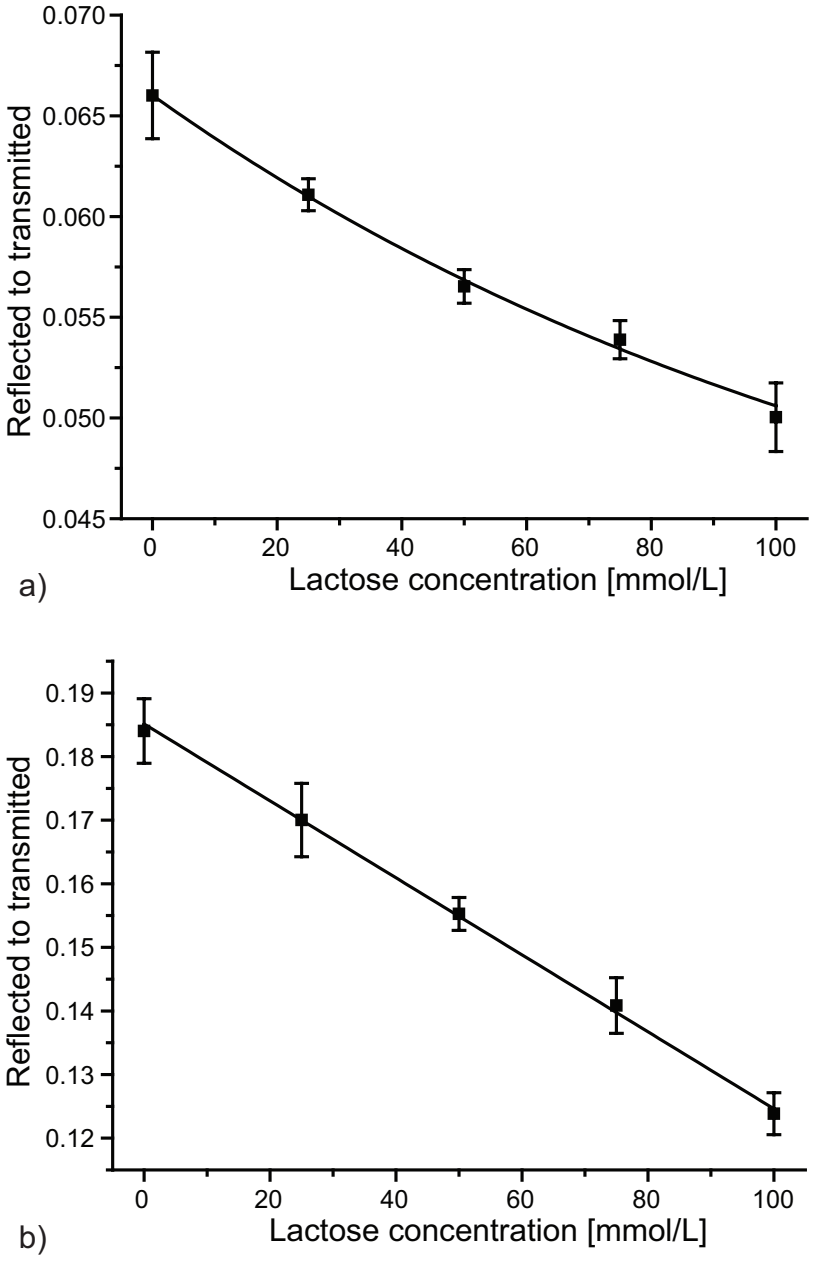

Figure 6.16: Sensor output of two different devices for complex analytes. Known concentrations of lactose are added to untreated lactose-free milk. The high optical absorbance of milk explains the increased standard deviations. (**a**) The device with an incident angle of 70.0° is operating outside the linear region. (**b**) The device with an incident angle of 72.5° allows operation in the linear range. An univocal discrimination of samples in a step size of below 25 mmol/L is feasible.

increase the overall refractive index of the buffer solution. At increased refractive indices, the device with an incident angle of 70.0° (Fig. 6.16a) is working outside the linear region. Using a device optimized for higher

refractive indices (incident angle of 72.5°, Fig. 6.16b) allows operation in the linear region again. Samples containing different concentrations of dissolved lactose in a step size of below 25 mmol/L can clearly be distinguished in the range of 0 to 100 mmol/L.

6.6 Determination of ethanol contents

As another application, a sensor optimized for the determination of ethanol contents is investigated [90,91]. The design of the device is followed by the results section proving the functionality of the system.

6.6.1 Device design

Fig. 6.17 illustrates the working principle of the device. Using a glass fiber

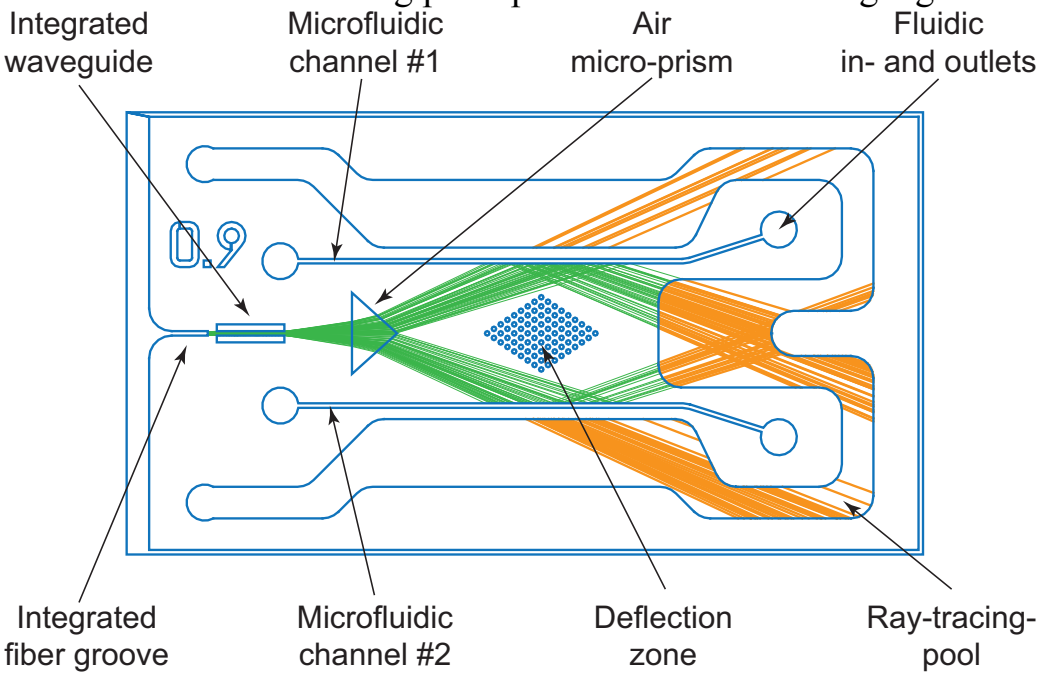

Figure 6.17: Schematic of the working principle for the determination of ethanol contents. Laser light (green) is expanded by an air micro-prism. Depending on the analytes light is partly transmitted through and partly reflected by the microfluidic channels. A ray-tracing pool is used for visualization of the exiting light rays (orange).

clamped into an integrated fiber groove, light is guided from the external light source onto the chip. An integrated waveguide ensures defined light conditions (light alignment and divergence) on-chip. The most essential

parts of the device are the air micro-prism and the two microfluidic channels. Defined by the shape of the prism, the two microfluidic channels are hit by light rays with different incident angles. Depending on the refractive indices of the analytes in the channels, and hence on their ethanol contents, at these solid-liquid interfaces incident light rays above the critical angle experience total internal reflection while the rest is partially transmitted. Both, the reflected as well as the transmitted light rays are visualized in a ray-tracing-pool (filled with a fluorophore). Digital image processing is then applied to calculate a ratio of reflected and transmitted light at the microfluidic channel #1, giving a measure for the ethanol content. The microfluidic channel #2 filled with DI water provides a reference value to minimize any errors in the measurements caused by, e.g., variations in laser light intensity. The devices are fabricated in PDMS and bonded to a glass microscope slide (Fig. 6.18).

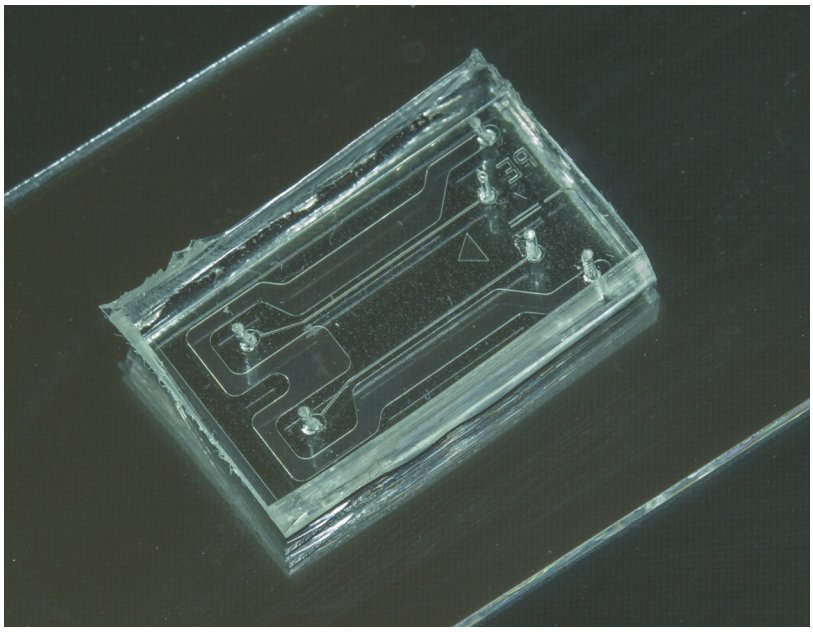

Figure 6.18: Photograph of the device for the analysis of the ethanol level in liquids. The PDMS device is bonded to a glass microscope slide.

6.6.2 Ethanol measurements

For the determination of the reflected and the transmitted light signals, the excited fluorescence in the ray-tracing pool is detected by an optical long-pass filter and a CCD camera. The captured images are segmented into 4 x 6 elements (Fig. 6.19). After gray-scale converting, segments 2/2 and 2/3 are integrated to obtain a value representing the transmitted light signal

of microfluidic channel #1. For the reflected light signal segments 3/3 and 3/4 are integrated. At the microfluidic channel #2 an analogous procedure is applied.

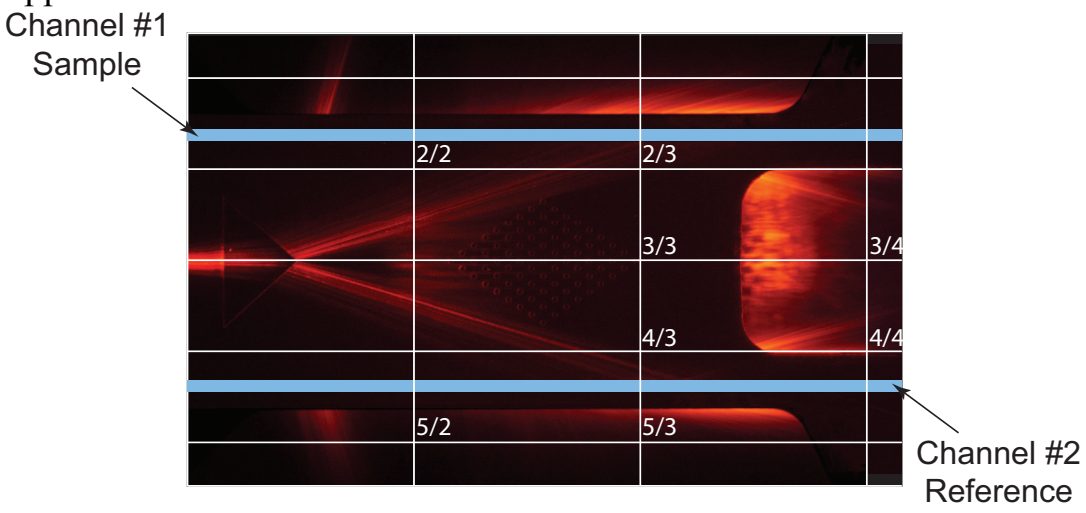

Figure 6.19: Fluorescence image taken during the analysis. Raster segments 2/2 and 2/3 are integrated for the transmitted signal of channel #1. Segments 3/3 and 3/4 represent the reflected signal of channel #1. Segments 5/2 and 5/3 as well as 4/3 and 4/4 are integrated in the same manner for channel #2. The blue lines in the figure illustrate the two microfluidic channels.

The results of ray tracing simulations and experimentally obtained values are illustrated in Fig. 6.20a and Fig. 6.20b, respectively. An increase in the ratio of reflected and transmitted light signal with decreasing ethanol concentration is evident in both diagrams.

In contrast to the experiments, the simulation results exponentially increase towards very high values for lower concentrations. This trend is suppressed in reality by an offset of the transmitted light signal. The working range can be defined by adapting the air micro-prism. The transitional phase of the fitted sigmoid curve (Device 84° and 90°) defines the lower end of the working range. At these points, the transmitted signals converge to the offset value and no significant change occurs anymore.

6.7 Characterization of micro-droplets

As another application, the sensor is optimized for the characterization and identification of micro-droplets. Implementing a similar sensor design as for the investigation of liquid concentrations, this device has proven suitable for counting, sizing, and identifying droplets in a flow-through manner.

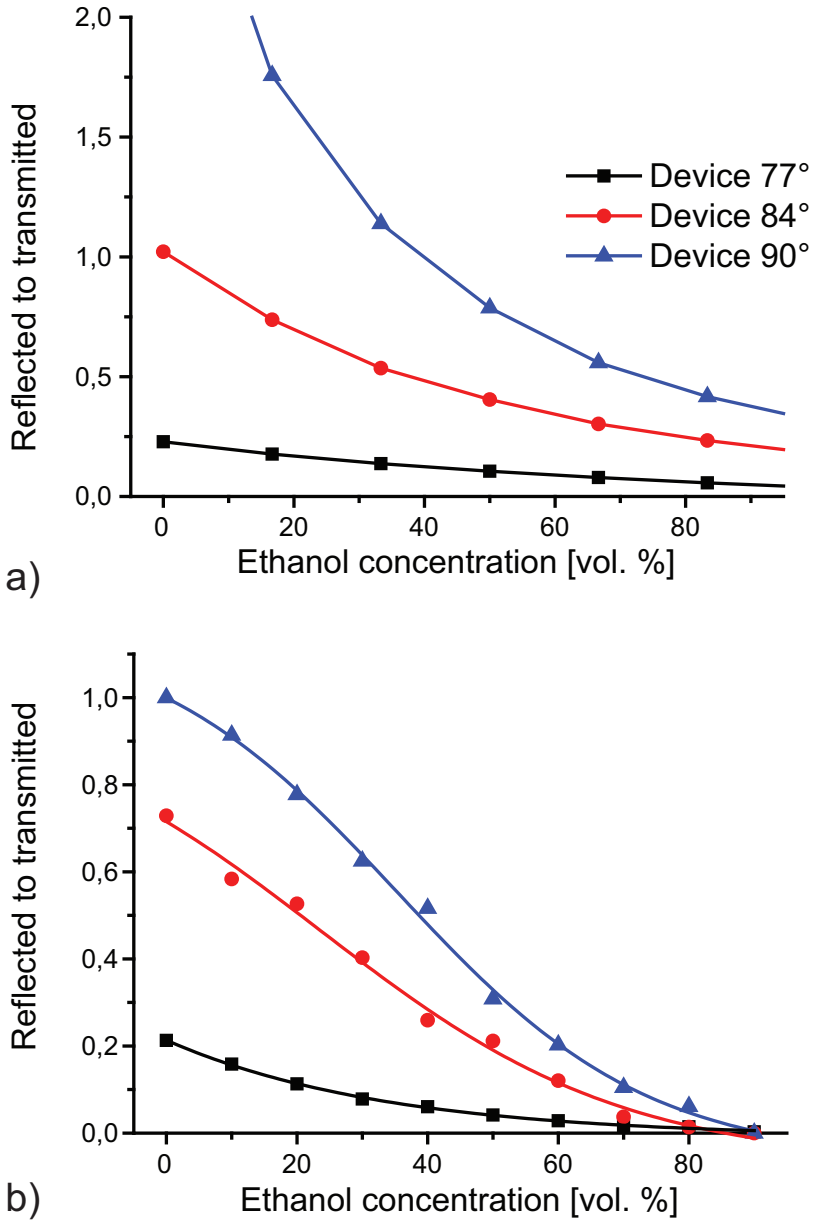

Figure 6.20: (a) Simulation results (ZEMAX, USA) for different ethanol concentrations. The ratio of reflected and transmitted light signals increases with decreasing alcohol content. Changing the angle of the incident light (by adapting the air micro-prism) results in different characteristics. Working ranges: Device 77° below 10%; Device 84° between 10 and 50%; Device 90° between 40 and 80%. **(b)** Experimentally obtained ratios of reflected and transmitted light signals measured on three different devices. The working ranges agree with those of the simulations.

6.7.1 Motivation

In the last decades, microfluidics has shown its capability of manipulating liquids on the microscale for various applications. Especially biological and medical analysis systems benefit from its novel possibilities [19, 92]. One limitation for applications in these disciplines often is the available sample volume. Small amounts should be sufficient for the analysis. As a new subfield of microfluidics, micro-droplets enable the formation of encapsulated environments with volumes in the range of pico-liters [93, 94]. Two or more immiscible fluids [95] are brought into the same channel and allow the controlled appearance of emulsions on-chip. Recent works have demonstrated manipulation of micro-droplets through microfluidic channel systems [96–99]. Zagnoni *et al.* [25] have shown coalescence of distinct droplets which facilitates fully controlled reactions on-chip. Investigated applications of micro-droplets include chemical and biochemical screening [100, 101], enzymatic assays [102], and single cell encapsulation [103, 104].

The monitoring of micro-droplets is as important as their generation and manipulation. Information about the volume and the content of the droplets allow one to accurately observe and detect changes during the performed experiments, such as cell growth or chemical reactions. Therefore, reliable and fast in-line characterization methods are required. For the analysis of particles and cells micro-flow cytometry is a promising approach for high-throughput screening [11, 105]. Fattaccioli *et al.* [106] utilized a bench-top flow cytometer which also allows the analysis of micro-droplets. Nevertheless, for systems dealing with micro-droplets, the monitoring is mostly performed using conventional light microscopes requiring bulky and expensive equipment. Different approaches have already been followed to realize integrated read-out systems. One approach employs a capacity sensor allowing on-chip detection and control of droplets [107]. Srisa-Art *et al.* [108] used an external optical setup for the detection of single DNA molecules based on fluorescent labeling. In other works, an optical interrogation point has been directly integrated on-chip [109–111]. In those works, the optical path is arranged perpendicular to the microfluidic channel. If droplets are passing this channel, the curvatures on both sides of the droplets result in light deflections which are detected in the signal recorded by an external avalanche photodiode. Droplets were analyzed with a throughput of 2.5 Hz. In that setup, there is no information gathered while the body of elongated droplets is passing the interrogation point. The height of the peaks in the signal is solely dependent on the radii of the droplet curvatures which, on the other

hand, is dependent on the contact angles of the employed liquids and the device material. Contact angles close to 90° could be critical for that principle. On the device presented by Shen *et al.* [112] a collimated light beam is directed towards a microfluidic channel. The reflected light signal is subsequently detected and used to derive information about the droplet size and content. In the following sections, an optofluidic sensor device is presented which exploits total internal reflection phenomena at the solid-liquid interface to characterize droplets in a microchannel.

6.7.2 Device design

The devices are fabricated in dry resist laminated on a polyester foil bonded to a PMMA microscope slide. The fluidic connections are managed by PTFE tubings glued to the microscope slide (Fig. 6.21).

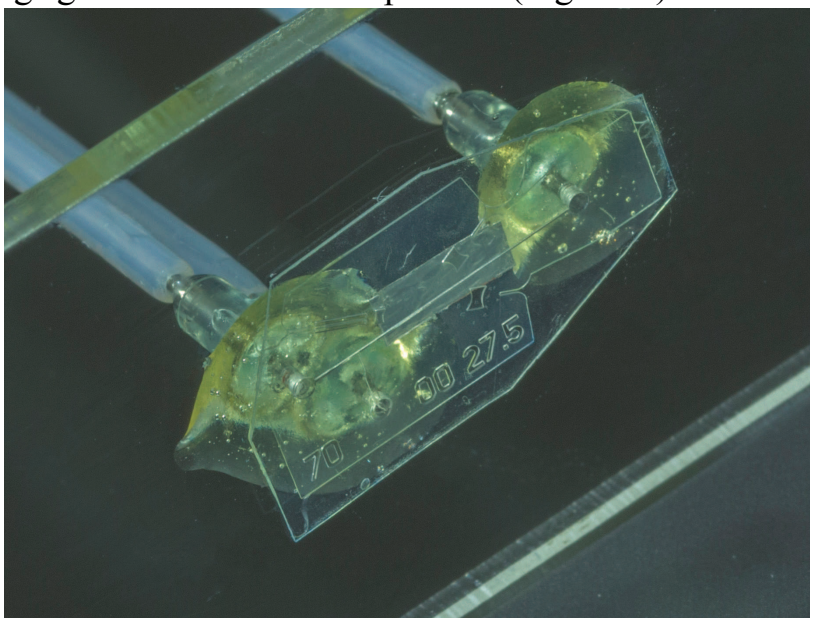

Figure 6.21: Photograph of the device for the analysis of micro-droplets. The dry resist devices on a polyester foil are bonded to a PMMA microscope slide. PTFE tubings are glued to the microscope slide to provide fluidic connections to the channels on the chip.

Fig. 6.22 depicts a schematic of the device design. Compared to the analysis of liquid concentration the liquid input region is adapted. A second fluidic inlet is placed on the device. A simple T-junction on-chip allows a stable formation of micro-droplets. The optical part of the device is identical to the one used for the study of liquid concentrations.

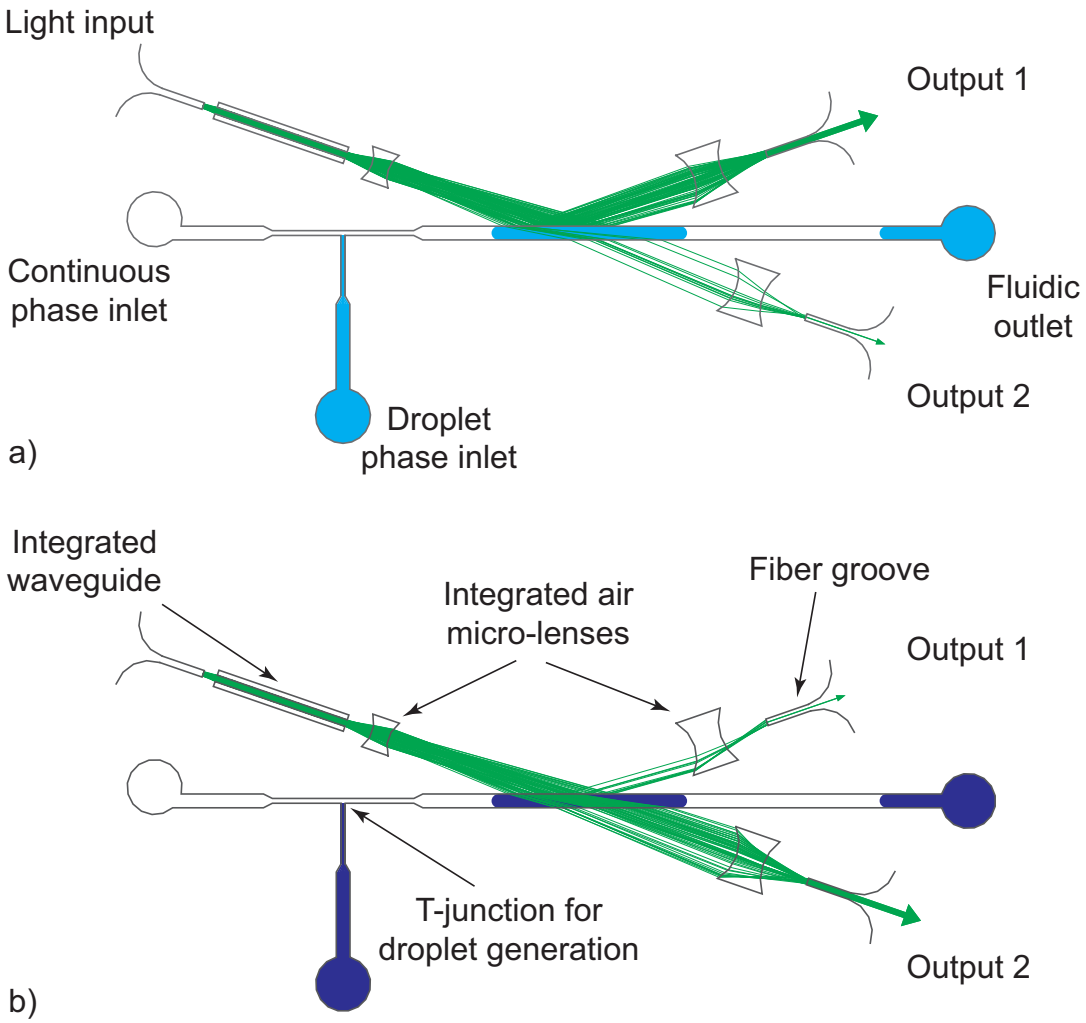

Figure 6.22: Illustrative schematic of the sensing principle; droplets having **(a)** a low refractive index result in a high signal in output 1 and a small signal in output 2; **(b)** a high refractive index result in a small signal in output 1 and a high signal in output 2.

6.7.3 Detection of micro-droplets

Droplets passing the interrogation point result in changes in both the reflected and the transmitted light signals. Due to the low refractive index of the droplet, the reflected light signal increases while the transmitted decreases simultaneously. Applying a peak-detection algorithm at either of those two signals allows the detection of single droplets. This peak-detection can be used to count droplets. In Fig. 6.23 signals recorded at the reflected output for two different droplet generation frequencies are shown.

Applying this procedure, droplets are successfully counted up to 320

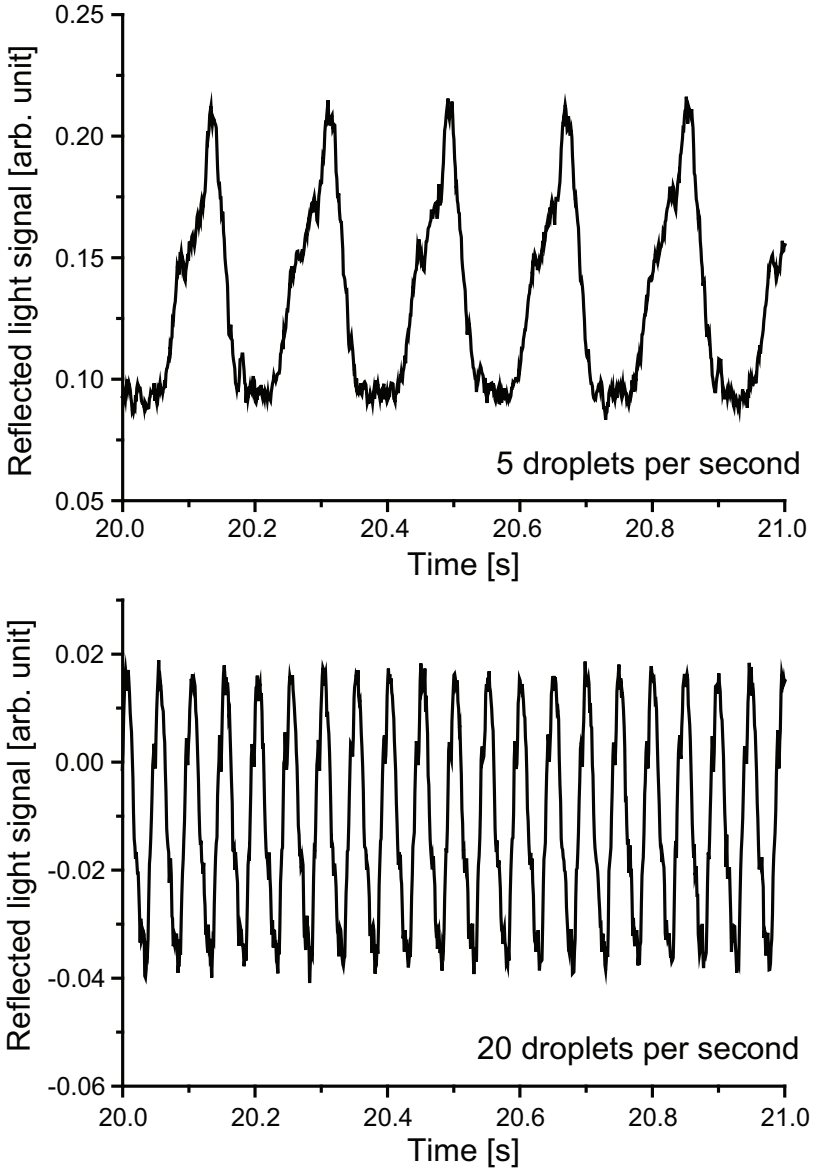

Figure 6.23: Signals recorded at the reflected output for two different droplet generation frequencies. Each peak in the signals represents a single droplet passing the interrogation point.

droplets per second. Above a droplet generation frequency of 320 droplets per second, the T-junction does not allow a stable formation of droplets anymore. At higher frequencies two streams of liquid, DI water next to oil, are achieved rather than a break-up into individual droplets. Implementation of other droplet generation units (e.g. cross-junction) would solve this issue. The proposed analysis principle itself is not limited here and can be applied for higher droplet generation frequencies as well.

6.7.4 Sizing of micro-droplets

Droplets of different shape generate different peaks in the reflected and the transmitted signals. In Fig. 6.24 elongated droplets, squeezed inside the channel as well as small spherical droplets are depicted. The droplet shape is defined by alternating the flow velocities of droplet and continuous phase. The total flow rate is kept at 6 µL/min.

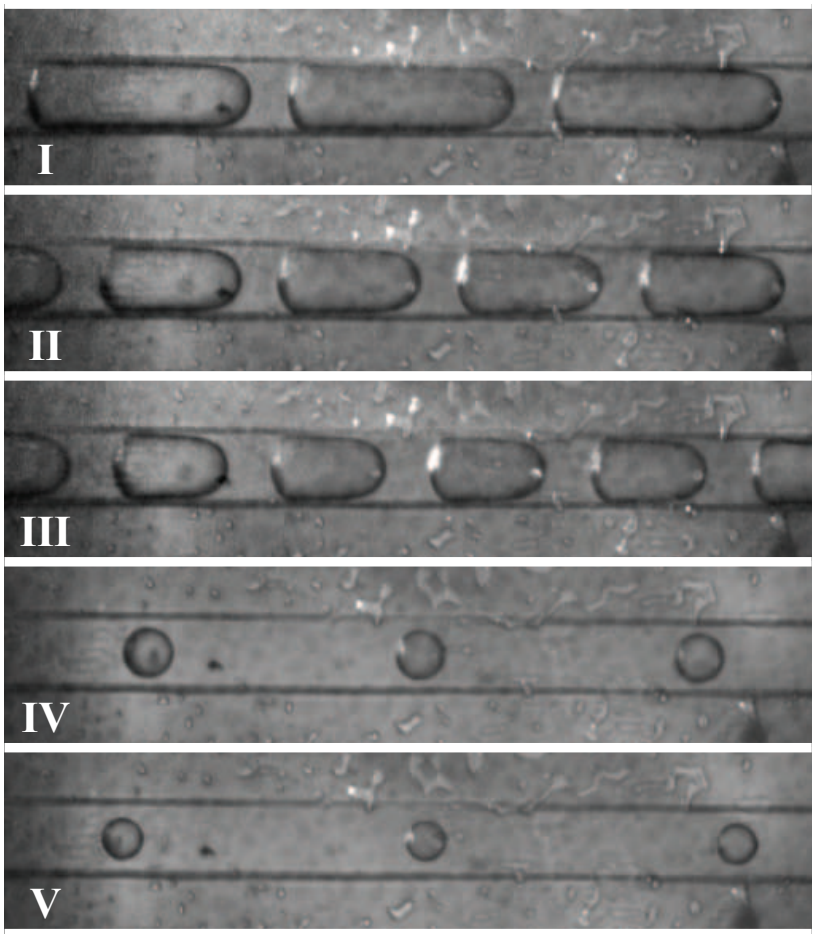

Figure 6.24: Micrographs of five droplet shapes. Elongated (I+II+III), as well as spherical droplets (IV+V) are shown. Depending on the droplet shape different peaks in the signals are obtained. The width of the microfluidic channel is 100 µm.

Both signals are examined separately. Each individual peak generated in the reflected signal by a passing droplet is integrated over time. The obtained values for all investigated droplet shapes are given in Fig. 6.25. For elongated droplets (shapes I, II, and III), the reflected signal can be used for sizing. The obtained values are clearly separated. With decreasing droplet size, the peaks in the reflected signal decrease proportionally. Once the droplet shape changes from elongated to spherical, an univocal discrimination of the droplets cannot be provided anymore. The obtained values

clearly overlap (shapes IV and V).

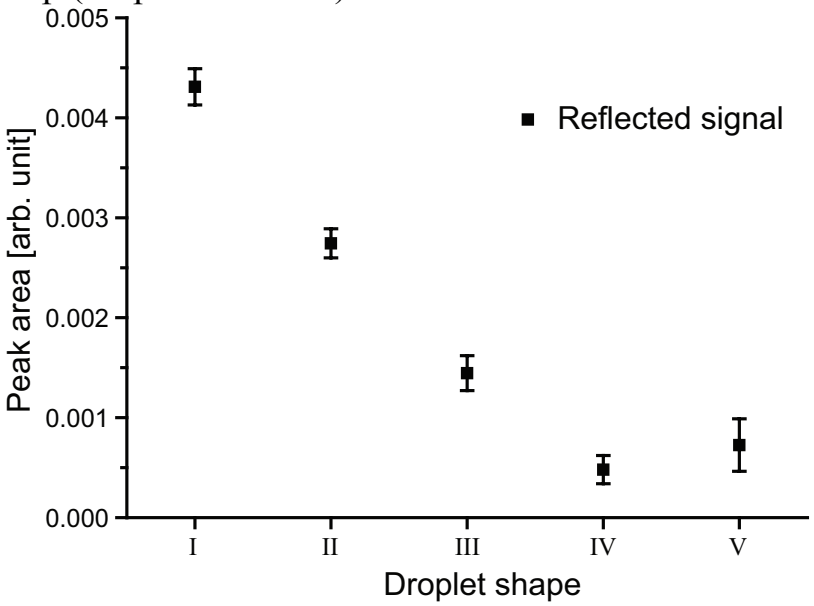

Figure 6.25: Peak integration applied on the reflected light signal for different droplet shapes. Elongated droplets (I, II, and III) can be discriminated. Spherical droplets not or hardly touching the channel walls result in a poor separation based on the reflected light signal (IV and V).

For the transmitted signal, the same procedure is applied. Each individual peak generated by a single droplet is integrated over time and plotted in Fig. 6.26. The behavior is the contrary compared to the analysis of the reflected signal. For elongated droplets (I, II, and III), no separation is possible. With decreasing droplet size the peaks in the transmitted signal increase. For spherical droplets (IV and V), a well-defined separation based on the droplet size is achieved. Exploiting the information obtained from both signals, droplets can be sized over a huge range of dimensions. Elongated as well as spherical droplets can be examined on one and the same device.

6.7.5 Identification of micro-droplets

The height of the reflected and the transmitted signals depends on the refractive index of the droplet phase. This circumstance can be exploited for the identification of the droplet content. Fig. 6.27 illustrates an univocal discrimination of 5 M $CaCl_2$ and DI water droplets. For both kind of droplets, the peaks in the reflected and transmitted signals are again integrated individually. The corresponding values of reflected and transmitted peak integration are then subtracted for each droplet and printed in the histogram.

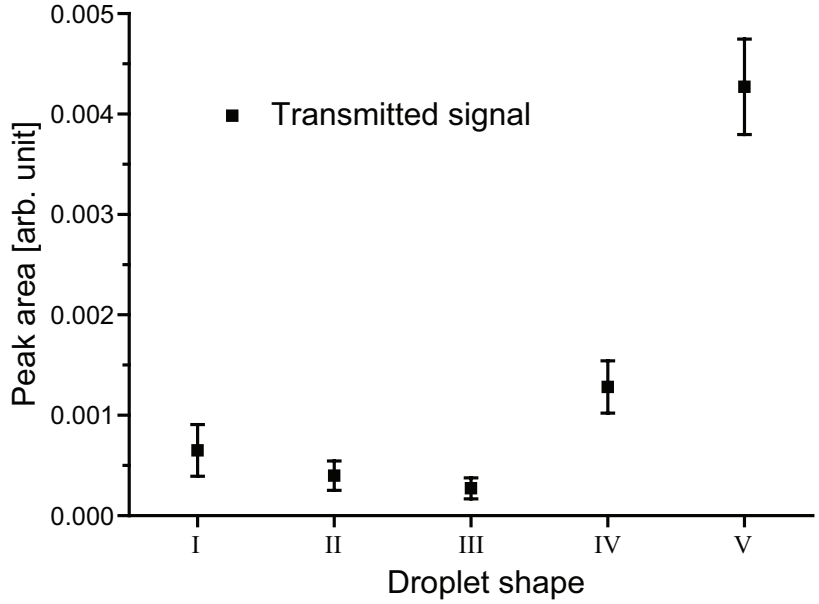

Figure 6.26: Peak integration applied on the transmitted light signal for different droplet shapes. Elongated droplets (I, II, and III) cannot be discriminated. Spherical droplets not or hardly touching the channel walls result in an excellent separation based on the transmitted light signal (IV and V).

To investigate the capability of the device to identify smallest changes in the droplet content, $CaCl_2$ solutions at different concentrations are sequentially used as droplet phase. The obtained results are given in Fig. 6.28. In this experiment, the total flow rate is set to 1.5 µL/min (continuous phase: 0.5 µL/min; droplet phase: 1 µL/min). The resulting droplet generation frequency is approx. 4.5 droplets per second. For each $CaCl_2$ concentration about 100 micro-droplets are analyzed.

With increasing $CaCl_2$ concentration, the refractive index of the droplet increases [83]. At higher refractive indices, the amount of transmitted light increases while the reflected signal decreases simultaneously. The results indicate highest sensitivity of the device at a $CaCl_2$ concentration of 5 M. In that region, changes in the concentration of approx. 70 mM can be detected. The range of sensitivity can be optimized for other refractive indices by redesigning the optical elements.

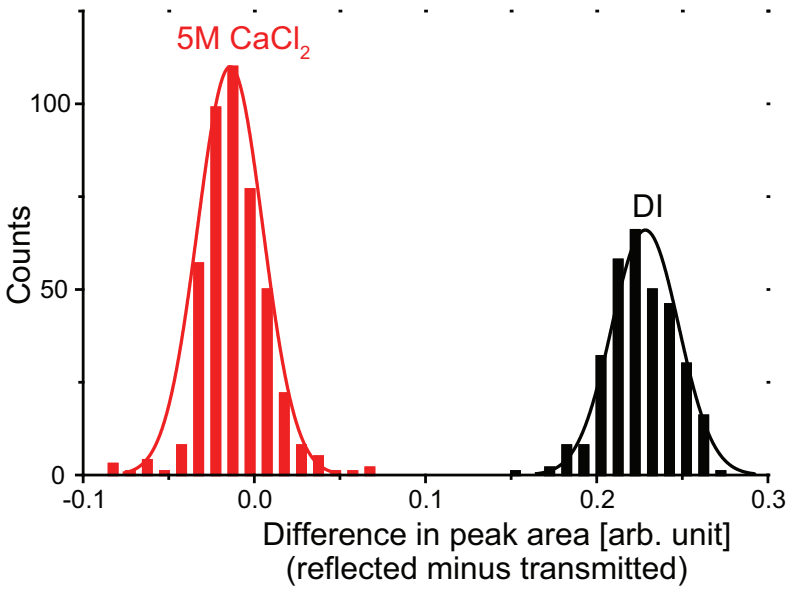

Figure 6.27: Difference in peak area of reflected and transmitted light signal of DI and 5 mol/L $CaCl_2$ droplets printed in a histogram. DI droplets, having a low refractive index (n of 1.33) result in more reflected and less transmitted light. Droplets containing 5 mol/L $CaCl_2$ (n of 1.44) result in a lower reflected and a higher transmitted signal. A full baseline resolved separation of the two clusters is achieved.

6.8 Conclusion

The presented sensor principle proved suitable for the detection of liquid concentrations in the range of a few tens of mmol/L to 5 mol/L. The typical resolution amounts to approx. 10 to 40 mmol/L depending on the investigated sample. The large working range provides high flexibility in application of the device. The simultaneous detection of two signals, reflected and transmitted, gives a permanent verification of the results. In addition, the use of the signal ratio for the sample analysis compensates for fluctuations in the light intensity due to laser instabilities which would destroy any validity in single signal approaches. The characterization of micro-droplets is another application of this device. In a simple and fast way, droplets are characterized based on different properties and provide valuable information for further analyses.

Especially the robustness, its simplicity and hence the ease in fabrication, and the tunability of the characteristics of the presented optofluidic analysis chip allow for sensitive, cost effective, flow-through, and non-invasive sensor implementations.

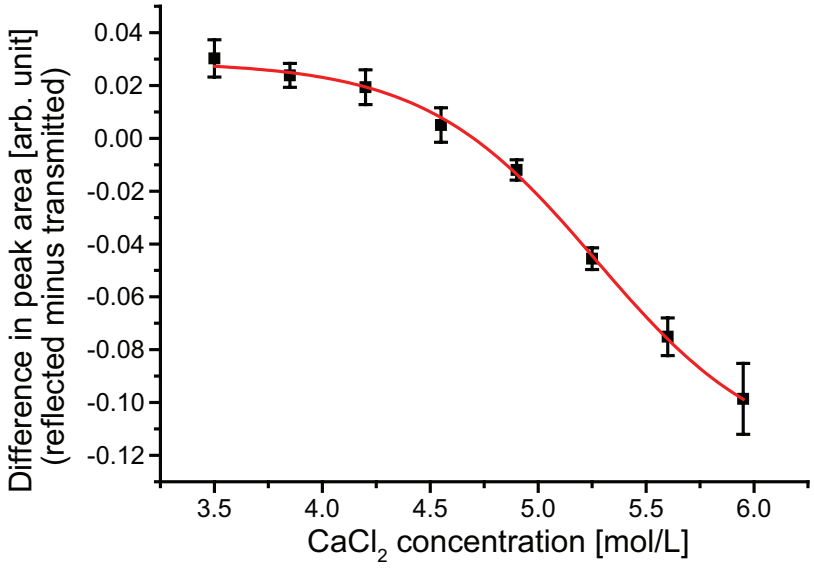

Figure 6.28: Difference in peak area of reflected and transmitted light signal for different $CaCl_2$ content in the droplets. The difference decreases with increasing refractive index meaning increasing $CaCl_2$ concentration. At approx. 5 M the device shows highest sensitivity. This range of sensitivity can be shifted by re-dimensioning of the optical elements on-chip.

Chapter 7

Conclusions and future perspectives

The dedicated goal of this thesis is the design and fabrication of applicable optofluidic sensing units for medical or biological purposes. Here the focus is to demonstrate optofluidics as a powerful tool providing extended functionality to the operator. The set objectives were achieved by the sensing system for liquid concentrations. Next to the development of this sensor device, an optofluidic actuator was realized and the new field of thermo-optofluidics was introduced for the first time. In the following sections, the major achievements of this thesis are shortly summarized and future perspectives are given.

Optofluidic light modulation

An optofluidic principle was exploited to design a fully functional on-chip light modulation unit. The focus was on operation without any mechanically moving elements. Furthermore, a minimum of peripheral equipment should be attached to end up with a compact overall system. The designed system features two microfluidic channels and micro-air lenses at the light in- and output region. Depending on the solutions in the two channels, the incident light is either fully transmitted or totally reflected at the solid-liquid interface. As required, the design has no mechanically moving elements integrated which ensures stable operation. Three possible light exiting positions can be randomly selected. The design is built such that further light exiting positions can easily be implemented. Besides the external light source no further peripheral instruments are needed. Since no restricted inflow conditions are required, the solutions can be filled in the channels in any way even by means of manual injection. In an experimental evaluation, the system has proven its functionality. The output was recorded by externally attached photodetectors and a clear on-off switching was demonstrated. In

future, this optofluidic light modulator can be integrated for on-chip fluorescence applications where the exposure time as well as the excited region has to be well confined. Providing multiple light exiting positions different parts of the analytes can be exposed one after each other in a well defined sequence.

Thermo-optofluidics

Thermo-optofluidics is a new subfield of optofluidics and was introduced in the course of this thesis for the very first time. It exploits the exceptional circumstance that with changing temperature the refractive index of solids and liquids change in opposite directions. This effect can be utilized to substantially increase the effective thermo-optic coefficient of optical elements implementing both liquids and solids. Using this concept, a light modulation unit was designed based on a liquid core solid cladding waveguide. At room temperature, this assembly provides the necessary difference in refractive index of core and cladding to allow wave guiding by total internal reflection. At altered temperature the refractive index of the liquid core decreases whereas the refractive index of the solid cladding increases. In that sense, light confinement inside the core of the waveguide is reversibly turned off. The practical experiments proved the functionality of the developed design. The output of the core of the waveguide was recorded by an external photodetector. The pulsed temperature profile triggered a shortly delayed on-off signal. For this evaluation, the temperature changes were introduced into the device by an underlying Peltier element. The integration of a thermo-element directly on-chip would drastically shorten the reaction time and allow higher modulation rates. This concept is unique and compared to thermo-optic devices solely based on solids, the effective thermo-optic coefficient is more than doubled allowing on-off modulations to be performed at less than half the temperature change. Assuming a linear heating rate of the assembly more than twice the modulation frequency can be achieved at the same input power.

Optofluidic sensing system

The main goal of this thesis was the design and development of an optofluidic sensing unit for biological/medical purposes. The developed device for the determination of liquid concentrations fully satisfies this objective. The

system is based on partial total internal reflection at the solid/liquid interface. The analyte is passed through the device in a straight microfluidic channel. This channel is hit by a slightly diverging light beam. Depending on the constitution of the analyte and hence its refractive index, a certain amount of the incident rays is totally reflected whereas the other part is transmitted as well. Both signals, the reflected as well as the transmitted one, are recorded. A ratio of those two signals is then used as a measure of the concentrations of certain molecules in the sample. The unique benefits of this system are the diverging light beam resulting in a span of incident angles and the recording of two read-out signals. Compared to analysis systems based on collimated beams, the diverging beam provides a linear relation between refractive index and reflected light intensity. This allows the optimal operation of the system over an increased working range. The use of the signal's ratio drastically improves the stability of the results. The outcome is not influenced by external parameters such as variations in the input power of the incident light beam. Furthermore, the system consists of just a few peripheral instruments allowing a space optimized measurement setup. Since the developed analysis principle doesn't need any visual inspection, all the experiments can be performed without an optical microscope which is one of the major space requiring factors in standard measurement systems for this application. Another feature of the designed analysis setup is its versatility. The system can be applied for the determination of any dissolved molecules as long as they have an adequate impact on the refractive index. In summary, a stable, compact, and versatile easy-to-use tool has been realized which is well suited for the field of biological sample analyses as well as for medical diagnosis applications.

Future perspectives

For each of the elaborated designs, a demonstrator was built up to prove its functionality. Although the sensing part of the systems, the optofluidic devices, were fully integrated on-chip not much attention was paid to the miniaturization of the peripheral setup. In future, the integration of all the system components should be tackled to develop the system towards handheld point of care analysis devices. Especially the integration of the light source, e.g. a diode or a laser diode, could be a big step towards applicable and user friendly devices. This would mean microfluidic elements and conventional semi-conductor technologies on one and the same chip.

Besides the pursuit for miniaturization of the overall systems, further research could be conducted to exploit the potential of optofluidics to a bigger extend. The developed sensing device was optimized for the analysis of concentrations of molecules of the same type. Here an excellent limit of detection could be achieved. Nevertheless, the device is not capable of distinguishing more than one type of dissolved molecule. One attempt to optimize the system in this direction could be a finger-print screening. Instead of using a monochromatic light source, multiple characteristic wavelengths can be used for the analysis. Each single wavelength could be chosen carefully to match the behavior of the refractive index change of the individual molecules. In such a way information about more than one dissolved molecule can be gathered.

The field of thermo-optofluidics was introduced and as a proof of concept an on-chip light modulator was built up. This was the very first step to demonstrate the functionality. Besides this application, one could also think of thermo-optofluidic sensing units. Exploiting the proposed principle in the reverse direction, highly accurate on-chip temperature sensors can be realized. The combination of the optical properties of solids and liquids allows the drastic improvement in performance of several thermo-optic systems solely based on solids and should be considered as a novel powerful tool.

Within the last years, optofluidics has evolved from just an idea to a powerful tool for on-chip analysis systems. Novel phenomena arise and can be exploited for different applications. The results of this thesis demonstrate the applicability of such systems in practical applications. It should provide a link between laboratory based and application oriented research. The work should serve as a reference and inspire future research in optofluidics since its limits are still far from being reached.

Acknowledgments

Success has many parents! The name under this thesis is mine, but the people behind who made this work possible deserve as much credit as I do. At the end of more than four years of work I would like to express my deepest gratitude to those who paved the way for this success.

Particular thanks go to Michael Vellekoop, my PhD supervisor, the one who initially pushed me to choose this way. Besides giving me the opportunity to work within his research group he inspired me in many technical aspects. He introduced me to the field of optofluidics and invited me to participate in international research activities which I enjoyed a lot. He has become my mentor throughout all this years of work. Dank je wel, Michiel!

Many thanks to Peter Verhaert from the Delft University of Technology for giving me the chance to join his analytical biotechnology group for the first period of my PhD. Additional thanks go to Martijn Pinkse for introducing me to the field of mass-spectrometry based protein analysis and for being a great soccer partner. During my time in the Netherlands I have found great new friends in Geisa and Joseph Evaristo, and Shrikanth Hari. Thanks for all the funny moments we have spent together!

I would like to thank Franz Keplinger from the Vienna University of Technology where I spent the second period of my PhD. He has supported me in technical questions and has critically reviewed our joint publications. Thanks also to my dear colleagues at the Institute of Sensor and Actuator Systems Dietmar Puchberger-Enengl, Christoph Haiden, and Martin Smolka for providing a pleasant working atmosphere at the institute and for having a beer together once in a while.

Many thanks to Mahmuda Akthar, Sander van den Driesche, and Lukas Brandhoff from the Institute for Microsensors, Actuators and Systems at the University of Bremen for accompanying me during the last year of my PhD. Special thanks to Sander, my office mate at the institute, who advised me in how to effectively finalize my thesis. Furthermore, thanks to all the technicians from the Delft University of Technology, the Vienna University of Technology, and the University of Bremen who supported me in biotechnology and micro-fabrication issues.

Many thanks for the financial support to the European Marie-Curie Ini-

tial Training Networks,"CellCheck - On-chip cell handling and analysis" project number MCRTN-CT-2006-035854 and "EngCaBra - Biomedical engineering for cancer and brain disease diagnosis and therapy development" project number PITN-GA-2010-264417. Additional thanks to all the colleagues in those two projects for being valuable discussion partners on different topics. Special thanks to Christine Hafner, Daniela Pucciarelli, and Heimo Breiteneder from the Medical University of Vienna for conducting infrared measurements on human biopsies and for sharing medical know-how.

Above all, however, the boundless support of my family was the key to my success. I am blessed with my parents Mechthilde and Gerhard. There is no way to express my gratefulness to the full extent. You have taught me the tools for life which made me the person I am today. Far from being perfect, but happy to be who I am.

Thanks to my two sisters Barbara and Elisabeth, and my brother Simon. Each one in her/his own way has given me strength to make my way through life. I will be happy to give you back all the great energy I have received from you.

At the end of my acknowledgments but on first place in my life I would like to say thank you to my wife Sylvia. You have convinced me of my own work in situations where I had lost sight of my goal. You have listened to my doubts and wiped them away with your positive attitude. Together with our son Samuel you are my rock in the waves. Thanks for being you!

List of Publications

Journal Papers

E. Weber and M. J. Vellekoop, "Optofluidic micro-sensors for the determination of liquid concentrations." *Lab on a Chip*, vol. 12, no. 19, pp. 3754–3759, Aug 2012. doi:10.1039/c2lc40616k. [Online]. Available: http://dx.doi.org/10.1039/c2lc40616k

E. Weber, F. Keplinger, and M. J. Vellekoop, "Detection of dissolved lactose employing an optofluidic micro-system," *Diagnostics*, vol. 2, no. 4, pp. 97–106, 2012. doi:10.3390/diagnostics2040097. [Online]. Available: http://www.mdpi.com/2075-4418/2/4/97

E. Weber, F. Keplinger, and M. J. Vellekoop, "On-chip light modulation applying optofluidic principles," *IEEE Sensors Journal*, vol. accepted, 2013.

E. Weber, D. Puchberger-Enengl, F. Keplinger, and M. J. Vellekoop, "In-line characterization and identification of micro-droplets on-chip," *Optofluidics*, vol. 1, pp. 11–18, 2013. doi:10.2478/optof-2013-0002

Proceedings International Conferences

E. Weber, F. Keplinger, and M. J. Vellekoop, "Optofluidic, contact-free 1x3 light-switch fabricated on a mono-layer device," in *Proc. of the 3rd European Conference on Microfluidics*, Heidelberg, Germany, 2012.

E. Weber, D. Puchberger-Enengl, and M. J. Vellekoop, "In-line characterization of micro-droplets based on partial light reflection at the solid-liquid interface." in *Proc. of the ASME 2012 10th ICNMM*, Puerto Rico, USA, 2012, pp. 589–595. doi:10.1115/ICNMM2012-73155

E. Weber and M. J. Vellekoop, "Thermo-optofluidics - on-chip light modulation as an application," in *Proc. of IEEE Sensors*. IEEE, 2012, pp. 1–4. [Online]. Available: http://ieeexplore.ieee.org/xpls/abs_all.jsp?arnumber=6411223

E. Weber, F. Keplinger, and M. J. Vellekoop, "Optofluidic analysis system for ethanol solutions," *Procedia Engineering*, vol. 47, pp. 651–654, 2012. [Online]. Available: http://www.sciencedirect.com/science/article/pii/S1877705812042944

E. Weber, M. Rosenauer, P. D. E. M. Verhaert, and M. J. Vellekoop, "Optofluidic microsystem for on-chip l2-waveguide modulation featuring flow stabilization and a novel input coupling region." *Procedia Engineering*, vol. 5, pp. 452–455, 2010. [Online]. Available: http://www.sciencedirect.com/science/article/pii/S1877705810006910

Other publications

M. J. Vellekoop and E. Weber, "Microfluidics and optofluidics for sensing applications," in *Hauptvortrag: 13th Meachatronics Forum, Linz (invited) 2012*.

D. Puchberger-Enengl, E. Weber, C. Krutzler, and M. J. Vellekoop, "Flexible microfluidics: Low cost fabrication of plastic lab-on-a-chip devices," in *Informationstagung Mikroelektronik 2012*, 2012.

Publications Related to other Projects

Journal Papers

E. Weber, M. W. Pinkse, E. Bener-Aksam, M. J. Vellekoop, and P. D. Verhaert, "Miniaturized mass-spectrometry-based analysis system for fully automated examination of conditioned cell culture media," *International journal of proteomics*, vol. 2012, 2012. doi:10.1155/2012/290457. [Online]. Available: http://www.hindawi.com/journals/ijpro/2012/290457

M. Rosenauer, E. Weber, J. Stampfl, and M. J. Vellekoop, "Optofluidische komponenten in der flüssigkeitssensorik optofluidic elements in liquid-based sensor systems," *tm-Technisches Messen*, vol. 77, no. 2, pp. 89–94, 2010. [Online]. Available: http://www.oldenbourg-link.com/doi/pdf/10.1524/teme.2010.0019

Proceedings International Conferences

E. Weber, M. Rosenauer, W. Buchegger, P. D. E. M. Verhaert, and M. J. Vellekoop, "Fluorescence based on-chip cell analysis applying standard viability kits." in *Proc. of the microTAS 2011*, Seattle, USA, 2011, pp. 1716–1718. [Online]. Available: http://www.rsc.org/images/LOC/2011/PDFs/Papers/573_0465.pdf

E. Weber, I. Finoulst, P. Vazquez, W. Svendsen, H. Walgraeve, E. Bener-Aksam, M. W. Pinkse, and P. Verhaert, "Microfluidics for in-line analysis of peptide based cell-to-cell communication in yeast cultures by mass spectrometry," in *Proc. of Netherlands MicroNano Conference*, 2010.

E. Weber, I. Finoulst, P. Vazquez, W. Svendsen, M. W. Pinkse, E. Bener-Aksam, and P. Verhaert, “In-line identification of peptides secreted from yeast cells by use of tandem mass spectrometry,” in *Proc. of 1st AB Sciex European Conference on MS/MS*, 2010.

C. Haiden, T. Wopelka, M. Jech, D. Puchberger-Enengl, E. Weber, F. Keplinger, and M. J. Vellekoop, “A microfluidic system for visualisation of individual sub-micron particles by light scattering,” *Procedia Engineering*, vol. 47, pp. 680–683, 2012. [Online]. Available: http://www.sciencedirect.com/science/article/pii/S1877705812043019

L. Brandhoff, E. Weber, S. van den Driesche, M. Bü lters, R. B. Bergmann, and M. J. Vellekoop, “Optofluidic multiplexing and switching device,” in *Solid-State Sensors, Actuators and Microsystems Conference, 2013. Transducers 2013. International*, 2013.

D. Pucciarelli, E. Weber, S. van den Driesche, M. J. Vellekoop, H. Breiteneder, and C. Hafner, “Macromolecular changes in melanoma cells observes by a mid-infrared sensor system after treatment with vemurafenib,” in *Proc. of the ESDR International Investigateive Dermatology 2013*, 2013.

V. Fioravanti, D. Pucciarelli, E. Weber, S. van den Driesche, C. Hafner, H. Breiteneder, and M. J. Vellekoop, “Biopsy analysis using a quadruple infrared sensor,” in *Proc. of IEEE Sensors*. IEEE, 2013, pp. 1–4.

Other publications

E. Weber, I. Finoulst, P. Vazquez, M. W. Pinkse, W. Svendsen, and P. Verhaert, “Miniaturization of mass spectrometry based analysis setup for identification of signalling peptides in yeast cultures,” in *Proc. of the Netherlands Proteomics Center*, 2011.

Bibliography

[1] G. E. Moore, "Cramming more components onto integrated circuits," *Electronics*, vol. 38, pp. 114–117, 1965. doi:10.1109/jproc.1998.658762

[2] B. Jakoby and M. Vellekoop, "Physical sensors for liquid properties," *Sensors Journal, IEEE*, vol. 11, no. 12, pp. 3076–3085, 2011. [Online]. Available: http://ieeexplore.ieee.org/xpls/abs_all.jsp?arnumber=6017086

[3] M. J. Vellekoop and E. Weber, "Microfluidics and optofluidics for sensing applications," in *Hauptvortrag: 13th Meachatronics Forum, Linz (invited) 2012*.

[4] H.-T. Chen and Y.-N. Wang, "Optical microflow cytometer for particle counting, sizing and fluorescence detection." *Microfluidics and Nanofluidics*, vol. 6, no. 4, pp. 529–537, Aug. 2008. doi:10.1007/s10404-008-0335-z. [Online]. Available: http://www.springerlink.com/index/10.1007/s10404-008-0335-z

[5] S. H. Cho, C. H. Chen, F. S. Tsai, J. M. Godin, and Y.-H. Lo, "Human mammalian cell sorting using a highly integrated micro-fabricated fluorescence-activated cell sorter (microFACS)." *Lab on a Chip*, vol. 10, no. 12, pp. 1567–1573, Jun 2010. doi:10.1039/c000136h. [Online]. Available: http://dx.doi.org/10.1039/c000136h

[6] A. Cleary, S. Garcia-Blanco, A. Glidle, J. S. Aitchison, P. Laybourn, and J. M. Cooper, "An integrated fluorescence array as a platform for lab-on-a-chip technology using multimode interference splitters," *Sensors Journal, IEEE*, vol. 5, no. 6, pp. 1315–1320, 2005. [Online]. Available: http://ieeexplore.ieee.org/xpls/abs_all.jsp?arnumber=1532272

[7] C. Bernabini, D. Holmes, and H. Morgan, "Micro-impedance cytometry for detection and analysis of micron-sized particles and bacteria." *Lab on a Chip*, vol. 11, no. 3, pp. 407–412, Feb. 2011. doi:10.1039/c0lc00099j. [Online]. Available: http://www.ncbi.nlm.nih.gov/pubmed/21060945

[8] M. J. Kennedy, S. J. Stelick, L. G. Sayam, A. Yen, D. Erickson, and C. A. Batt, "Hydrodynamic optical alignment for microflow cytometry." *Lab on a Chip*, vol. 11, no. 6, pp. 1138–1143, Mar. 2011. doi:10.1039/c0lc00500b. [Online]. Available: http://www.ncbi.nlm.nih.gov/pubmed/21279198

[9] M. Rosenauer and M. J. Vellekoop, "Miniaturized absorbance based cell analysis system with integrated microfluidic and optical elements." in *Proc. of the IEEE Sensors 2009*, 2009, pp. 1567–1570. [Online]. Available: http://ieeexplore.ieee.org/stamp/stamp.jsp?tp=&arnumber=5398484

[10] M. Rosenauer and M. J. Vellekoop, "Characterization of a microflow cytometer with an integrated three-dimensional optofluidic lens system." *Biomicrofluidics*, vol. 4, no. 4, p. 43005, 2010. doi:10.1063/1.3502672. [Online]. Available: http://dx.doi.org/10.1063/1.3502672

[11] E. Weber, M. Rosenauer, W. Buchegger, P. D. E. M. Verhaert, and M. J. Vellekoop, "Fluorescence based on-chip cell analysis applying standard viability kits." in *Proc. of the microTAS 2011*, Seattle, USA, 2011, pp. 1716–1718. [Online]. Available: http://www.rsc.org/images/LOC/2011/PDFs/Papers/573_0465.pdf

[12] D. Erickson, "Special issue on optofluidics." *Microfluidics and Nanofluidics*, vol. 4, no. 1-2, pp. 1–2, Sep. 2007. doi:10.1007/s10404-007-0226-8. [Online]. Available: http://www.springerlink.com/index/10.1007/s10404-007-0226-8

[13] C. Monat, P. Domachuk, and B. Eggleton, "Integrated optofluidics: A new river of light," *Nature Photonics*, vol. 1, no. 2, pp. 106–114, 2007. [Online]. Available: http://www.nature.com/nphoton/journal/v1/n2/abs/nphoton.2006.96.html

[14] A.-Q. Liu, "Approach of optofluidics from optics to photonics," in *Proc. Int Optical MEMS and Nanophotonics (OMN) Conf*, 2012, pp. 53–54. doi:10.1109/OMEMS.2012.6318798. [Online]. Available: http://ieeexplore.ieee.org/stamp/stamp.jsp?arnumber=6318798

[15] M. Rosenauer and M. J. Vellekoop, "Characterization of an on-chip reconfigurable 3d optofluidic microlens by confocal laser scanning microscopy." *Procedia Engineering*, vol. 5, pp. 440–443, 2010. [Online]. Available: http://www.sciencedirect.com/science/article/pii/S1877705810006880

[16] M. Rosenauer and M. J. Vellekoop, "3d fluidic lens shaping-a multiconvex hydrodynamically adjustable optofluidic microlens." *Lab on a Chip*, vol. 9, no. 8, pp. 1040–1042, Apr. 2009. doi:10.1039/b822981c. [Online]. Available: http://www.ncbi.nlm.nih.gov/pubmed/19350083

[17] W. R. Dean, "Note on the motion of fluid in a curved pipe," *Philosophical Magazine*, vol. 4, pp. 208–223, 1927.
[18] W. R. Dean, "The stream-line motion of fluid in a curved pipe," *Philosophical Magazine*, vol. 5, pp. 673–695, 1928.
[19] G. M. Whitesides, "The origins and the future of microfluidics." *Nature*, vol. 442, no. 7101, pp. 368–373, Jul 2006. doi:10.1038/nature05058. [Online]. Available: http://dx.doi.org/10.1038/nature05058
[20] J.-C. Baret, "Surfactants in droplet-based microfluidics." *Lab on a Chip*, vol. 12, no. 3, pp. 422–433, Feb 2012. doi:10.1039/c1lc20582j. [Online]. Available: http://dx.doi.org/10.1039/c1lc20582j
[21] L. A. Lyon, C. D. Keating, A. P. Fox, B. E. Baker, L. He, S. R. Nicewarner, S. P. Mulvaney, and M. J. Natan, "Raman spectroscopy," *Analytical Chemistry*, vol. 70, pp. 341–362, 1998. doi:10.1021/a1980021p
[22] J. R. Baena and B. Lendl, "Raman spectroscopy in chemical bioanalysis," *Current Opinion in Chemical Biology*, vol. 8, pp. 534–9, 2004. doi:10.1016/j.cbpa.2004.08.014
[23] P. Abbyad, R. Dangla, A. Alexandrou, and C. N. Baroud, "Rails and anchors: guiding and trapping droplet microreactors in two dimensions." *Lab Chip*, vol. 11, no. 5, pp. 813–821, Mar 2011. doi:10.1039/c0lc00104j. [Online]. Available: http://dx.doi.org/10.1039/c0lc00104j
[24] I. Doh, E. Y. Erdem, and A. P. Pisano, "Trapping and collection of uniform size droplets using a well array inside a microchannel," in *Micro Electro Mechanical Systems (MEMS), 2012 IEEE 25th International Conference on*, 2012, pp. 1113–1116. doi:10.1109/MEMSYS.2012.6170357. [Online]. Available: http://ieeexplore.ieee.org/stamp/stamp.jsp?arnumber=6170357
[25] M. Zagnoni and J. M. Cooper, "On-chip electrocoalescence of microdroplets as a function of voltage, frequency and droplet size." *Lab on a Chip*, vol. 9, pp. 2652–2658, 2009. doi:10.1039/B906298J
[26] N.-T. Nguyen and S. T. Wereley, *Fundamentals and applications of microfluidics*. Artech House, 2002.
[27] H. Bruus, *Theoretical microfluidics*. Oxford University Press, 2008, vol. 18.
[28] J. Berthier and P. Silberzan, *Microfluidics for biotechnology*. Artech House, 2010.
[29] O. C. Zienkiewicz and R. L. Taylor, *The finite element method*. McGraw-hill London, 1977, vol. 3.
[30] T. Thorsen, R. W. Roberts, F. H. Arnold, and S. R. Quake, "Dynamic pattern formation in a vesicle-generating microfluidic device," *Physical review letters*, vol. 86, no. 18, p. 4163, 2001. [Online]. Available: http://prl.aps.org/abstract/PRL/v86/i18/p4163_1
[31] P. Garstecki, M. J. Fuerstman, H. A. Stone, and G. M. Whitesides, "Formation of droplets and bubbles in a microfluidic t-junctionscaling and mechanism of break-up," *Lab on a Chip*, vol. 6, no. 3, pp. 437–446, 2006. [Online]. Available: http://pubs.rsc.org/en/content/articlehtml/2006/lc/b510841a
[32] G. A. Reider, *Photonik*. Springer DE, 2005.
[33] F. de Fornel, *Evanescent waves: from Newtonian optics to atomic optics*. Springer, 2001, vol. 73.
[34] E. D. Palik, *Handbook of Optical Constants of Solids, Five-Volume Set, Volume 1-5: Handbook of Thermo-Optic Coefficients of Optical Materials with Applications (v. 1-5)*. Academic Press, 1997.
[35] C. R. Pollock and M. Lipson, "Graded index waveguides," *Integrated Photonics*, pp. 149–163, 2003. doi:10.1007/978-1-4757-5522-0
[36] E. Weber, F. Keplinger, and M. J. Vellekoop, "On-chip light modulation applying optofluidic principles," *IEEE Sensors Journal*, vol. accepted, 2013.
[37] E. Weber, F. Keplinger, and M. J. Vellekoop, "Detection of dissolved lactose employing an optofluidic micro-system," *Diagnostics*, vol. 2, no. 4, pp. 97–106, 2012. doi:10.3390/diagnostics2040097. [Online]. Available: http://www.mdpi.com/2075-4418/2/4/97
[38] E. Weber, F. Keplinger, and M. J. Vellekoop, "Optofluidic, contact-free 1x3 light-switch fabricated on a mono-layer device," in *Proc. of the 3rd European Conference on Microfluidics*, Heidelberg, Germany, 2012.
[39] E. Weber, F. Keplinger, and M. J. Vellekoop, "Optofluidic analysis system for ethanol solutions," *Procedia Engineering*, vol. 47, pp. 651–654, 2012. [Online]. Available: http://www.sciencedirect.com/science/article/pii/S1877705812042944
[40] E. Weber, D. Puchberger-Enengl, F. Keplinger, and M. J. Vellekoop, "In-line characterization and identification of micro-droplets on-chip," *Optofluidics*, vol. 1, pp. 11–18, 2013. doi:10.2478/optof-2013-0002
[41] E. Weber, D. Puchberger-Enengl, and M. J. Vellekoop, "In-line characterization of micro-droplets based on partial light reflection at the solid-liquid interface." in *Proc. of the ASME 2012 10th ICNMM*, Puerto Rico, USA, 2012, pp. 589–595. doi:10.1115/ICNMM2012-73155
[42] E. Weber and M. J. Vellekoop, "Thermo-optofluidics - on-chip light modulation as an application," in *Proc. of IEEE Sensors*. IEEE, 2012, pp. 1–4. [Online]. Available: http://ieeexplore.ieee.org/xpls/abs_all.jsp?arnumber=6411223
[43] K. R. Williams and R. S. Muller, "Etch rates for micromachining processing," *Journal of*

Microelectromechanical Systems, vol. 5, no. 4, pp. 256–269, 1996. doi:10.1109/84.546406. [Online]. Available: http://ieeexplore.ieee.org/stamp/stamp.jsp?arnumber=546406

[44] M. A. Green, "Self-consistent optical parameters of intrinsic silicon at 300k including temperature coefficients," *Solar Energy Materials and Solar Cells*, vol. 92, pp. 1305–1310, 2008. doi:10.1016/j.solmat.2008.06.009. [Online]. Available: http://dx.doi.org/10.1016/j.solmat.2008.06.009

[45] www.thorlabs.de, "Transmission spectrum of n-bk7 borosilicate glass," http://www.thorlabs.de/newgrouppage9.cfm?objectgroup_id=6973&ispreview=yes&tabname=N-BK7, online; accessed 31-Dec-2013. [Online]. Available: http://www.thorlabs.de/newgrouppage9.cfm?objectgroup_id=6973&ispreview=yes&tabname=N-BK7

[46] A. D. Campo and C. Greiner, "SU-8: A photoresist for high-aspect-ratio and 3d submicron lithography." *Journal of Micromechanics and Microengineering*, vol. 17, no. 6, pp. R81–R95, Jun. 2007. doi:10.1088/0960-1317/17/6/R01. [Online]. Available: http://stacks.iop.org/0960-1317/17/i=6/a=R01?key=crossref.5f54d4397fa259758a20d0ac229f2a2c

[47] www.microchem.com, "Transmission spectrum of n-bk7 borosilicate glass," http://http://microchem.com/pdf/SU-82000DataSheet2100and2150Ver5.pdf, online; accessed 31-Dec-2013. [Online]. Available: http://microchem.com/pdf/SU-82000DataSheet2100and2150Ver5.pdf

[48] H. H. Li, "Refractive index of silicon and germanium and its wavelength and temperature derivatives," *Journal of Physical and Chemical Reference Data*, vol. 9, pp. 561–658, 1980. doi:10.1063/1.555624. [Online]. Available: http://dx.doi.org/10.1063/1.555624

[49] P. Vulto, N. Glade, L. Altomare, J. Bablet, L. D. Tin, G. Medoro, I. Chartier, N. Manaresi, M. Tartagni, and R. Guerrieri, "Microfluidic channel fabrication in dry film resist for production and prototyping of hybrid chips." *Lab on a Chip*, vol. 5, no. 2, pp. 158–162, Feb 2005. doi:10.1039/b411885e. [Online]. Available: http://dx.doi.org/10.1039/b411885e

[50] S. N. Kasarova, N. G. Sultanova, C. D. Ivanov, and I. D. Nikolov, "Analysis of the dispersion of optical plastic materials." *Optical Materials*, vol. 29, no. 11, pp. 1481–1490, Jul. 2007. doi:10.1016/j.optmat.2006.07.010. [Online]. Available: http://linkinghub.elsevier.com/retrieve/pii/S0925346706002473

[51] D. Puchberger-Enengl, E. Weber, C. Krutzler, and M. J. Vellekoop, "Flexible microfluidics: Low cost fabrication of plastic lab-on-a-chip devices," in *Informationstagung Mikroelektronik 2012*, 2012.

[52] M. Focke, D. Kosse, C. Mller, H. Reinecke, R. Zengerle, and F. von Stetten, "Lab-on-a-foil: Microfluidics on thin and flexible films." *Lab on a Chip*, vol. 10, no. 11, pp. 1365–1386, Jun 2010. doi:10.1039/c001195a. [Online]. Available: http://dx.doi.org/10.1039/c001195a

[53] Y. C. Tsai, S. J. Yang, H. T. Lee, H. P. Jen, and Y. Z. Hsieh, "Fabrication of a flexible and disposable microreactor using a dry film photoresist." *Journal of the Chinese Chemical Society*, vol. 53, pp. 683–688, 2006.

[54] J. C. McDonald and G. M. Whitesides, "Poly(dimethylsiloxane) as a material for fabricating microfluidic devices." *Acc Chem Res*, vol. 35, no. 7, pp. 491–499, Jul 2002. doi:10.1021/ar010110q

[55] J. M. K. Ng, I. Gitlin, A. D. Stroock, and G. M. Whitesides, "Components for integrated poly(dimethylsiloxane) microfluidic systems." *Electrophoresis*, vol. 23, no. 20, pp. 3461–3473, Oct 2002. doi:3.0.CO;2-8. [Online]. Available: http://dx.doi.org/3.0.CO;2-8

[56] G. Whitesides, E. Ostuni, S. Takayama, X. Jiang, and D. Ingber, "Soft lithography in biology and biochemistry," *Annual review of biomedical engineering*, vol. 3, no. 1, pp. 335–373, 2001. [Online]. Available: http://www.annualreviews.org/doi/pdf/10.1146/annurev.bioeng.3.1.335

[57] E. Weber, "Optimization and fabrication of optofluidic micro-systems," Master's thesis, Vienna University of Technology, 2009.

[58] E. Weber, M. Rosenauer, P. D. E. M. Verhaert, and M. J. Vellekoop, "Optofluidic microsystem for on-chip l2-waveguide modulation featuring flow stabilization and a novel input coupling region." *Procedia Engineering*, vol. 5, pp. 452–455, 2010. [Online]. Available: http://www.sciencedirect.com/science/article/pii/S1877705810006910

[59] H. Shao, D. Kumar, and K. L. Lear, "Single-cell detection using optofluidic intracavity spectroscopy," *Sensors Journal, IEEE*, vol. 6, no. 6, pp. 1543–1550, 2006. [Online]. Available: http://ieeexplore.ieee.org/xpls/abs_all.jsp?arnumber=4014191

[60] F. Baldini, A. Carloni, A. Giannetti, A. Mencaglia, G. Porro, L. Tedeschi, and C. Trono, "Optical pmma chip suitable for multianalyte detection," *Sensors Journal, IEEE*, vol. 8, no. 7, pp. 1305–1309, 2008. [Online]. Available: http://ieeexplore.ieee.org/xpls/abs_all.jsp?arnumber=4567454

[61] R. Bernini, N. Cennamo, A. Minardo, and L. Zeni, "Planar waveguides for fluorescence-based biosensing: optimization and analysis," *Sensors Journal, IEEE*, vol. 6, no. 5, pp. 1218–1226, 2006. [Online]. Available: http://ieeexplore.ieee.org/xpls/abs_all.jsp?arnumber=1703481

[62] E. Jung, A. Chung, and D. Erickson, "Analysis of liquid-to-solid coupling and other performance parameters for microfluidically reconfigurable photonic systems," *Optics Express*, vol. 18, no. 11, pp. 10 973–10 984, 2010. [Online]. Available: http://www.opticsinfobase.org/abstract.cfm?URI=oe-18-11-10973

[63] Z. Li, Z. Zhang, T. Emery, A. Scherer, and D. Psaltis, "Single mode optofluidic distributed feedback dye laser." *Optics Express*, vol. 14, no. 2, pp. 696–701, Jan 2006. doi:10.1364/OPEX.14.000696

[64] W. Song and D. Psaltis, "Pneumatically tunable optofluidic dye laser," *Applied Physics Letters*, vol. 96, no. 8, pp. 081 101–081 101, 2010. [Online]. Available: http://ieeexplore.ieee.org/xpls/abs_all.jsp?arnumber=5419542

[65] D. Wolfe, R. Conroy, P. Garstecki, B. Mayers, M. Fischbach, K. Paul, M. Prentiss, and G. Whitesides, "Dynamic control of liquid-core/liquid-cladding optical waveguides," *Proceedings of the National Academy of Sciences of the United States of America*, vol. 101, no. 34, pp. 12 434–12 438, 2004. [Online]. Available: http://www.pnas.org/content/101/34/12434.short

[66] A. Chung and D. Erickson, "Optofluidic waveguides for reconfigurable photonic systems," *Optics Express*, vol. 19, no. 9, pp. 8602–8609, 2011. [Online]. Available: http://www.opticsinfobase.org/oe/fulltext.cfm?uri=oe-19-9-8602&id=212830

[67] J. Lim, J. Urbanski, T. Thorsen, and S. Yang, "Pneumatic control of a liquid-core/liquid-cladding waveguide as the basis for an optofluidic switch," *Applied Physics Letters*, vol. 98, no. 4, pp. 044 101–044 101, 2011. [Online]. Available: http://ieeexplore.ieee.org/xpls/abs_all.jsp?arnumber=5705303

[68] X. Mao, B. Juluri, S. Lin, J. Shi, M. Lapsley, and T. Jun Huang, "In-plane tunable optofluidic microlenses," in *IEEE/LEOS Summer Topical Meetings, 2008 Digest of the*. IEEE, 2008, pp. 201–202. [Online]. Available: http://ieeexplore.ieee.org/xpls/abs_all.jsp?arnumber=4590559

[69] W. Xu, X. G. Huang, and J. S. Pan, "A simple fiber-optic refractive index sensor based on fresnel reflection and optical switch," *IEEE Sensors Journal*, 2013, early Access. [Online]. Available: http://ieeexplore.ieee.org/xpls/abs_all.jsp?arnumber=6395799

[70] W. Song and D. Psaltis, "Pneumatically tunable optofluidic 2 x 2 switch for reconfigurable optical circuit." *Lab on a Chip*, vol. 11, no. 14, pp. 2397–2402, Jul 2011. doi:10.1039/c1lc20220k. [Online]. Available: http://dx.doi.org/10.1039/c1lc20220k

[71] K. Campbell, A. Groisman, U. Levy, L. Pang, S. Mookherjea, D. Psaltis, and Y. Fainman, "A microfluidic 2x2 optical switch." *Applied Physics Letters*, vol. 85, no. 25, pp. 6119–6121, 2004. doi:10.1063/1.1839281

[72] Y. Seow, S. Lim, and H. Lee, "Tunable optofluidic switch via hydrodynamic control of laminar flow rate," *Applied Physics Letters*, vol. 95, no. 11, pp. 114 105–114 105, 2009. [Online]. Available: http://ieeexplore.ieee.org/xpls/abs_all.jsp?arnumber=5281706

[73] A. J. Chung, E. Jung, and D. Erickson, "Reconfigurable photonics from microfluidic waveguides," in *Proc. Conf. Lasers and Electro-Optics (CLEO) and Quantum Electronics and Laser Science Conf. (QELS)*, 2010, pp. 1–2. [Online]. Available: http://ieeexplore.ieee.org/stamp/stamp.jsp?arnumber=5500124

[74] M. I. Lapsley, S.-C. S. Lin, X. Mao, and T. J. Huang, "An in-plane, variable optical attenuator using a fluid-based tunable reflective interface." *Applied Physics Letters*, vol. 95, p. 083507, 2009. doi:10.1063/1.3213348

[75] D. Psaltis, S. R. Quake, and C. Yang, "Developing optofluidic technology through the fusion of microfluidics and optics." *Nature*, vol. 442, no. 7101, pp. 381–386, Jul. 2006. doi:10.1038/nature05060. [Online]. Available: http://www.ncbi.nlm.nih.gov/pubmed/16871205

[76] R. C. Kamikawachi, I. Abe, A. S. Paterno, H. J. Kalinowski, M. Muller, and F. J. L. Pinto, J L and, "Determination of thermo-optic coefficient in liquids with fiber bragg grating refractometer." *Optics Communications*, vol. 281, pp. 621–625, 2008. doi:10.1016/j.optcom.2007.10.023. [Online]. Available: http://dx.doi.org/10.1016/j.optcom.2007.10.023

[77] S. K. Tang, B. T. Mayers, D. V. Vezenov, and G. M. Whitesides, "Optical waveguiding using thermal gradients across homogeneous liquids in microfluidic channels," *Applied physics letters*, vol. 88, no. 6, pp. 061 112–061 112, 2006. [Online]. Available: http://ieeexplore.ieee.org/xpls/abs_all.jsp?arnumber=4821251

[78] V. Pilla, E. Munin, and M. R. Gesualdi, "Measurement of the thermo-optic coefficient in liquids by laser-induced conical diffraction and thermal lens techniques," *Journal of Optics A: Pure and Applied Optics*, vol. 11, no. 10, p. 105201, 2009. [Online]. Available: http://iopscience.iop.org/1464-4258/11/10/105201

[79] Y. H. Kim, S. J. Park, S.-W. Jeon, S. Ju, C.-S. Park, W.-T. Han, B. H. Lee *et al.*, "Thermo-optic coefficient measurement of liquids based on simultaneous temperature and refractive index sensing capability of a two-mode fiber interferometric probe," *Opt. Express*, vol. 20, pp. 23 744–23 754, 2012.

[80] T. Chu, H. Yamada, S. Ishida, and Y. Arakawa, "Compact 1× n thermo-optic switches based on silicon photonic wire waveguides," *Optics Express*, vol. 13, no. 25, pp. 10 109–10 114, 2005. [Online]. Available: http://www.opticsinfobase.org/abstract.cfm?id=86452

[81] J. Komma, C. Schwarz, G. Hofmann, D. Heinert, and R. Nawrodt, "Thermo-optic coefficient of silicon at 1550 nm and cryogenic temperatures," *Applied Physics Letters*, vol. 101, no. 4, pp. 041 905–041 905, 2012. [Online]. Available: http://ieeexplore.ieee.org/xpls/abs_all.jsp?arnumber=6248441

[82] R. L. Espinola, M. C. Tsai, J. T. Yardley, and J. Osgood, R. M., "Fast and low-power thermooptic switch on thin silicon-on-insulator." *IEEE Photonics Technology Letters*, vol. 15, no. 10, pp. 1366–1368, 2003. [Online]. Available: http://ieeexplore.ieee.org/stamp/stamp.jsp?tp=&arnumber=1232959

[83] D. Lide, *CRC Handbook of Chemistry and Physics*, 88th ed., P. J. Mohr and B. N. Taylor, Eds. Boca Raton, 2007.

[84] E. Weber and M. J. Vellekoop, "Optofluidic micro-sensors for the determination of liquid concentrations." *Lab on a Chip*, vol. 12, no. 19, pp. 3754–3759, Aug 2012. doi:10.1039/c2lc40616k. [Online]. Available: http://dx.doi.org/10.1039/c2lc40616k

[85] N. K, S. T, G. Rao, and M. Varma, "Analysis of integrated optofluidic lab-on-a-chip sensor based on refractive index and absorbance sensing," *Sensors Journal, IEEE*, 2013, early Access. doi:10.1109/JSEN.2013.2243429. [Online]. Available: http://ieeexplore.ieee.org/stamp/stamp.jsp?arnumber=6423198

[86] M. I. Lapsley, I.-K. Chaing, Y. B. Zheng, X. Ding, X. Mao, and T. J. Huang, "A single-layer, planar, optofluidic mach-zehnder interferometer for label-free detection." *Lab on a Chip*, vol. 11, pp. 1795–1800, 2011. doi:10.1039/c0lc00707b

[87] K.-S. Chao, T.-Y. Lin, and R.-J. Yang, "Two optofluidic devices for the refractive index measurement of small volume of fluids." *Microfluidics and Nanofluidics*, vol. 12, no. 5, pp. 697–704, 2012. doi:10.1007/s10404-011-0915-1

[88] Y. C. Seow, S. P. Lim, B. C. Khoo, and H. P. Lee, "An optofluidic refractive index sensor based on partial refraction." *Sensors and Actuators B: Chemical*, vol. 147, no. 2, pp. 607–611, 2010. doi:10.1016/j.snb.2010.03.076. [Online]. Available: http://dx.doi.org/10.1016/j.snb.2010.03.076

[89] Bundesministerium für Gesundheit, "Zusatzstoff-zulassungsverordnung - ZZuLV." http://www.gesetze-im-internet.de/bundesrecht/zzulv_1998/gesamt.pdf, 1998, online; accessed 31-Dec-2013. [Online]. Available: http://www.gesetze-im-internet.de/bundesrecht/zzulv_1998/gesamt.pdf

[90] L. Lei, I. Mattos, and Y. Chen, "Microfluidic devices for optical determination of ethanol concentration." *Microelectronic Engineering*, vol. 85, no. 5-6, pp. 1318–1320, May 2008. doi:10.1016/j.mee.2008.01.076. [Online]. Available: http://linkinghub.elsevier.com/retrieve/pii/S016793170800035X

[91] C. Meneghini, S. Caron, A. Claire, J. Poulin, A. Proulx, F. Émond, P. Paradis, C. Paré, and A. Fougères, "Determination of ethanol concentration by raman spectroscopy in liquid-core microstructured optical fiber." *IEEE Sensors Journal*, vol. 8, no. 7, pp. 1250–1255, 2008. [Online]. Available: http://ieeexplore.ieee.org/stamp/stamp.jsp?tp=&arnumber=4567485

[92] S. Haeberle, G. Roth, F. von Stetten, R. Zengerle *et al.*, "Microfluidic lab-on-a-chip platforms: requirements, characteristics and applications," *Chemical Society Reviews*, vol. 39, no. 3, pp. 1153–1182, 2010. [Online]. Available: http://pubs.rsc.org/en/content/articlehtml/2010/cs/b820557b

[93] A. Huebner, S. Sharma, M. Srisa-Art, F. Hollfelder, J. B. Edel, and A. J. deMello, "Microdroplets: A sea of applications?" *Lab on a Chip*, vol. 8, pp. 1244–1254, 2008. doi:10.1039/B806405A

[94] X. C. i. Solvas and A. deMello, "Droplet microfluidics: Recent developments and future applications." *Chemical Communications*, vol. 47, pp. 1936–1942, 2011. doi:10.1039/C0CC02474K

[95] S. Hardt and T. Hahn, "Microfluidics with aqueous two-phase systems." *Lab on a Chip*, vol. 12, pp. 434–442, 2012. doi:10.1039/C1LC20569B

[96] S. S. Bithi and S. A. Vanapalli, "Behavior of a train of droplets in a fluidic network with hydrodynamic traps." *Biomicrofluidics*, vol. 4, p. 044110, 2010. doi:10.1063/1.3523053

[97] M. Abdelgawad and A. R. Wheeler, "The digital revolution: A new paradigm for microfluidics." *Advanced Materials (Weinheim, Germany)*, vol. 21, pp. 920–925, 2009. doi:10.1002/adma.200802244

[98] L. Malic, D. Brassard, T. Veres, and M. Tabrizian, "Integration and detection of biochemical assays in digital microfluidic LOC devices." *Lab on a Chip*, vol. 10, pp. 418–431, 2010. doi:10.1039/B917668C

[99] Z. Wang and J. Zhe, "Recent advances in particle and droplet manipulation for lab-on-a-chip devices based on surface acoustic waves." *Lab on a Chip*, vol. 7, pp. 1280–1285, 2011. doi:10.1039/C0LC00527D

[100] H. Song, M. R. Bringer, J. D. Tice, C. J. Gerdts, and R. F. Ismagilov, "Experimental test of scaling of mixing by chaotic advection in droplets moving through microfluidic

channels," *Applied Physics Letters*, vol. 83, no. 22, pp. 4664–4666, 2003. [Online]. Available: http://ieeexplore.ieee.org/xpls/abs_all.jsp?arnumber=4871194

[101] H. Song, J. D. Tice, and R. F. Ismagilov, "A microfluidic system for controlling reaction networks in time." *Angewandte Chemie International Edition*, vol. 42, pp. 768–772, 2003. doi:10.1002/anie.200390203

[102] H. Song and R. F. Ismagilov, "Millisecond kinetics on a microfluidic chip using nanoliters of reagent." *Journal of the American Chemical Society*, vol. 125, pp. 14 613–14 619, 2003. doi:10.1021/ja0354566

[103] J. F. Edd, D. Di Carlo, K. J. Humphry, S. Kster, D. Irimia, D. A. Weitz, and M. Toner, "Controlled encapsulation of single-cells into monodisperse picolitre drops." *Lab on a Chip*, vol. 8, pp. 1262–1264, 2008. doi:10.1039/B805456H

[104] T. Konry, M. Dominguez-Villar, C. Baecher-Allan, D. A. Hafler, and M. L. Yarmush, "Droplet-based microfluidic platforms for single t cell secretion analysis of IL-10 cytokine." *Biosensors and Bioelectronics*, vol. 26, pp. 2707–2710, 2011. doi:10.1016/j.bios.2010.09.006

[105] M. Rosenauer, W. Buchegger, I. Finoulst, P. Verhaert, and M. Vellekoop, "Miniaturized flow cytometer with 3d hydrodynamic particle focusing and integrated optical elements applying silicon photodiodes." *Microfluidics and Nanofluidics*, vol. 10, no. 4, pp. 761–771, Oct. 2010. doi:10.1007/s10404-010-0707-z. [Online]. Available: http://www.springerlink.com/index/10.1007/s10404-010-0707-z

[106] J. Fattaccioli, J. Baudry, J.-D. merard, E. Bertrand, C. Goubault, N. Henry, and J. Bibette, "Size and fluorescence measurements of individual droplets by flow cytometry." *Soft Matter*, vol. 11, pp. 2232–2238, 2009. doi:10.1039/B814954B

[107] X. Niu, M. Zhang, S. Peng, W. Wen, and P. Sheng, "Real-time detection, control, and sorting of microfluidic droplets." *Biomicrofluidics*, vol. 1, p. 044101, 2007. doi:10.1063/1.2795392

[108] M. Srisa-Art, A. J. deMello, and J. B. Edel, "High-throughput confinement and detection of single DNA molecules in aqueous microdroplets." *Chemical Communications*, vol. 43, pp. 6548–6550, 2009. doi:10.1039/B917721C

[109] N.-T. Nguyen, S. Lassemono, and F. A. Chollet, "Optical detection for droplet size control in microfluidic droplet-based analysis systems." in *Digest of Technical Papers, TRANSDUCERS 2005*, vol. 2, 2005, pp. 1557–1560. [Online]. Available: http://ieeexplore.ieee.org/stamp/stamp.jsp?tp=&arnumber=1497382

[110] N.-T. Nguyen, S. Lassemono, and F. A. Chollet, "Optical detection for droplet size control in microfluidic droplet-based analysis systems." *Sensors and Actuators B: Chemical*, vol. 117, pp. 431–436, 2006. doi:10.1016/j.snb.2005.12.010

[111] N.-T. Nguyen, S. Lassemono, F. A. Chollet, and C. Yang, "Interfacial tension measurement with an optofluidic sensor." *IEEE Sensors Journal*, vol. 7, no. 5, pp. 692–697, 2007. [Online]. Available: http://ieeexplore.ieee.org/stamp/stamp.jsp?tp=&arnumber=4154687

[112] Z. Shen, Y. Zou, and X. Chen, "Characterization of microdroplets using optofluidic signals." *Lab Chip*, vol. 12, no. 19, pp. 3816–3820, Aug 2012. doi:10.1039/c2lc40758b. [Online]. Available: http://dx.doi.org/10.1039/c2lc40758b

About the Author

Weber Emanuel was born in Oberpullendorf, Austria in 1983. In 2003 he passed his Matura with distinction at the Federal Higher Technical Institute for Educating and Experimenting for Electrical Engineering (Höhere Technische Bundes- Lehr- und Versuchsanstalt) in Wr. Neustadt. In 2009, he finished his studies on Electrical Engineering and Microtechnology at the Vienna University of Technology, Austria and received his Dipl.-Ing. degree (equivalent to M.Sc.). In 2010 he spent one year at the Delft University of Technology in the Netherlands at the Department of Biotechnolgy under the framework of a European Marie-Curie Initial Training Network, CellCheck. In 2011 he returned to the Vienna University of Technology and joined the Institute of Sensor and Actuator Systems working on his Ph.D. degree on optofluidic systems for biomedical devices. In 2012 he moved to the Institute for Microsensors, -Actuators and -Systems at the University of Bremen, Germany and continued his work on optofluidics under the framework of a second European Marie-Curie Initial Training Network, EngCaBra. He authored journal papers and conference contributions and gave presentations at international conferences. His research activities concern optofluidic micro-systems, micro-fabrication technologies, as well as thermo-optofluidics.